2023

COMBINING CHIRAL CHROMATOGRAPHIC STATIONARY PHASES AND N-DERIVATIZATION STRATEGIES FOR THE QUALITATIVE AND QUANTITATIVE ANALYSIS OF D-AMINO ACIDS, D-AMINO ACID CONTAINING PEPTIDES AND D-AMINO ACID RELATED SECONDARY METABOLITES USING LIQUID CHROMATOGRAPHY

Sam Sung

COMBINING CHIRAL CHROMATOGRAPHIC STATIONARY PHASES AND N-DERIVATIZATION STRATEGIES FOR THE QUALITATIVE AND QUANTITATIVE ANALYSIS OF D-AMINO ACIDS, D-AMINO ACID CONTAINING PEPTIDES AND D-AMINO ACID RELATED SECONDARY METABOLITES USING LIQUID CHROMATOGRAPHY

by

Yu-Sheng Sung

Presented to the Faculty of the Graduate School of

The University of Texas at Arlington in Partial Fulfillment

of the requirements for the Degree of

DOCTOR OF PHILOSOPHY

THE UNIVERSITY OF TEXAS AT ARLINGTON

May 2023

Acknowledgements

First and foremost, I would like to take the opportunity to express my sincere gratitude to my Ph.D advisor Prof. Daniel W. Armstrong for his mentorship, guidance, and constant support during my graduate studies. As a teacher and mentor, he has provided a supportive and engaging working environment that has allowed me to grow and learn.

I would also like to thank Prof. Kevin A. Schug for his guidance when I was still an undergraduate researcher in his lab as well as making state-of-the-art mass spectrometer widely available to student researchers at the University of Texas at Arlington.

I also sincerely thank Dr. Siqi Du, for her mentorship, leadership and support when I first started as a graduate student in the Armstrong Lab. It was a highly enjoyable experience and honor for me to be under her mentorship. She further encouraged me during my internship at AbbVie Inc. and is still a strong role model for me in my career pursuits.

I want to say thanks to Joshua Putnam, my coworker and friend that I collaborated with on multiple research projects. He also provided intellectually stimulating conversations both inside and outside of the laboratory. I would like to thank Umang Dhaubhadel, another coworker that I completed multiple projects with. It is highly encouraging to see younger scientists progress in their understanding. I also would like to thank my good friends, Dr. Elizabeth Readel and Dr. Abiud Portillo, who I would brainstorm with about our projects. Seeing them complete their doctoral studies was highly motivating for me to do the same. A sincere thank you to the other members of the Armstrong lab, Dr. J.T. Lee, Dr. John Lang, Dr. Alain Berthod, Arzoo, and Troy, who provided valuable feedback during group meeting presentations. A monumental thank you to Anne, who was a great help in the logistical planning of acquiring chemicals, scheduling of events, and submission of academic research papers.

I would like to thank my close friends Kate and Chris, whom I befriended throughout my graduate studies and liked me enough to endure a drive time of 16 hours with me from Arlington to Chicago during my internship.

A great thank you to my parents and all the members in my family, who I love dearly. To my parents, who brought me to the US at a young age and supported me through my graduate studies. To my brothers and their families, whom I have learned valuable life lessons from. To my girlfriend, Julissa, thank you for the love and support you have shown me in the time that I've known you.

April 12, 2023

Abstract

COMBINING CHIRAL CHROMATOGRAPHIC STATIONARY PHASES AND N-DERIVATIZATION STRATEGIES FOR THE QUALITATIVE AND QUANTITATIVE ANALYSIS OF D-AMINO ACIDS, D-AMINO ACID CONTAINING PEPTIDES AND D-AMINO ACID RELATED SECONDARY METABOLITES USING LIQUID CHROMATOGRAPHY

Yu-Sheng Sung Ph. D

The University of Texas at Arlington, 2023

Supervising Professor: Daniel W. Armstrong

Amino acids are essential building blocks in all life on Earth. It was first mistakenly believed that only L-amino acids were of biological relevance in higher organisms, and D-amino acids were laboratory artifacts or biologically irrelevant. It is well accepted today that various D-amino acids exist in different organisms, including humans, and some even play critical roles in biological pathways and processes. In addition, aberrant levels of certain D-amino acids have been reported in patients with varying diseases. It has been proposed that the aberrant variations in the levels of D-amino acids in biological fluids may serve as biomarkers for disease in humans. However, due to the lack of a comprehensive and robust analytical platform a full understanding of D-amino acids remains elusive and most of D-amino acids and their biological roles are not well investigated. An analytical challenge is the analysis of D-amino acids in biological samples, because dominant L-amino acid signals and a mix of other endogenous compounds can interference with detection and quantitation of the trace analytes of interest. Additionally, current methods for the comprehensive analysis of D-amino acids are time

consuming. Therefore, the main goals of this dissertation are to a) enhance the sensitivity of current analytical methods and platforms for D-amino acid analysis in biological samples, and b) provide information and methodologies that future studies can use to investigate the roles of D-amino acids in biological systems. A comparison between using UV, MS single quad, multiple reaction monitoring (MRM) detection modes was investigated to determine limits of detection (LOD) for the analysis of AQC-amino acids. This achiral method showed improved detection sensitivity as low as pg and sub-pg levels when using high sensitivity detection modes such as MRM and fluorimetry. A separate study reported the first comprehensive analysis of the intracellular and extracellular profiles of L- and D-amino acid in human breast cancer cells (MCF-7) and non-tumorigenic epithelial breast cells (MCF10A) using HPLC-MS/MS. This study further advanced our knowledge of how D-amino acids can interact with the NMDA receptors in cancer cells. For the differentiation of peptides containing D-amino acids, a novel enzymatic technique using carboxypeptidase Y, coupled with selective retention of D-amino acids and D-amino acid containing peptides on teicoplanin type stationary phases was developed. This enzyme hydrolytically cleaves L-amino acids at the peptide bond from the C-terminus of peptides, but its catalytic efficiency decreases dramatically when confronted with a C-terminal D-amino acid. The strong retention of D-amino acids and D-amino acid containing peptides on teicoplanin stationary phases was then exploited to analyze intact fragments of the carboxypeptidase hydrolysis by LC-MS/MS with little to no interference from more abundant L-amino acid peptides. A fully comprehensive, highly sensitive and selective 2D-HPLC-MS/MS chiral separation method was developed along with a complementary GC-MS/MS method for the study of L- and D-homoserine lactone homologues in the extracellular media of gram-negative bacteria.

Table of Contents

List of Figures

List of Tables

Chapter 1 Introduction

Chapter 1.1 Chirality of amino acids

Chirality is an important consideration for pharmaceutical compounds, foods, agrochemicals and biologically active compounds.[1-3] Amino acids are essential to life and serve multiple fundamental roles as the building blocks of proteins, intermediates in metabolic processes, and cell signaling.[4-6] All proteinogenic amino acids except for glycine, possess a chiral center stemming from the alpha carbon, which is attached to an amine, carboxylate and hydrogen. Traditionally, L-amino acids were the only enantiomer thought to be biologically consequential and D-amino acids were thought of as "unnatural" and detrimental to life (both are shown in Fig 1.1). However, as separation and sensitive analytical techniques grew and developed, there was mounting evidence to challenge the view that life was exclusively homochiral (the L-form).

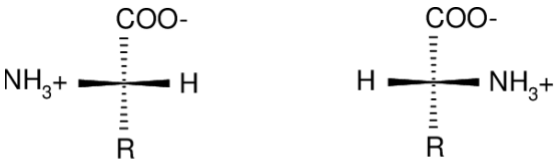

Figure 1.1 Chirality of amino acids

1.2 D-amino acids in living organisms

The presence of D-amino acids in living organisms was first reported in cancerous cell tissue proteins in 1939.[7,8]. D-amino acids would then be discovered in the acid hydrolysate of bacteria cells a few years later in 1948.[9] It was determined that bacteria peptidoglycan was partly comprised of D-Ala and D-Glu and that these D-amino acids served an essential role in cell wall assembly.[10,11] We now know that the evolutionary drive towards incorporations of D-amino

acids in bacteria include resilience to protease hydrolysis, resistance to antibiotics, regulating peptidoglycan structure.[12-13] Free D-amino acids can also be used by certain species of bacteria to inhibit biofilm formation in rival bacterial species.[14]

In the present day, both free and peptide bound D-amino acids have been confirmed to exist in living organisms and can be produced in a variety of ways.[15] D-amino acids can be produced by racemaces and aminotransfereases,[16-18] whereas peptide bound D-amino acids can result from epimerases,[19] and natural isomerism in the case of Asp isomerization.[20] It was recently discovered that D-Cys levels were endogenous modulators of neural progenitor cell dynamics in development in mammalian brains.[21] D-Ser is also an important agonist for NMDA receptors, a transmembrane protein which serves as an ion channel and highly expressed in brain tissue.[22,23] This is further evidenced by the discovery of the first mammalian amino acid racemace, serine racemace, now known to be common in mammalian brain tissue.[24]

1.3 D-amino acids in human diseases

Abnormal levels of D-amino acids have been linked to diseases in humans. Elevated levels of D-Asp, D-Ser and D-Ala have been reported in skin and breast cancer cells,[25] D-Ser, D-Asp, D-Pro and D-Asn present in urine have been used to evaluate kidney health,[26] and abnormal levels of D-Asp, D-Ser, D-Ala and D-Leu associated with neurological diseases such as Alzheimer's disease,[27] schizophrenia[28] and epilepsy.[29]

1.4 Analytical approaches to D-amino acid analysis

The first chiral separation of natural amino acids in liquid chromatography (LC) was presented in 1972 on a ligand exchange column packed with a chloromethylated styrene polymer with 0.8% divinyl benzene that had been reacted with L-Pro in the presence of sodium iodide catalyst and subsequently saturated with Cu^{2+} ions.[30] Until the introduction of macrocyclic

glycopeptide antibiotic stationary phases by Armstrong in 1994, most chiral separations in HPLC were performed with ligand-type exchange, pi-stacking, cyclodextrin, chiral crown ethers or cellulose type phases.[1,31] Since then, the flurry of development in instrumentation and column manufacturing technologies have made the resolution of stereoisomers and enantiomers commonplace. However, the detection of trace levels of D-amino acids and D-amino acid bound peptides in living organisms still presented an analytical challenge. Quantitation of trace D-amino acids are also difficult if the second eluting enantiomer was a D-amino acid which was often hidden by the dominant L-enantiomer if there was insufficient enantioresolution. There was also a demand for sensitive instrumentation and bioanalytical methods to interrogate biological sources for trace amounts of D-amino acids. As mentioned earlier, initial methods of determining D-amino acid content in peptides and proteins used acid hydrolysis.[9] The main problem with this method was that it induces partial racemization of all hydrolyzed amino acids to different extents.[32] Aspartic and glutamic acid are especially difficult to quantify as they are the most susceptible to deamination, converting to asparagine and glutamine respectively in the hydrolysis process.[33] Additionally, the indole group on tryptophan is completely destroyed during acid hydrolysis.[33] Alternatively, hydrolyzing with DCl as opposed to HCl can produce more reliable results as any racemized amino acid would contain a deuterium on the hydrolysis site and Asp to Asn/Glu to Gln conversions would be discernable.[34] Another method to differentiate peptide isomers is using MS/MS techniques although this would ideally require a synthesized standard to confirm the identity of the peptide.[35] Thus, there is an increasing demand in the field of bioanalytics for highly sensitive and robust techniques for the detection of both free and peptide bound D-amino acids to further understand their biological roles.

1.5 Research objectives and organization of the dissertation

This dissertation will encompass five academic research papers. The first will describe the separation and detection studies of α-amino acids derivatized with 6-aminoquinolyl-N-hydroxysuccimidyl carbamate and their respective limits of detection (LOD) via four commonly used detection modes.[36] It will also explain the idiosyncrasies of detecting certain traditionally problematic amino acids using these detectors. The second paper will describe the abnormal levels of D-amino acids and their physiological impact on NMDA receptors in cancerous skin tissue.[25] This article also describes a method of using AQC-derivatization to better resolve low abundance D-enantiomers on a modified quinine stationary phase with the optimal order of elution (D-enantiomer first) that was used for bioanalysis. The third paper incorporates the use of enzymatic stereospecific differentiation of D-amino acid containing peptides based on rates of hydrolysis with carboxypeptidase Y, a serine protease.[37] This type of enzyme hydrolytically cleaves L-amino acids from the C-terminus of peptides but can be inhibited upon encountering a D-amino acid. AQC-derivatization was also incorporated as it has been shown that large N-blocking groups increase the susceptibility of short peptides to carboxypeptidase hydrolysis. In addition, AQC-derivatization increases the detectability of some hydrolysis products. The fourth paper demonstrates the merits of using teicoplanin aglycone CSP, a macrocyclic glycopeptide antibiotic, as an extraction media for free D-amino acids and C-terminal D-amino acid containing peptides.[38] This selective preference of the CSP towards D-amino acids was then combined with the use of CPY to generate the C-terminal D-amino acid containing peptides which were then analyzed on a teicoplanin stationary phase. The last paper features a comprehensive chiral LC-MS/MS as well as a complementary GC-MS/MS method for the identification and quantitation of DL-homoserine lactones.[39] These quorum sensing molecules

are produced from L-Met through biosynthetic pathways. This method will greatly enhance the analytical toolbox of scientists when searching for the elusive D-homoserine lactones.

Chapter 2 A closer examination of 6-aminoquinolyl-N-hydroxysuccimidyl carbamate amino acid derivatization in HPLC with multiple detection modes

Abstract

6-Aminoquinolyl-*N*-hydroxysuccinimidyl carbamate is a well-known reagent used to derivatize amino acids (AAs) into their aminoquinolyl carbamate (AQC) analogs. Originally, AQC derivatization was used to enhance UV detection of amino acids (and amines) and to provide a fluorescent derivative for further enhanced detection. Subsequently, it was found that AQC derivatization could also enhance mass spectrometry (MS) detection. It is sometimes assumed that since the AQC tag is identical for all amino acids, that their detection will be similar for a given detection mode. However, this is often not the case. Sometimes there are extreme exceptions, for example, cysteine and tryptophan, which are simply ignored in the literature. Herein, four detection modes were compared: two optical spectroscopic modes, 254 nm UV and fluorimetry, and two mass spectrometry (MS) modes, single ion analysis and multiple reaction monitoring (MRM). The most sensitive detection modes were fluorimetry and MRM which were able to detect down to the tens of femtomoles of injected AAs. But single quad MS and classical UV detection could quantitate most AQC-AAs down to the picomole level in most instances. The differences between detection modes and within each of the four detection modes are examined and discussed for the first time. The possible reasons for extreme differences in the detectability of specific amino acids are considered.

2.1 Introduction

Cohen and Michaud introduced 6-aminoquinolyl-*N*-hydroxysuccinimidyl carbamate (AQC) as a derivation agent for amino acids (AA) that subsequently could be analyzed by reverse phase liquid chromatography (RPLC).[40,41] This derivatization method quickly became popular since it provided easily functionalized amino acids that were stable, less polar, and highly UV detectable compounds given the large hydrophobic chromophore. The aminoquinolyl group, also being a fluorophore, means that the AQC-AA derivatives can exploit highly sensitive fluorometric detection.[42-45] With the rapid improvements in mass spectrometers (MS), and their interfaces with HPLC instruments, MS has become one of the more common and powerful liquid chromatography detectors. MS detection of native amino acids can be difficult due to the presence of buffer salts and analyte masses below 200, resulting in interference from the mobile phase and considerable noise.[46,47] However, AQC derivatization increases the amino acid masses by 170 Da and produces positively charged species in all cases, facilitating their ESI–MS detection (Fig. 2.1).

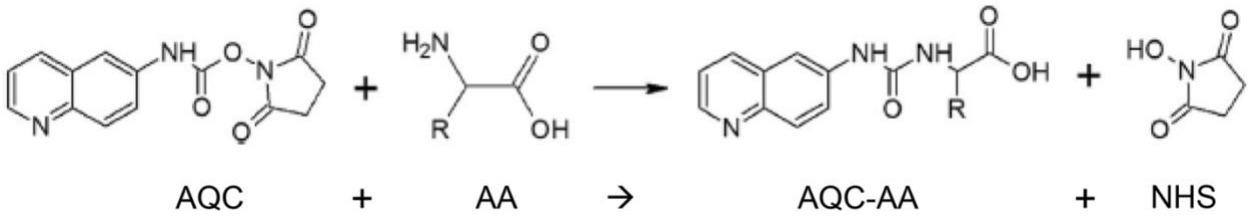

Fig 2.1 Reaction of 6-aminoquinolyl-*N*-hydroxysuccinimidyl carbamate (AQC, m.w. 285.3) with amino acids (AA) producing the AQC-AA derivative (m.w. AA + 170.2) and N-hydroxysuccinimide (NHS, m.w. 115.1)

The simplicity of AQC derivatization and its compatibility with buffer salts have made it one of the preferred choices for MS detection of amino acids in complex samples.[25,48-53] There

are 20 proteinogenic amino acids, but often the published data in many papers involving quantitative amino acid analyses do not list the full set of LODs for the 20 AQC derivatized amino acids. [44,48,49,54,55] It has been stated that asparagine and glutamine were missing from acidic solutions because of amide hydrolysis which produced aspartic and glutamic acids, respectively. Tryptophan has been excluded due to its "instability" during protein hydrolysis and cysteine often was not listed due to its ability to dimerize into cystine and also due to its destruction during acid hydrolysis of proteins.[56,57] In direct amino acid analyses of biological or environmental samples, i.e. without harsh acidic hydrolysis, tryptophan is the only native amino acid that can be determined by fluorescence. All other AAs must be derivatized. However, AQC-tryptophan shows a poor limit of detection with fluorescence compared to the other AQC-AAs.[53, 54, 58] Cysteine also seems difficult to analyze in any sample by any detection method.[44, 48, 49, 55, 58] All other AQC derivatized amino acids show good sensitivity by each of various detection approaches. Since the pendant AQC group (Fig. 2.1) is the moiety that is mainly responsible for detection, it may be thought that most AQC-AAs will have similar limits of detection (LODs) when using the same detector.

In this work, the AQC derivatization of amino acids was used to detect AQC-AAs with high sensitivity and comparing three detection approaches: UV, fluorimetry and MS upon separation with UPLC. Two different modes were used with MS detection: the simple single quadrupole (SQ) monitors a specific *m*/*z* ratio and the MS/MS mode with multiple reaction monitoring (MRM) focusing on a dominant product ion fragment coming from a selected *m*/*z* precursor under optimal conditions. The cases of AQC derivatized AAs with poor detectability are examined in detail for the first time.

2.2 Methods

2.2.1 Materials

Native L-AAs were obtained from Sigma-Aldrich (MilliporeSigma, Saint-Louis, MO, USA) except L-tyrosine that came from TCI Chemicals (Thermo Fisher Scientific, Pittsburg, PA, USA). HPLC grade solvents and ammonium formate were from Sigma. 10 mM stock solutions of each AA in 10% methanol were kept frozen at −4 °C as well as a 0.10 mM norvaline solution. 250 µL of each 10 mM AA standard solution were mixed together making a 5 mL of stock solution of a 500 µM for each 20 AAs. This solution was serially diluted to standard concentrations of 200, 100, 50, 25, 10, 5, 1, and 0.25 µM to prepare AA calibration curves for UV, fluorescence, and MS detection. 100 µL of the 0.1 mM norvaline solution was added as internal standard (IS) to each 1 mL of AA mixes for UV and MS detection so that all standards contain 10 µM of norvaline IS. For fluorometric detection, the calibration concentrations ranged from 100 µM down to 0.25 µM with all mixes containing 10 µM norvaline as the internal standard.

2.2.2 Amino acid derivatization

The AccQ-Tag Ultra "3X" derivatization kit from Waters (Milford, MA, USA) was used to obtain the AQC-AA derivatives mostly following the manufacturer procedure. The kit contains three different groups of vials: one containing a 0.2 mM borate buffer solution at pH 8.8, the second one contains the dry powdered AQC reagent and the third one contains acetonitrile that needs to be added to the second vial to obtain a 10 mM AQC reagent solution. The ratio by volume of borate buffer to AA mix to AQC reagent was 70:10:20 producing AQC-AA mixes with a 10 times lower concentration than that of the initial mixes. The mixture was

then briefly vortexed and heated for 15 min at 55 °C and left standing overnight at room temperature prior to analysis.

2.2.3 HPLC instrumentation and method

A Thermo Scientific Vanquish UHPLC Focus instrument was used for AQC-AA UV calibration curves obtained at 254 nm using the Chromeleon 7.2 SR4 software for data handling. A Prominence HPLC system (Shimadzu, Columbia, MD, USA) equipped with a RF-20A XS fluorescence detector and using the LabSolutions data handling software gave the fluorescence calibration curves with an excitation wavelength of 248 nm and emission monitored at 395 nm for the AQC-AA compounds. A Shimadzu LCMS 8040 using the LabSolution Insight software was used for single quad (SQ) and multiple reaction monitoring (MRM) MS AQC-AA detections. ESI nebulizing and drying gas flow of 2 and 15 L/min, respectively. Desolvation line and heat block temperature used were 275 and 400 °C, respectively. Dwell time for all analytes was 25 ms in both MS methods. Table 2.1 lists the experimental conditions used for each AQC-AA. The precursor ion in MRM detection was the Table 1.1 listed SQ *m*/*z* ion. The product ion monitored in MRM was always the aminoquinolyl fragment with a *m*/*z* of 171.0 ± 0.01. The CID gas pressure used was 230 kPa and the collision cell voltage is given in Table 2.1

Table 2.1 Experimental conditions used for the single quad (SQ and multiple reaction monitoring (MRM) mass spectrometry detection of AQC-derivatized amino acids[a]

Amino acid	Code	AA m.w	SQ *m/z*	MRM			
				Monitored *m/z*	Q1 bias V	Collision cell V	Q3 bias V
Alanine	Ala	89.1	260.1	171.0	− 29	− 17	− 17
Arginine	Arg	174.2	345.2	171.0	− 17	− 26	− 15
Asparagine	Asn	132.1	303.1	171.0	− 15	− 22	− 15
Aspartic acid	Asp	133.1	304.1	171.0	− 15	− 23	− 26
Cysteine	Cys	121.2	292.2	171.0	− 14	− 26	− 15
Glutamine	Gln	146.1	317.1	171.0	− 14	− 21	− 15
Glutamic acid	Glu	147.1	318.1	171.0	− 16	− 22	− 15
Glycine	Gly	75.1	246.1	171.0	− 17	− 23	− 16
Histidine	His	155.2	326.2	171.0	− 12	− 22	− 15
Isoleucine	Ileu	131.2	302.2	171.0	− 16	− 16	− 16
Leucine	Leu	131.2	302.2	171.0	− 15	− 23	− 15
Lysine	Lys	146.2	244.1[b]	171.0	− 17	− 25	− 27
Methionine	Met	149.2	320.2	171.0	− 14	− 31	− 25
Phenylalanine	Phe	165.2	336.2	171.0	− 16	− 25	− 16
Proline	Pro	115.1	286.1	171.0	− 30	− 23	− 26
Serine	Ser	105.1	276.1	171.0	− 17	− 23	− 15

Threonine	Thr	119.1	290.1	171.0	− 14	− 17	− 15
Trans-L-hydroxy proline	Tr-L-Hyp	131.1	302.1	171.0	− 14	− 21	− 16
Tryptophan	Trp	204.2	375.2	171.0	− 15	− 18	− 15
Tyrosine	Tyr	181.2	352.2	171.0	− 15	− 22	− 25
Valine	Val	117.1	288.1	171.0	− 15	− 21	− 15

[a]The precursor MRM ion is the listed SQ ion; the dwell time was always 25 ms
[b]The lysine has two AQC groups attached. MRM monitors 487.2 *m*/*z* as the precursor ion

A 15-cm Poroshell 120 EC-C18 Infinite column (4.6 mm i.d., 2.7 µm superficially porous particles) and 3 µL injections were used for all three LC methods with the same mobile phase gradient profile. All separations used a flow rate of 0.4 mL/min. Only 1 µL injections were used with fluorescent detection due to the high sensitivity of the detector. Mobile phase A was 25 mM ammonium formate pH 6 buffer in Millipore filtered water, mobile phase B was LC/MS grade acetonitrile. The gradient conditions were: 0–13 min hold at 8% B, 13–25 min 0.66%/min ramp from 8 to 16% B, 25–35 min 1.6%/min ramp from 16 to 32% B, 35–38 min 2%/min ramp from 32 to 38% B, 38–43 min hold at 38% B, 43–53 min fast return and hold at 8% B.

2.2.4 Spectral data

All UV and fluorescent spectra shown were collected with stand-alone spectrophotometers with no prior chromatographic separation. UV spectra were collected with a Shimadzu UV-2600 UV–vis double beam spectrophotometer. Wavelength range was 210–400 nm with a sampling interval of 1 nm and a lamp source transition at 326 nm from a tungsten source to a deuterium source. A quartz cuvette was used with a path length of 1 cm. Collection software used was UVProbe 2.42. Fluorescence spectra were collected with a Jobin Yvon Horiba

FluoroMax-3 single beam fluorimeter. Excitation wavelength was 248 nm and emission wavelengths were collected from 300 to 450 nm with a sampling interval of 1 nm. Signal formula used was S1-R1 with an accumulation of three average scans. Cuvette used was a Shimadzu 10 mm quartz Cell Fluorimeter. Data collection software used was FluorEssence V3.9.

2.2.5 Miscellaneous details

The LODs were calculated according to Ref 55 where the $LOD = \frac{3.3\sigma}{m}$, σ is the standard deviation of the lowest concentration, and *m* is the slope of the calibration curve. The LOD concentration was subsequently converted to absolute picomole values using injection volume to account for differences in injection volume between fluorescence and the other three modes of detection.

The 3D modeling and analysis software Chem3D Ultra® from CambridgeSoft (Cambridge, MA, USA) were used on a personal computer for molecular modeling with energy minimization.

2.3 Results and Discussion

2.3.1 Detection modes

Native AAs are poorly UV absorbing molecules when the only chromophore is the carboxylic acid group. Three AAs, phenylalanine, tyrosine, and tryptophan contain, respectively, a benzyl, phenol and indol aromatic group that increases their UV detectability. The AQC derivatization adds an aminoquinolyl chromophore group, enhancing the UV absorbance of all amino acids by two to three orders of magnitude.[42,59] Figure 2.2, top inset, shows the UV absorbance spectra of the three aromatic AAs (solid lines) as well as those of their respective AQC derivatives (dotted lines). At a 5 μM concentration in a 1 cm-path length cell, the 254 nm UV absorbance of the native aromatic AAs reaches 0.03 unit (upper Fig. 2.2 inset) when, in the

same conditions, their AQC derivatives have almost two orders of magnitude more absorbance. The similarity of the three AQC-aromatic AA UV spectra clearly shows that the absorbance is due to the aminoquinoline group.

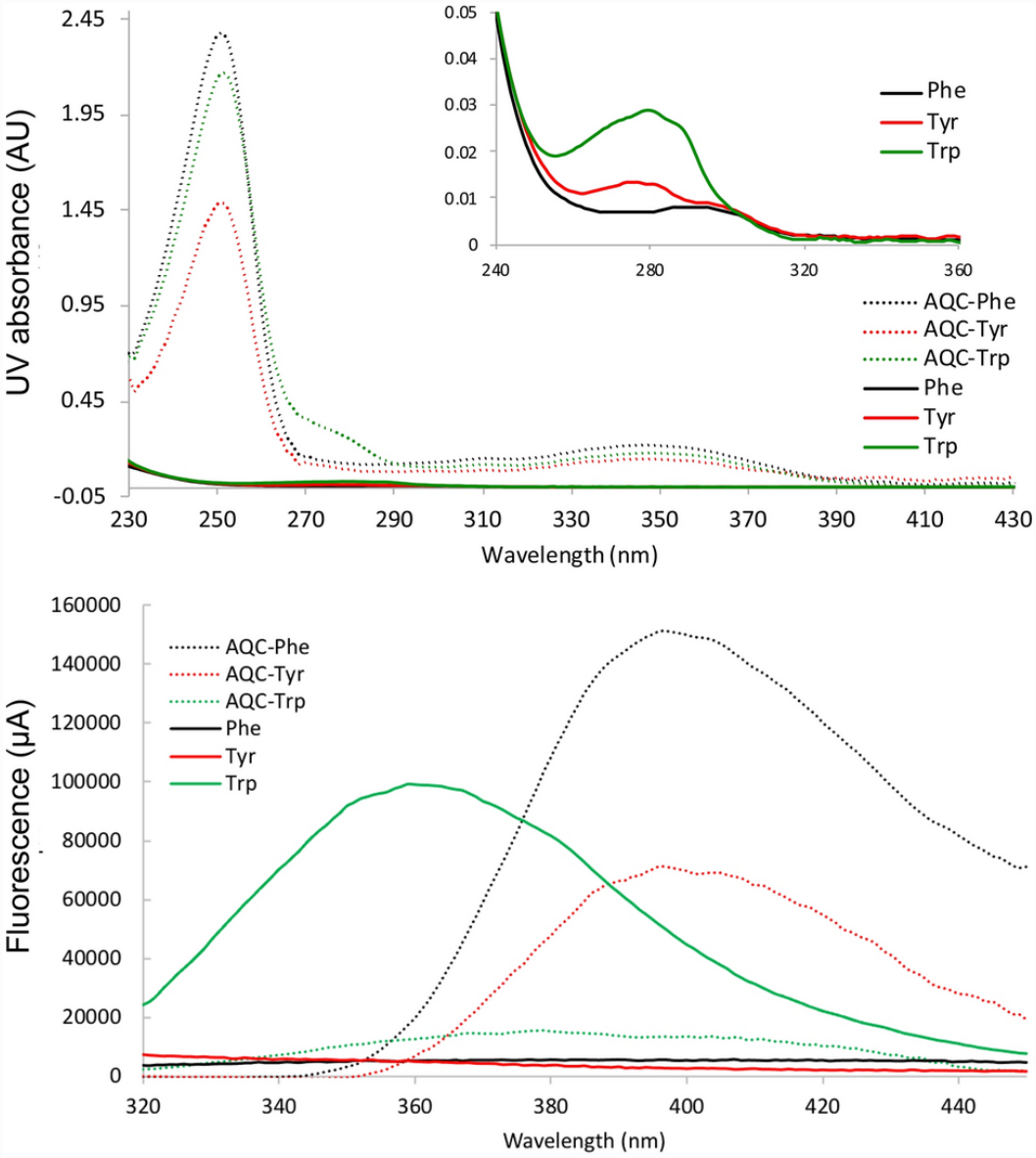

Fig 2.2 Background corrected UV spectra of three underivatized aromatic amino acids (upper inset, *full lines*) and their aminoquinolyl derivatives (AQC-AA, *dotted lines*) showing the differences in 254 nm UV absorbance (top) and background corrected fluorescence emission with 248 nm excitation (bottom). Amino acid concentration: 5 µM, cell path: 1 cm

Given the Fig. 2.2 AQC absorbance spectra of the three aromatic amino acids and other AQC-AAs, it might be assumed that their UV limits of detection (LODs) could be similar. Native aromatic AAs could be UV detected underivatized at a short 210–220 nm wavelength but with a much weaker absorbance than their AQC counterparts (Fig. 2.2, top).

Fluorescence is intrinsically a much more sensitive detection mode than UV since it is far easier to observe light emitted by a fluorescent molecule on a black background than counting absorbed photons in a bright UV beam. Tryptophan is the only naturally fluorescent AA, a widely important and utilized property for protein analyses.[60] Two other aromatic AAs, phenylalanine and tyrosine, have a very weak fluorescence at short wavelength (solid lines, Fig. 2.2, bottom). It is generally assumed that all AQC derivatized AAs are strongly fluorescent due to the added aminoquinolyl group. All AQC-AAs were well detected by fluorescence except AQC-tryptophan which shows a very weak emission spectra (dotted green line, Fig. 2.2 bottom) as noted in different works.[53,54,58] This point will be further discussed in a subsequent section. Again, it might be thought that the AQC-AAs could have similar fluorescence intensities and LODs as they all have the same 6-aminoquinolyl functional group. Figure 2.3 compares the chromatograms of the proteinogenic derivatized amino acids obtained under the same conditions with UV and fluorescence detection. Degradation products of the AQC derivatization reaction are identified as N-hydroxysuccinimide, aminoquinoline, and bis-aminoquinoline carbamate, the AQC-derivative of aminoquinoline.

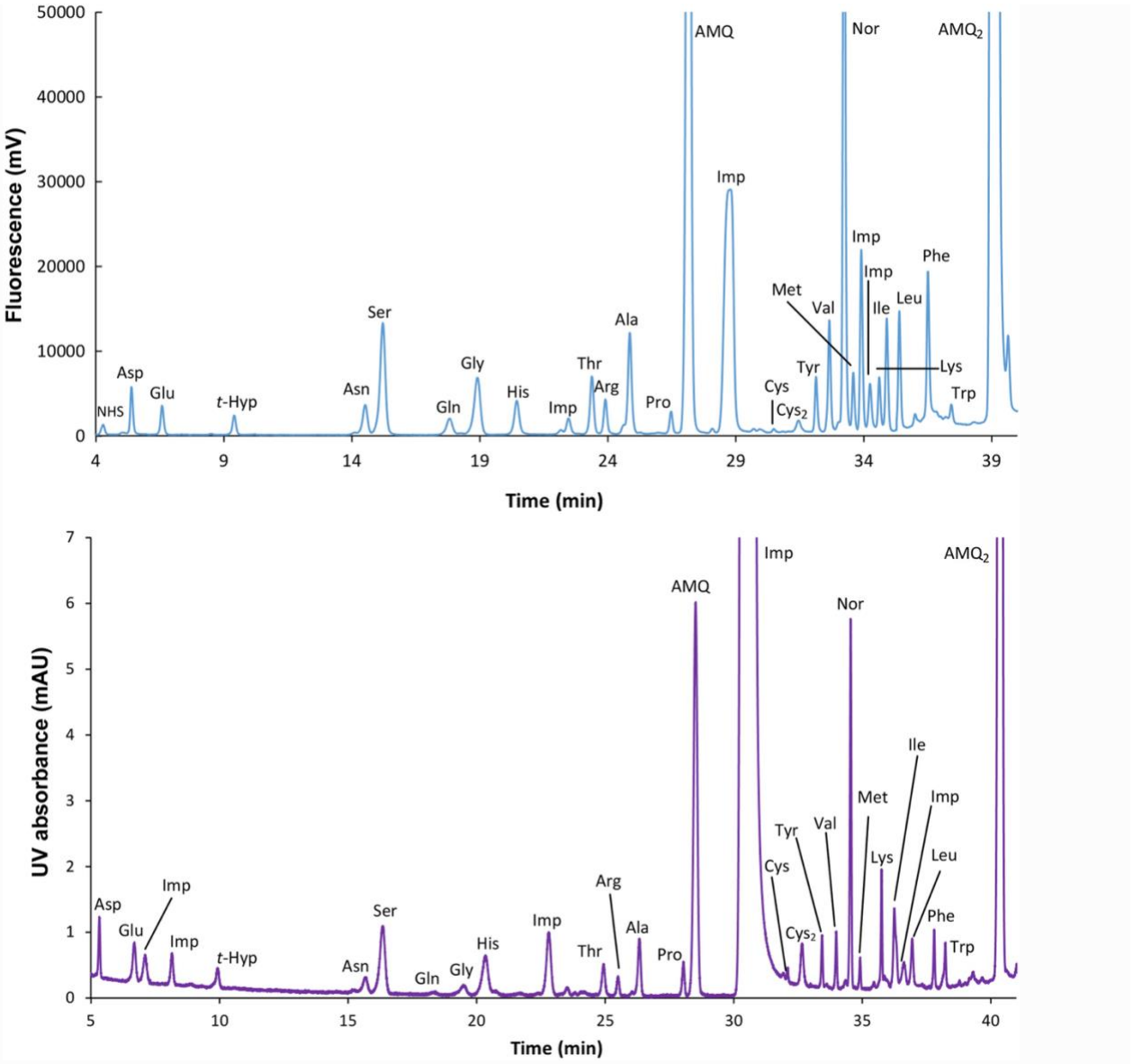

Fig 2.3 Chromatograms of AQC-amino acids detected by fluorimetry (top) with λ_{ex} 248 nm and λ_{em} 395 nm and UV 254 nm (bottom). 1 and 3 µL of 0.1 µM AQC-AA mix were injected (0.1 and 0.3 pmol of each AQC-AA), for fluorimetry and UV detection, respectively, on a 15-cm Poroshell 120 EC-C18 Infinite column (4.6 mm i.d., 2.7 µm superficially porous particles) and eluted with a 25 mM ammonium formate pH 6 buffer/acetonitrile gradient (see Experimental section). *AMQ* 6-aminoquinoline; *NHS* N-hydroxysuccinimide; *AMQ2* di-aminoquinolinyl carbamate; *Cys2* cystine; *Nor* norvaline internal standard

The injected AQC-AA concentrations for this chromatogram were all 0.1 µM, and 0.3 pmol with a 3 µL injection volume. This is not the case for fluorometric detection which contains 0.1 pmol with a 1 µL injection volume, with peaks well above LODs except for cysteine and tryptophan (these unique cases will be discussed subsequently).

Single quadrupole MS detection used the positive mode, corresponding to the amino acid molecular weight plus 171.0 for the added aminoquinolyl group (see Table 2.1). AQC-lysine was monitored at a m/z 244.1 in single quadrupole MS corresponding to its molecular weight plus two AQC groups, because both of its two primary amines were derivatized with both acquiring a charge during the ionization process. MRM optimization for AQC-lysine favored the singly charged precursor from 487.2 to 171.0 transition. With no exception, the precursor ion was also the [amino acid + 171.0] *m*/*z* ion listed under the SQ heading in Table 2.1. The monitored fragment was the aminoquinolyl ion at *m*/*z* 171.0 ± 0.01 (Table 2.1). The AQC-Arg precursor ion at *m*/*z* 345.3 gave two strong fragments: the *m*/*z* 171.0 expected fragment and also the close *m*/*z* 174.2 fragment of arginine ion. Both fragments were monitored for the best AQC-arginine detection with a lower MRM LOD obtained using the *m*/*z* 171.0 fragment.

2.3.2 Limits of Detection

Calibration curves for the 20 proteinogenic AAs plus the collagen forming trans-L-hydroxyproline were obtained with 32 experiments done in triplicate: for each of the four detection modes. The eight amino acid mixtures were injected in increasing concentration in the UHPLC system described in the Experimental to prevent crossover. The AQC-AAs were separated on the same 15 cm Poroshell 120 EC-C_{18} column eluted with the same pH 6 buffer/acetonitrile gradient. Figure 2.3 gives an example of UV and fluorometric detection

chromatograms. Table 2.2 lists the limits of detection (LOD) obtained with the four detection modes: UV, fluorimetry and the two MS modes, SQ and MRM. The limits of quantitation are not listed since they can easily be estimated, being three times the LODs. Figure 2.4 presents the LOD data with a log scale for easy comparison.

Table 2.2 Limit of detection of AQC derivatized amino acids in four detection modes[a]

Amino acid	Code	UV–Vis (pmol)	Fluorimetry (pmol)	MS-SQ (pmol)	MS-MRM (pmol)
Alanine	Ala	0.096	0.043	0.36	**0.030**
Arginine	Arg	0.14	**0.018**	0.63	0.033
Asparagine	Asn	0.48	0.062	0.42	**0.048**
Aspartic acid	Asp	0.15	**0.040**	0.78	0.054
Cysteine	Cys	*1.1*	***0.16***	*1.6*	*1.2*
Glutamine	Gln	0.92	0.057	0.51	**0.024**
Glutamic acid	Glu	0.090	0.051	0.48	**0.048**
Glycine	Gly	0.34	**0.055**	1.1	0.099
Histidine	His	0.090	**0.018**	0.22	0.054
Isoleucine	Ileu	0.27	**0.010**	0.12	0.027
Leucine	Leu	0.24	**0.009**	0.16	0.018
Lysine	Lys	0.040	**0.007**	0.063	0.030

Methionine	Met	0.18	**0.008**	0.16	0.012
Phenylalanine	Phe	0.12	0.019	0.042	**0.015**
Proline	Pro	0.18	0.037	0.45	**0.021**
Serine	Ser	0.11	0.038	0.13	**0.018**
Threonine	Thr	0.16	0.030	0.35	**0.015**
Trans-L-hydroxy proline	Tr-L-Hyp	0.14	**0.024**	0.63	0.030
Tryptophan	Trp	0.20	*0.35*	0.42	**0.018**
Tyrosine	Tyr	0.14	0.024	0.48	**0.012**
Valine	Val	0.064	0.032	0.20	**0.030**

Bold values correspond to the lowest limit of detection for a given AA; italicized values are discussed in text

[a]*AQC* aminoquinolyl derivative; *SQ* single quad mass spectrometry; *MRM* multiple reaction monitoring

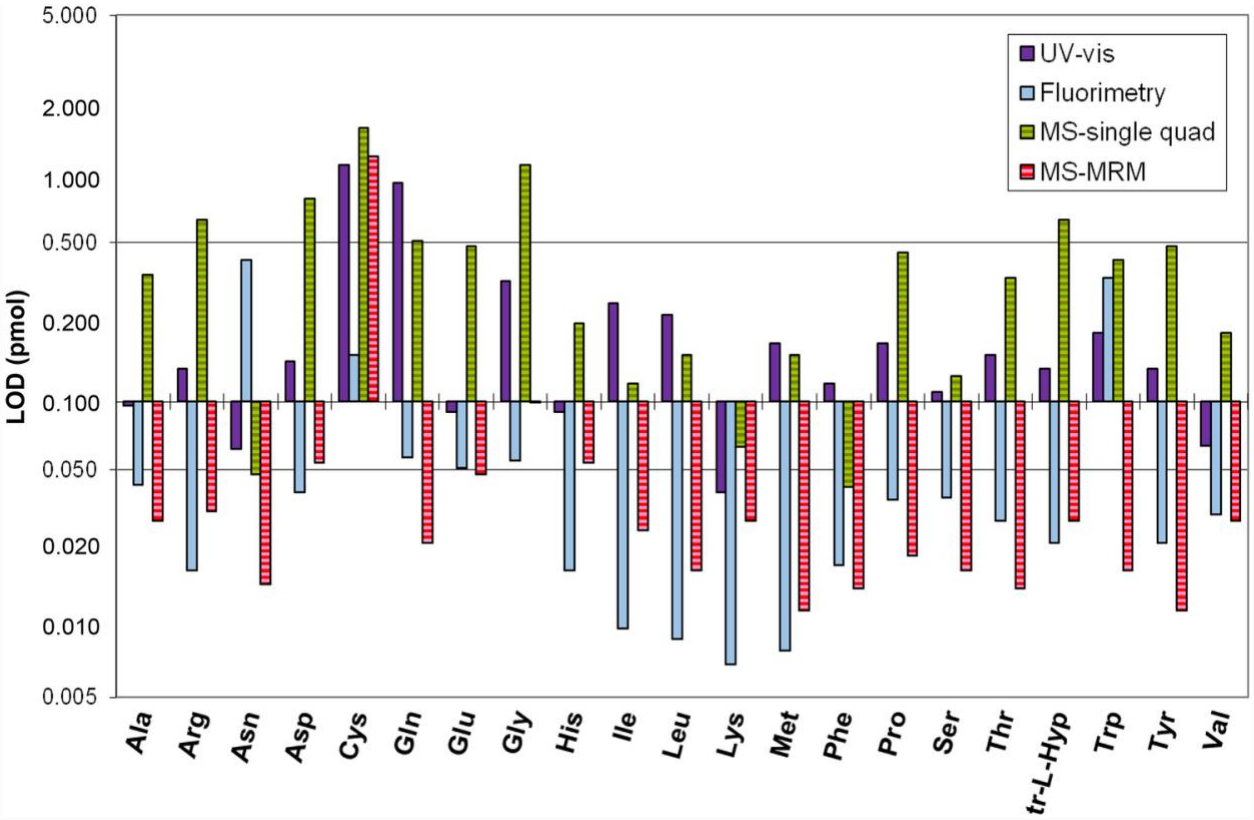

Fig. 2.4 Numerical limits of detection (LODs) for the determination of AQC derivatized amino acids by UHPLC and four different detection modes (note that the *y*-axis is log scale, but the values of the bars in the graph are not). See Table 2.1 and text for full MS experimental information

The LOD results clearly show that "one pot" AQC derivatization does not produce even roughly equivalent results within any one of these four detection modes. Significant sensitivity differences are observed between AQC-AAs. Except for cysteine (which will be discussed subsequently), these differences are not associated to a particular amino acid. The lowest UV AQC-AA LOD is lysine (0.040 pmol) and the highest is cysteine (1.1 pmol), a 27-fold difference. For fluorescence, the lowest LOD is AQC-lysine (0.007 pmol) and the highest is AQC-asparagine (0.062 pmol) excluding AQC-tryptophan and AQC-cysteine (see below), a near

ninefold difference. The best MS-SQ detection was obtained for the AQC-phenylalanine (0.042 pmol) and the highest LOD was with AQC-glycine (1.1 pmol), nearly a 26-fold difference when excluding cysteine. The lowest MRM LOD was observed for AQC-tyrosine (0.012 pmol) and the highest was for AQC-glycine (0.099 pmol), an approximately eightfold difference when excluding cysteine. AQC-glutamine is known to be more difficult to detect than other AQC-AA derivatives, often being omitted in several works.[44,48,55] However, its LOD is quite good in MRM (Fig. 2.4). Placing the *Y*-axis bar at the 0.1 pmol level in Fig. 2.4 clearly shows that UV and SQ LODs are mostly higher than 0.1 pmol while fluorescence and MRM LODs are all lower than that level. But differences between AQC-AA LODs obtained with the same detection mode can reach to over an order of magnitude.

The MRM detection mode with the convenient *m*/*z* 171.0 fragment provides the lowest LODs for the majority of the AQC-AA derivatives. It goes down to 0.3 pmol injected onto the UHPLC column. However, fluorimetry gave comparable and even lower LODs than MS-MRM for approximately half of the AQC-amino acids listed (Table 2.2). Considering the equipment costs, fluorimetry must be viewed as a very appropriate HPLC detector for AQC-AA analysis at the ultra-trace level. When AA concentrations are in the 1 µM range or higher, the simple and classic UV detector is as capable as MS in obtaining reliable quantitative results. Further, the UV LODs were frequently comparable to or better than simple quadrupole MS detection (Fig. 2.4 and Table 2.2).

2.3.3 Poor detection of Cysteine

Far and away, cysteine gave the poorest results, being difficult to detect and having the highest LODs in all detection modes except fluorescence (Fig. 2.4). Cysteine has a known tendency to oxidize to cystine. Approximately, 40% of cysteine can be oxidized in cystine after

24 h in boiling water and at neutral pH.[60] To check for cysteine oxidation, a solution of 100 µM cysteine alone was prepared and derivatized strictly following the protocol used with the amino acid mixtures. Under our conditions, it was not expected that a significant part of the added cysteine had enough time to oxidize. However, a significant AQC-cystine peak was observed soon after derivatization in our chromatographic conditions. It should be noted that AQC-cystine has had both of its amine groups AQC derivatized. Further, it is clear that cysteine does not react well with the AQC reagent and it is possible that reagent decomposition occurs as a result of the reactive thiolate group. At the borate buffer pH, cysteine can form di-anions with its carboxylic acid, –COOH, group and also with its acidic sulfhydryl, –SH, group as shown by Fig. 2.5.[61]

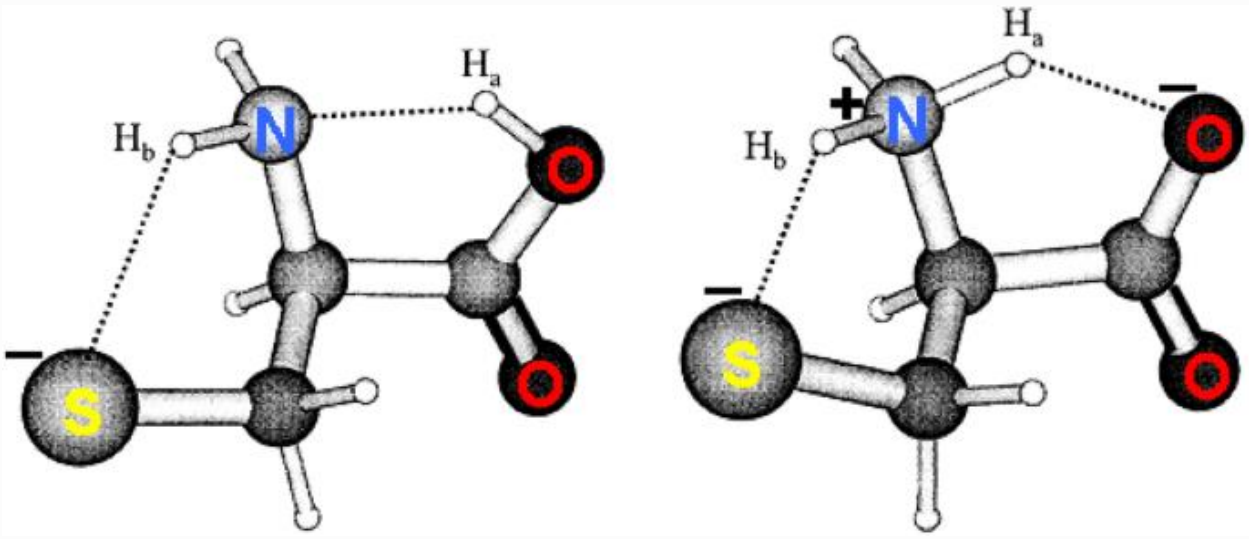

Fig 2.5 Possible amine–sulfur interaction in the two possible anionic forms of cysteine in solution, adapted from ref 61. Cysteine –COOH $pKa_1 = 5.1$, –SH $pKa_2 = 8.1$, borate buffer pH = 9.0

The thiolate ($–S^-$) group is a strong nucleophile that will react much faster with the AQC reagent than any amine group. However, the thiocarbamate formed is not very stable and may decompose during the 15-min 55 °C heating step.[62,63] This thiolate reactivity peculiar to cysteine

could explain the low AQC derivation. If only a fraction of cysteine is derivatized and it also forms some derivatized cystine, this likely explains the low response observed in all detection modes. Further, the standard curves for cysteine were unlike those of all other AQC-AAs in that they were nonlinear and with concurrent poor R^2 values. However good linearity was observed with cystine standards which further indicates that the problem lies with the reactive thiol group and that other competing reactions were occurring.

2.3.4 Low Fluorescence of Derivatized Tryptophan

The AQC-tryptophan derivative shows an abnormally low response only with fluorometric detection, its 0.35 pmol LOD being the highest of all AQC-AAs tested and being higher by an order of magnitude than most other AQC-AA LODs (Table 2.2). It is the only AQC-AA that is better detected by UV (LOD 0.20 pmol) than by fluorimetry (Table 2.2). Native tryptophan also is the only strongly fluorescent amino acid (Fig. 2.2, full green line). Thus, the low LOD of AQC-Trp in fluorescence may not be a coincidence. Molecular modeling of AQC-Trp was performed using the AQC-Trp structure and using the "minimize energy" routine of the software (see Experimental). Figure 2.6 shows the resulting conformation.

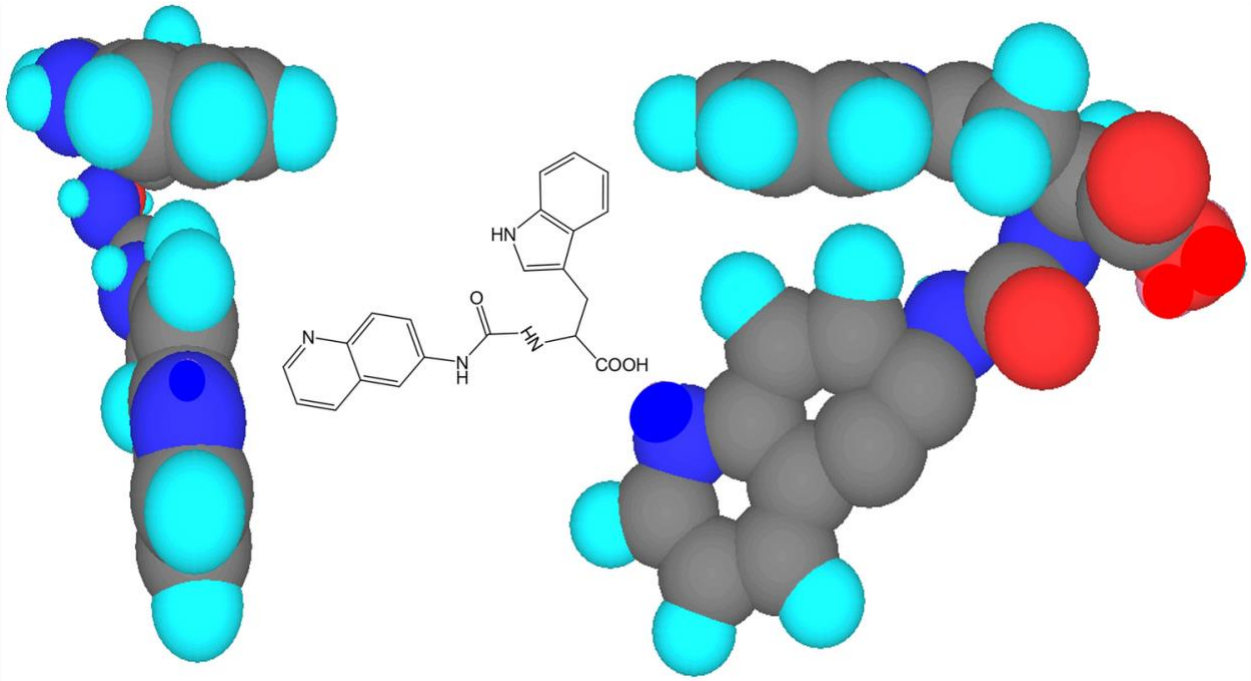

Fig 2.6 Energy minimized 3D modeling of the aminoquinolyl derivatized tryptophan molecule seen on 90° angles. Carbon atoms are *black spheres*; hydrogen, *light blue*; nitrogen, *dark blue*; and oxygen, *red.*

The aminoquinolyl group is at a right angle to the indol tryptophan group, i.e., in the face-to-edge conformation. Such an arrangement of the two fluorescent moieties present in the AQC-tryptophan molecule may result in significant self-quenching, experimentally observed by the intramolecular Dexter effect.[64] We acknowledge that such energy minimization calculations are done for a molecule in vacuo, free of any other external molecular interactions. However, intramolecular quenching and especially tryptophan fluorescence quenching have previously been observed in peptides.[65,66,67]Aside from the MRM detection of AQC-Trp (Table 2.2), fluorescence detection of native tryptophan is the easiest way to detect and to quantitate it at trace levels.

2.4 Conclusions

The AQC derivation of AAs produces relatively easily stable UV absorbent and fluorescent derivatives that are also better detected by MS than their native counterparts. A ubiquitous UV detector can quantitate these AQC-AA derivatives down to a tenth of picomole injected on a 15-cm 4.6 mm column. Fluorimetry and MS/MS detection can go two orders of magnitude lower (Table 2.2 and Fig. 2.4). No particular problems were encountered with AQC-asparagine and AQC-glutamine, two AA derivatives often omitted in published works.[48,55] Possible explanations for the systematic difficult detection of cysteine and lack of usable fluorescence for AQC-tryptophan were proposed. Cysteine may not have complete AQC derivation given competing reactions promulgated by its thiolate group. Also, it may be possible that its target amine moiety is "blocked" by its ionized sulfur group. An intramolecular indole-quinoline quenching may inhibit the AQC-tryptophan fluorescence.

Chapter 3 Altered profiles and metabolism of L- and D-amino acids in cultured human breast cancer cells vs non-tumorigenic human breast epithelial cells

Abstract

N-methyl-D-aspartate (NMDA) receptors, which are widely present in the central nervous system, have also been found to be up-regulated in a variety of cancer cells and tumors and they can play active roles in cancer cell growth regulation. NMDA receptor antagonists have been found to affect cancer cell viability and interfere with tumor growth. Moreover, cancer cells also have been shown to have elevated levels of some D-amino acids. Two human skin cell lines: Hs 895.T skin cancer and Hs 895.Sk skin normal cells were investigated. They were derived from the same patient to provide tumor and normal counterparts for comparative studies. The

expression of specific NMDA receptors was confirmed for the first time in both skin cell lines. Dizocilpine (MK-801) and memantine, NMDA receptor channel blockers, were found to inhibit the growth of human skin cells by reducing or stopping NMDA receptor activity. Addition of D-Ser, D-Ala, or D-Asp, however, significantly reversed the antiproliferative effect on the human skin cells triggered by MK-801 or memantine. Even more interesting was the finding that the specific intracellular composition of a few relatively uncommon amino acids was selectively elevated in skin cancer cells when exposed to MK-801. It appears that a few specific and upregulated D-amino acids can reverse the drug-induced antiproliferative effect in skin cancer cells via the reactivation of NMDA receptors. This study provides a possible innovative anticancer therapy by acting on the D-amino acid pathway in cancer cells either blocking or activating their regulatory enzymes.

3.1 Introduction

N-methyl-D-aspartate (NMDA) receptors are glutamate-gated transmembrane ion channels that play essential roles in synaptic plasticity and memory function.[68] NMDA receptors are so named due to the receptors' very selective synthetic agonist, NMDA. NMDA was synthesized in 1960s and eventually used for determining the pharmacological properties of different excitatory amino acid receptors in the 1990s.[69] The initial investigations on their structures and functions were mostly performed on neuronal NMDA receptors as they are widely distributed in the central nervous system (CNS).[70] NMDA receptors are assembled as heterotetramers with subunits derived from three subfamilies: the GluN1 subunit, the GluN2 subunit (GluN2A, GluN2B, GluN2C, GluN2D), and the GluN3 subunit (GluN3A and GluN3B).[71] The existence of seven distinct subunits of NMDA receptors allows for various combinations of subunit assembly, giving rise to the different biophysical and pharmacological properties and thus the functional

diversity of NMDA receptors.[72] Typically, NMDA receptors consist of two GluN1 subunits and two of the GluN2 subunits or a mixture of GluN2 and GluN3 subunits.[73] GluN1 subunits are obligatory and essential for the receptor assembly, and GluN2A and GluN2B from the GluN2 subfamily are the predominant subunits in the adult CNS.[72] Activation of NMDA receptors requires both the binding of glutamate and a co-agonist, which was presumed to be Gly.[74,75] In late 1990s, D-Ser and its biosynthetic enzyme serine racemase were discovered in mammalian brains.[76-78] The localization pattern of D-Ser and serine racemase coincided more closely with NMDA receptors as compared to Gly.[79-80] Furthermore, selective degradation of D-Ser in neuronal cells by D-amino acid oxidase (DAAO) diminished NMDA receptor-mediated neurotransmission, which established D-Ser as an endogenous co-agonist of NMDA receptors.[81] In addition to D-Ser, D-Ala and D-Asp have also been indicated as co-agonists of NMDA receptors.[75,82-85] It is increasingly recognized that many CNS diseases are linked to the dysfunction of NMDA receptors. Hyperactivity of NMDA receptors has been implicated in Alzheimer's disease (AD) and Huntington's disease,[86-88] while hypofunction of NMDA receptors is believed to contribute to the pathophysiology of schizophrenia.[89]

While the structures, distributions, and functions of NMDA receptors are extensively characterized in neuronal cells, NMDA receptors are also expressed in a variety of non-neuronal cells in the CNS and peripheral tissues, including glial cells, brain endothelial cells, skin, heart, pancreas, lung, bone, kidney and others.[70] Additionally, expression of NMDA receptors subunits has been identified in a myriad of tumor tissues and human cancer cell lines.[70,90-92] The expression of NMDA receptors was found to be higher in prostate cancer compared to the normal prostate cells.[93] NMDA receptors in human keratinocytes were suggested to control epidermal renewal.[94,95] In addition, the growth of human prostate, breast, and pancreatic cancer

cells were stalled when NMDA receptor activity was blocked by an NMDA receptor channel blocker such as, dizocilpine (MK-801) or memantine.[93,96,97] While the precise mechanisms are not established, it is clear that NMDA receptors are involved in cancer cell proliferation and tumor growth, indicating that it could be a promising therapeutic target against cancer.[91] Recently, our group has discovered that the human breast cancer cell line MCF-7 has altered profiles and metabolisms of D- and L-amino acids.[53] MCF-7 cells can not only uptake D-amino acids from growth medium, but also secrete certain D-amino acids into the cell culture medium during proliferation. Most interestingly, intracellular D-Asp, D-Ser, and D-Ala concentrations in MCF-7 cells were significantly elevated compared to the non-tumorigenic breast cell line MCF-10A. Intriguingly, the three D-amino acids which were elevated intracellularly are also co-agonists of NMDA receptors. The question arises as to whether these three D-amino acids are crucial for cancer cell proliferation or can enhance cancer proliferation. Are D-amino acids required for the activation of NMDA receptors during cancer cell proliferation?

To answer these questions, we investigated how D-amino acids are associated with cancer cell proliferation via NMDA receptors. We studied the expression of NMDA receptors in human skin normal (Hs 895.Sk) and skin cancer (Hs 895.T) cells and profiled the NMDA receptors subunit types for the first time. We investigated the effect of NMDA receptor inhibition on cell proliferation for these two human skin cell lines. Moreover, we explored the effect of D-amino acid treatment on human skin cells exposed to NMDA inhibitors. Lastly, we delve into the changes in intracellular amino acid levels in the skin cancer cell line when exposed to an NMDA antagonist.

3.2 Experimental

3.2.1 Materials

Amino acid standards, formic acid, and ammonium formate were obtained from Sigma-Aldrich (Millipore, St. Louis, MO, USA). For ultra-sensitive detection, all amino acids were derivatized using 6-aminoquinolyl-N-hydroxysuccinimide carbamate (AQC) in borate buffer. The derivations were performed using the AccQ·Tag Ultra derivatization kit sold by Waters Corporation (Milford, MA, USA). HPLC–MS grade methanol and water were purchased from Sigma-Aldrich, and ultrapure water was obtained from a Milli-Q water system (Millipore, Bedford, MA, USA). Memantine hydrochloride and (+)-dizocilpine hydrogen maleate (MK-801) were obtained from Sigma. The bicinchoninic acid (BCA) protein assay kit was purchased from Thermo Fisher Scientific (Waltham, MA, USA), and the AlamarBlue® cell viability method (Bio-Rad, Life Science, Hercules, CA, USA) was used to monitor cell proliferation.

3.2.2 Cell lines and culture conditions

The human skin cells were CL-7636 Hs 895.Sk normal fibroblast cells and CRL-7635 Hs 895.T melanoma cancer fibroblast cells obtained from American Type Culture Collection (ATCC, Manassas, VA 20108, USA). The two cell lines came from the same Caucasian, 48 y.o. female. The cells were grown and maintained in Dulbecco's Modified Eagle Medium (DMEM) obtained from ATCC and supplemented with 10% fetal bovine serum (from Millipore Sigma) and 1% penicillin–streptomycin at 37 °C in a humidified atmosphere of 5% CO_2. To investigate the change of intracellular amino acid compositions when exposed to NMDA receptor antagonist, 300 µM and 700 µM of MK-801 were added into the Hs 895.T skin cancer cell plates. Triplicate plates were seeded for each experimental condition. Cells were harvested after

72 h growth and counted by conducting the Trypan blue assay using a hemacytometer (Sigma-Aldrich, St. Louis, MO).

3.2.3 RNS extraction, cDNA synthesis and quantitative real-time PCR (qRT-PCR)

Skin cells were homogenized in 300 µL TriReagent® (Molecular Research Center, Cincinnati, OH) using the Kontes Pellet Pestle (Sigma-Aldrich, St. Louis, MO). Total RNA was then extracted using the Direct-zol™ RNA MiniPrep Kit (Zymo Research, Irvine, CA) according to the manufacturer's instructions with optional on-column DNase treatment. Subsequently, 1 µg total RNA was used as template to synthesize cDNA with the High Capacity cDNA Reverse Transcription Kit (Applied Biosystems, Foster City, CA). Primers for all assays were designed using Primer 3. Melting curve analysis was performed to insure single-product amplification for all primer pairs.

Real time PCR was performed on the BioRad CFX384 Real Time System (BioRad, Hercules, CA) using assays specific to the genes of interest. Each reaction well contained 5 µL of PowerUp™ SYBR Green Master Mix (Applied Biosystems), cDNA equivalent to 20 ng of total RNA and 250 nM each of forward and reverse amplification primers in a final reaction volume of 10 µL. Cycling conditions were as follows: 95 °C for 10 min for polymerase activation, followed by 40 cycles of 95 °C for 15 s and 60 °C for 1 min. Data analysis was performed using CFX Manager software from BioRad, version 3.1. The experimental Cq (cycle quantification) was calibrated against the endogenous control products glyceraldehyde-3-phosphate dehydrogenase (GAPDH) and beta-Actin (ACTB). Samples were analyzed for relative gene expression by the ΔΔCt method.[98]

3.2.4 Protein extraction and Western blot

Western blot analysis was performed by RayBiotech (Peachtree Corners, GA, USA). The procedures are as follows: phosphate-buffered-saline (PBS) containing protease inhibitor was added into cell pellets, followed by resuspension and freeze–thaw for 5 cycles to lyse the cells. The cell lysate was then centrifuged at 20,000 g for 15 min at 4 °C, and the supernatant, which was the cytosolic fraction, was collected for GAPDH as loading control. The pellets were washed with cold PBS, and then lysed in cold radio immune-precipitation assay (RIPA) buffer with protease inhibitor, followed by incubation at 4 °C for 30 min and centrifugation at 20,000 g at 4 °C for 20 min. The supernatant, which contained the solubilized membrane fractions, was then collected. The BCA protein assay kit was used to measure the protein concentration in both cytosolic and membrane fractions. Samples were heated in a boiling water bath for 5 min and SDS–polyacrylamide gel electrophoresis (SDS-PAGE) was performed with 20 µg of total protein for each sample. Then the protein was transferred onto polyvinylidene fluoride (PVDF) membranes (Millipore, MS, USA). The membrane was blocked in 5% non-fat milk/0.1% Tween-20, and then was incubated with primary antibodies at 4 °C overnight with shaking. Commercially available antibodies for NMDAR1 was obtained from Cell Signaling (Danvers, MA, USA), NMDAR2 was purchased from Santa Cruz Biochemicals (Santa Cruz, CA, USA), NMDAR2D was obtained from Thermo Fisher Scientific (Waltham, MA, USA), and anti-GAPDH antibody was provided by (RayBiotech, GA, USA). Each protein band was visualized by ECL chemiluminescent reagent (Millipore, MA, USA).

3.2.5 Cell viability assay

Cell growth and viability were evaluated by the Alamar Blue assay. The Hs 895.Sk normal cells and Hs 895.T cancer cells were washed with FBS-free minimum essential medium

(obtained from Sigma) and plated onto 96 well plates, at a density of 500 cells/well, for 24 h. MK-801 (300 µM) or memantine (700 µM), amino acids (700 µM) and Alamar blue (1:10 dilution following the manufacturer's protocol) were added into the wells. Fluorescence readings were taken at periods representing 24, 48, and 72 h of incubation using FLUOstar Omega multi-mode microplate reader (BMG Labtech, Ortenberg, Germany) at excitation/emission wavelength of 544 nm and 590 nm.

3.2.6 Amino acid extraction and total protein content determination

Amino acids were extracted from the skin cells with 80/20 methanol/water (5% formic acid) v/v by sonication on ice for 30 s. Next the sample was centrifuged at 4 °C and 14,000 rpm for 20 min. The cell precipitate was used to determine the protein concentration by BCA assay. The supernatant was collected, evaporated, and resuspended in 90/10 v/v methanol/water. Then, 100 µM L-norvaline (L-Nva) and 0.1 µM D-norvaline (D-Nva) were added as internal standards. Cell medium was filtered and precipitated by addition of cold acetonitrile, followed by centrifugation, evaporation and resuspension like the cell lysate. All amino acids were analyzed as AQC derivatives as described in our recent articles.[42,52,53]

3.2.7 Amino acid analysis

The HPLC–MS/MS analyses were performed on a LCMS-8040 Shimadzu instrument (Shimadzu Scientific, Columbia, MD, USA) with triple quadrupole spectrometer and electrospray ionization. Two different chiral stationary phases were used. A 2.7 µm superficially porous particle silica 150 × 3 mm Q-Shell (quinine based)[99] and TeicoShell (teicoplanin macrocyclic glycopeptide selector)[100] columns were used. Both columns were obtained from AZYP LLC (Arlington, TX, USA). Gradients were performed on both columns. Solvent A was methanol-ammonium formate 50 mM pH 6 (90/10 v/v) and Solvent B was methanol-ammonium

formate 50 mM pH 4.5 (90/10 v/v) for the Q-shell column. Solvent A was ammonium formate 5 mM pH 4 and Solvent B was pure acetonitrile for the TeicoShell column. Full experimental details for method validation can be found in our previous work.[52]

3.3 Results

3.3.1 Expression of NMDA receptors in HS 895.Sk and Hs 895.T human skin cells

To investigate the expression of NMDA receptors in both human skin cancer (Hs 895.T) and skin normal (Hs 895.Sk) cell lines, RT-PCR was performed for different NMDA receptor subunits: GluN1, GluN2A, GluN2B, GluN2C, and GluN2D. GluN1mRNA (GRIN1) and Glu2D mRNA (GRIN2D) were detected in both skin cancer and skin normal cell lines (Fig. 3.1a). Hs 895.Sk skin normal cells showed higher levels of GRIN1 and GRIN2D compared to Hs 895.T skin cancer cells. Interestingly, no GRIN2A, GRIN2B, and GRIN2C mRNA were detected in either of the skin cell lines. The expression of NMDA receptor subunit proteins (GluN1 and GluN2A-2D) in both cell lines was further investigated by Western blot analysis. As shown in Fig. 3.1b, membrane protein extracts from both cell lines recognized a band of approximately 120 kDa corresponding to the GluN1 subunit, and a band of 165 kDa corresponding GluN2D subunit. No GluN2A-2C proteins were detected in either of the skin cell lines (data not shown). Using RT-PCR and western blot data, we confirmed the expression of GluN1 and GluN2D NMDA receptor subunits in both Hs 895.T and Hs 895.Sk human skin cell lines.

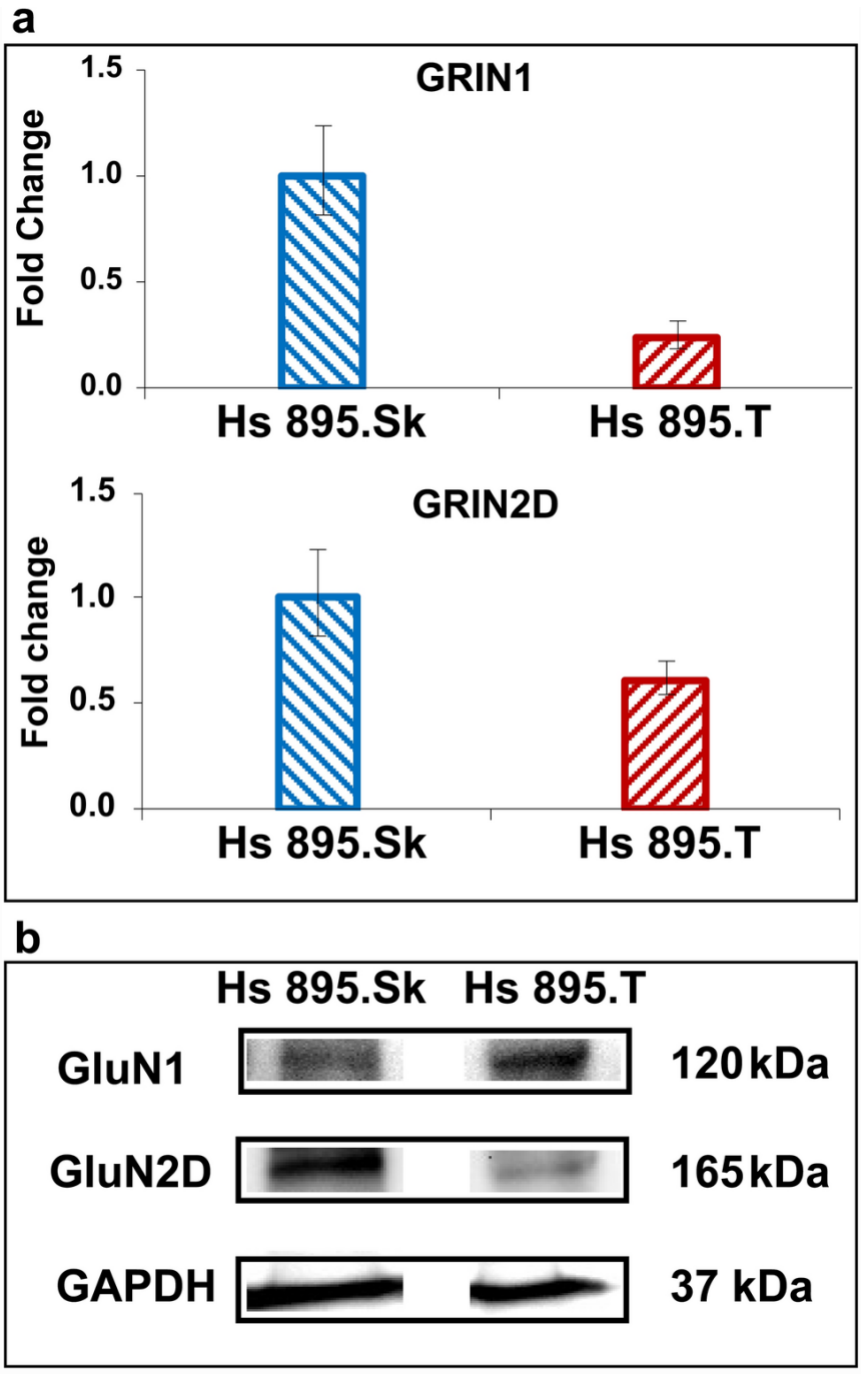

Fig 3.1 Expression of NMDA receptors in Hs 895.Sk skin normal and Hs 895.T skin cancer cells. **a)** qRT-PCR analysis showed the expression of GRIN1 and GRIN2D, and **b)** Western blot analysis confirmed the expression of GluN1 and GluN2D proteins in both human skin normal and skin cancer cell lines

3.3.2 Effect of NMDA receptor blockade on HS 895.T human skin cancer cell proliferation

Cell viability after the treatment of NMDA receptor antagonists was evaluated by the Alamar blue assay. The advantage of this assay is the ability to continuously monitor cell proliferation during the culture period without harm to the cells.[101] Cell growth of Hs 895.T skin cancer cells was examined at 24 h, 48 h, and 72 h upon the addition of NMDA receptor antagonists, MK-801 or memantine. MK-801 and memantine significantly reduced Hs 895.T skin cancer cell growth in a concentration-dependent manner (Fig. 3.2). MK-801 inhibited the growth of Hs 895.T cancer cells with IC_{50} at 72 h of ~ 1200 µM (Fig. 3.2a), while memantine produced dramatic decreases in cell viability with IC_{50} at 72 h of ~ 400 µM (Fig. 3.2b). Thus, inhibition of NMDA receptor activity, by adding channel blocker drugs inhibited cell proliferation, with memantine being more effective compared to MK-801 for Hs 895.T skin cancer cells.

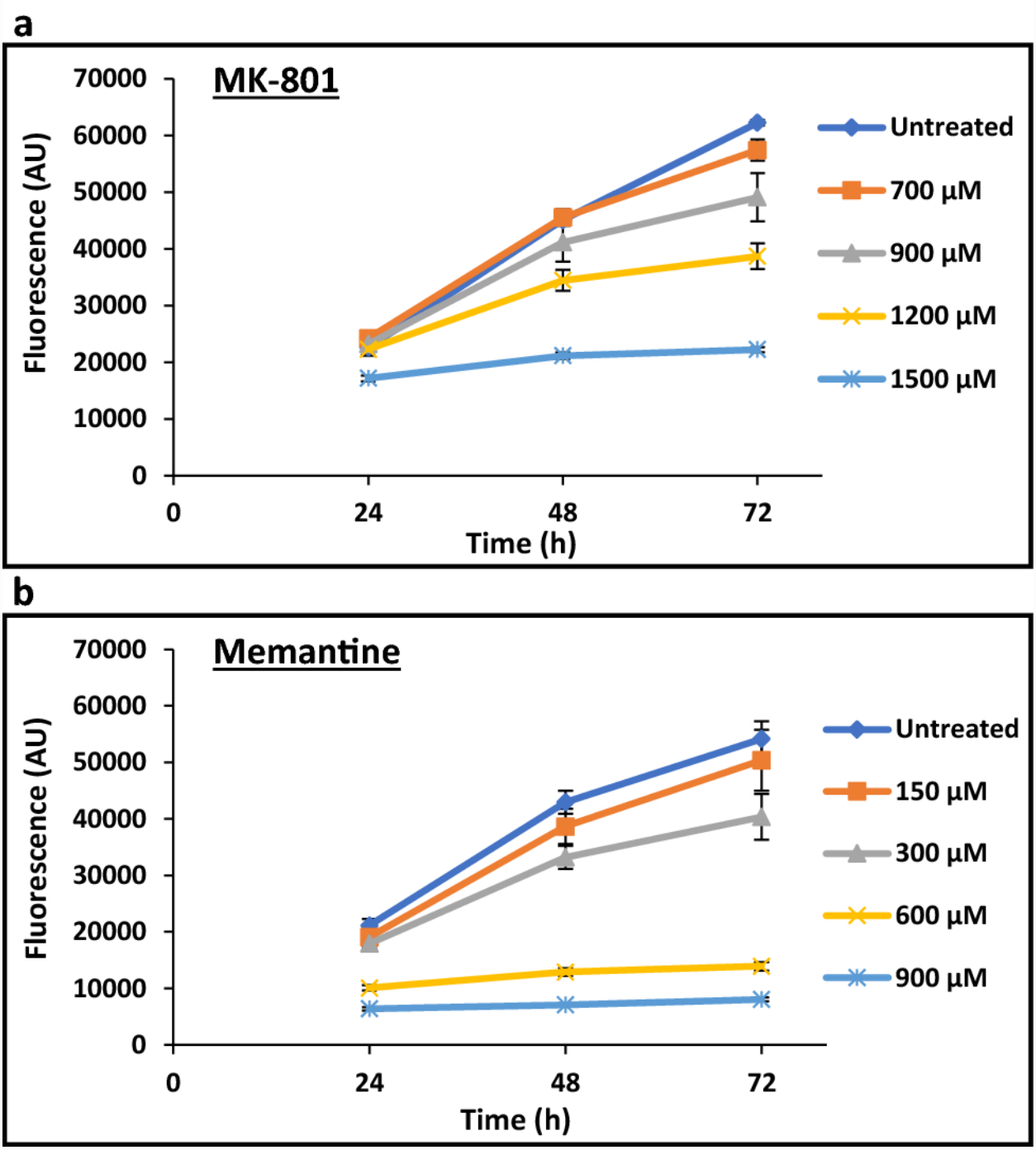

Fig 3.2 Effect of NMDA antagonists on the growth of Hs 895.T skin cancer cells. Reduction in cell viability of Hs 895.T cells depicted as estimated cell growth (mean ± SEM) produced in the presence of different concentration (µM) of NMDA receptor antagonists **a)** MK-801 and **b)** memantine after 24 h, 48 h, and 72 h of treatment.

3.3.3 Effect of D-amino acids addition on cell proliferation of Hs 895.Sk and Hs 895.T cells exposed to NMDA receptor agonists

Hs 895.T and Hs 895.Sk were grown in FBS-free minimum essential medium. Cell viability measurements were taken at 3 h, 24 h, 48 h, and 72 h after the addition of MK-801(700 µM) or memantine (300 µM) and D-amino acids (700 µM). For the 3 h measurement, the untreated and the corresponding experimental groups (treatment with antagonists and amino acids) showed the same fluorescence reading (Fig. 3.3 a–d), indicating the initial condition for all the groups were the same. After 48 h and 72 h, significant growth inhibition was observed for both Hs 895.T and Hs 895.Sk cells with MK-801 or memantine treatment compared to the untreated cells (Fig. 3.3 a–d). No significant growth differences were observed for Hs 895.T and Hs 895.Sk cells grown in the minimum essential medium with the addition of D-Ser, D-Asp, or D-Ala (see Fig. S2). However, when D-amino acids were added to the cells exposed to either MK-801 or memantine, significant rescue effects were observed. Figure 3.3a and b showed the growth curves of Hs 895.T skin cancer cells subject to MK-801 and memantine treatment, respectively. D-Ser, D-Asp, or D-Ala reduced the growth inhibition of Hs 895.T cells caused by NMDA receptor antagonists. Similarly, D-Ser, D-Asp, or D-Ala also recovered the growth of Hs 895.Sk skin normal cells when treated with MK-801 and memantine, respectively (Fig. 3.3 c, d), but the magnitude of the rescue was less substantial.

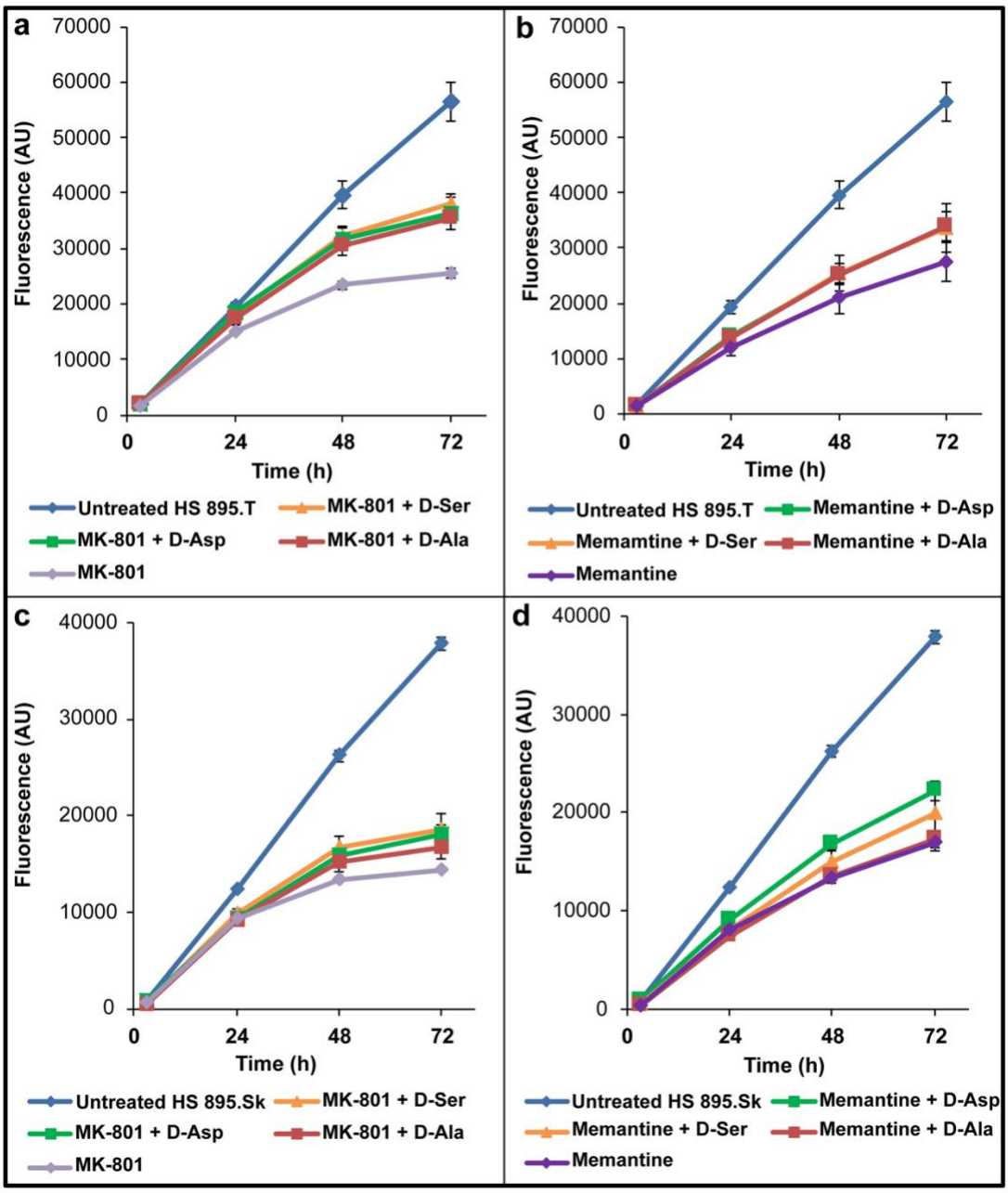

Fig 3.3 Effect of D-amino acids on Hs 895.Sk and Hs 895.T cell proliferation and viability. Addition of D-Ser, D-Asp, or D-Ala appeared to reverse the antiproliferative effect caused by NMDA antagonists in **a)** Hs 895.T skin cancer cells with MK-801 treatment, **b)** Hs 895.T skin cancer cells with memantine treatment, **c)** Hs 895.Sk skin normal cells with MK-801 treatment, and **d)** Hs 895.Sk skin normal cells with memantine treatment

3.3.4 Intracellular amino acid levels in Hs 895.T skin cancer cells exposed to MK-801

Intracellular D- and L-amino acid levels were analyzed in the Hs 895.T skin cancer cells grown in FBS-free minimum essential medium subjected to MK-801 treatment. Figure 3.4 shows the change in the levels of L-amino acids, D-amino acids, and %D-amino acids in Hs 895.T skin cancer cells compared to the untreated cells. Intracellular L-amino acid levels were decreased in Hs 895.T cells exposed to 300 µM and 700 µM of MK-801(Fig. 3.4a). Intracellular D-amino acid levels were slightly decreased or remained constant, except for D-Ala, which showed a dramatic increase in Hs 895.T cells exposed to MK-801 (Fig. 3.4b). %D-Ala was four-fold higher in Hs 895.T cells exposed to 300 µM MK-801 compared to the control, while greater than five-fold higher when treated with 700 µM MK-801 (Fig. 3.4c). A similar but less pronounced effect was obtained with Asp. The %D-Asp was nearly three times higher in cells exposed to 700 µM of MK-801 compared the control (only 150% higher with 300 µM MK-801) (Fig. 3.4c). Much smaller or non-significant changes were observed for the other amino acids as shown in Fig. 3.4.

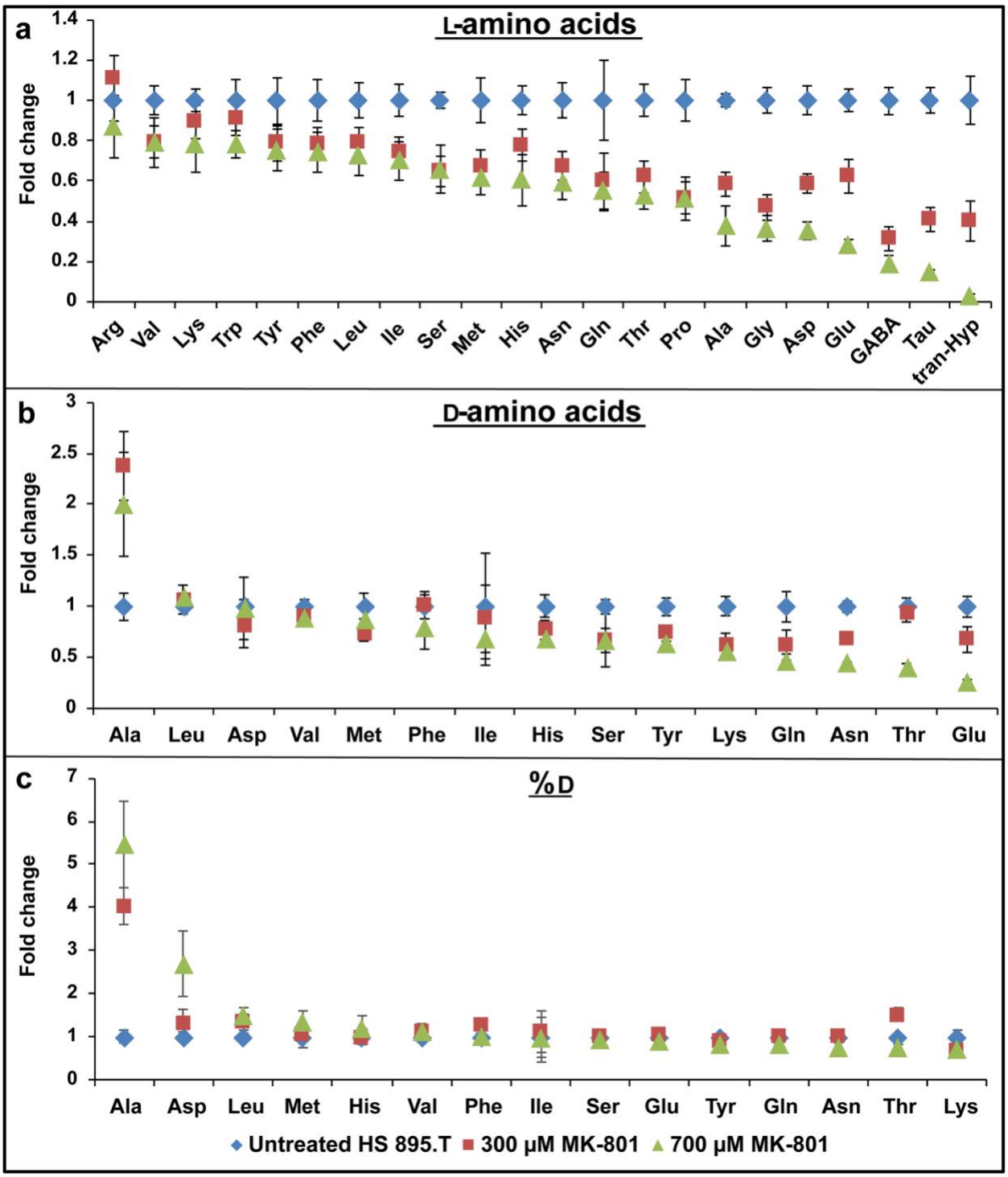

Fig 3.4 Changes of intracellular amino acid levels in Hs 895.T skin cancer cells after MK-801 treatment. **a)** Fold change of L-amino acids compared to the control, **b)** Fold change of D-amino acids compared to the control, **c)** Fold change of %D values compared to the control

3.4 Discussion

NMDA receptors in the CNS are well-characterized and known to play essential functions in neurodegenerative diseases. However, recent studies have demonstrated that non-neuronal cells including cancer cells also express functional NMDA receptors. Indeed, in this study, the expression of NMDA receptors was confirmed for the first time in Hs 895.T human skin cancer cells and Hs 895.Sk skin normal cells, which were derived from the same patient to provide tumor and normal counterparts for comparative studies. Furthermore, the subunit types of NMDA receptors were examined, and both skin cell lines expressed GluN1 and GluN2D subunits of NMDA receptors. Functional NMDA receptors require both GluN1 subunits (necessary for calcium conductivity of the channel) and Glu2 and/or Glu3 subunits (which determine the pharmacological responses of the receptors).[71] GluN1 subunits are widely identified in a variety of neuronal and non-neuronal cells, but the presence of Glu2D subunits is limited to a small numbers of cells in selected brain regions, i.e., diencephalon and brainstem.[102] In addition, the expression of GluN2D subunits in the brain is found to change substantially during development. GluN2D were present at high levels in the embryonic brain, but dropped markedly after birth.[103,104] Interestingly, a recent study has reported the presence of Glu2D subunits in 11 cancer cell lines, including human rhabdomyosarcoma/medulloblastoma, neuroblastoma, thyroid carcinoma, lung carcinoma, astrocytoma, multiple myeloma, glioma, colon adenocarcinoma, T cell leukemia cells, breast carcinoma, and colon adenocarcinoma, as well as in normal human skin fibroblasts.[90] It is believed that the re-expression of GluN2D subunits in cancer cells may aid their proliferation.[90]

MK-801, memantine, and ketamine, which are known to be NMDA receptor channel blockers, were found to limit the growth of several types of human cancer cells.[96,97,105,106] In this study, we have observed similar results in human skin cancer Hs 895.T and skin normal Hs 895.Sk cells. Both MK-801 and memantine inhibited proliferation and decreased viability of the two skin cell lines examined, with memantine being the more effective agent. The results obtained here corroborate previously published results on human breast cancer cells.[96] NMDA receptors play active roles during the human skin cancer cell proliferation. Recent reports revealed that blockage of NMDA receptor activity disrupted the extracellular signal-regulated kinase (ERK) pathway in lung and colorectal cancer cells.[106,107] Such a disruption of the ERK pathway was achieved by suppressing the expression and activity of growth and transcription factors which control the proliferation of cancer cells.[106,107] These findings revealed the possible mechanism of the antiproliferative action caused by NMDA receptor antagonists. However, it is not clear whether the anti-proliferative effect caused by NMDA receptor blockage on the two human skin cell lines in this study was due to the disruption of ERK pathway. Another study has shown that D-Asp regulates production of testosterone in rats through NMDA receptors and the ERK pathway.[108] Additionally, it has been postulated that D-Asp may enhance spermatogonia propagation via NMDA activation of Akt and ERK pathways, which could increase PCNA and Aurora B protein expression.[109] These studies show further links between non-neuronal NMDA receptors and various other proteins.

A recent study showed that N-methyl-D-aspartate, a synthetic and specific agonist of NMDA receptors, reversed the MK-801 blockage of these receptors and restored their receptor currents.[110] As D-Ser, D-Asp, and D-Ala are endogenous agonists of NMDA receptors, we investigated whether these D-amino acids would restore the activity of NMDA receptors under

conditions of antagonist exposure. Indeed, the cell viability studies showed that the growth of Hs 895.T and to a lesser extent Hs 895.Sk cells was rescued by the addition of these D-amino acids when exposed to MK-801 or memantine. Thus, D-Ser, D-Asp, or D-Ala appear to be capable of reversing the anti-proliferative effect on human skin cells caused by NMDA blockage. Furthermore, we analyzed the change of intracellular amino acid composition in Hs 895.T skin cancer cells treated with MK-801. Interestingly, Hs 895.T skin cancer cells showed significant increases in D-Ala and D-Asp when exposed to MK-801 compared to the untreated cells. As the growth medium (FBS-free minimum essential medium) for this experiment does not contain D-Ala and D-Asp, these D-amino acids could possibly be generated endogenously by the skin cancer cells when exposed to MK-801 to activate NMDA receptors. This endogenous production of D-amino acids implicates the presence of possible undiscovered D-amino acid racemases or other methods of D-amino acid production in skin cancer cells.

3.5 Conclusions

We have confirmed the expression and subunit types of NMDA receptors in Hs 895.T human skin cancer and Hs 895.Sk skin normal cells for the first time. Blockage of NMDA receptors by MK-801 or memantine significantly reduced or stopped the cell growth for both human skin cell lines. Addition of D-Ser, D-Asp, or D-Ala appeared to restore the cell growth from the antiproliferative effect of MK-801 and memantine. Finally, Hs 895.T skin cancer cells exhibited higher percent values of D-Ala and D-Asp when treated by a NMDA receptor inhibitor, MK-801. This work indicates the possible endogenous production of D-Ala, D-Asp and D-Ser by skin cancer cells in the presence of NMDA receptor inhibitors. If skin cancer cells can reverse the antiproliferative effects of NMDA receptor inhibitors by endogenous generation of the appropriate D-amino acids, a promising new anticancer therapy could be envisaged. The

regulatory enzymes involved in D-amino acid pathways in cancer cells could be identified and targeted, either to inhibit the activity of enzymes that generate D-amino acids (e.g., racemases), or enhance the activity of enzymes that degrade D-amino acids (e.g., DAAO).

Chapter 4 Enhanced carboxypeptidase efficacies and differentiation of peptide epimers

Abstract

Carboxypeptidases enzymatically cleave the peptide bond of C-terminal amino acids. In humans, it is involved in enzymatic synthesis and maturation of proteins and peptides. Carboxypeptidases A and Y have difficulty hydrolyzing the peptide bond of dipeptides and some other amino acid sequences. Early investigations into different N-blocking groups concluded that larger moieties increased substrate susceptibility to peptide bond hydrolysis with carboxypeptidases. This study conclusively demonstrates that 6-aminoquinoline-N-hydroxysuccimidyl carbamate (AQC) as an N-blocking group greatly enhances substrate hydrolysis with carboxypeptidase. AQC addition to the N-terminus of amino acids and peptides also improves chromatographic peak shapes and sensitivities via mass spectrometry detection. These enzymes have been used for amino acid sequence determination prior to the advent of modern proteomics. However, most modern proteomic methods assume that all peptides are comprised of L-amino acids and therefore cannot distinguish L-from D-amino acids within the peptide sequence. The majority of existing methods that allow for chiral differentiation either require synthetic standards or incur racemization in the process. This study highlights the resistance of D-amino acids within peptides to enzymatic hydrolysis by Carboxypeptidase Y. This stereoselectivity may be advantageous when screening for low abundance peptide stereoisomers.

4.1 Introduction

Carboxypeptidases sequentially hydrolyze peptide bonds by removing single amino acids from the C-terminus of peptides.[111-113] In humans these enzymes perform a role in post-translational modification and enzymatic synthesis of proteins as well as regulating biological processes through the biosynthesis of neuroendocrine peptides such as insulin.[114-116] Prior to the advent of modern proteomics, these enzymes were used for amino acid sequence determinations of peptides.[117] Two carboxypeptidases commonly used in peptide sequencing were Carboxypeptidase A (CPA) and Carboxypeptidase Y (CPY). CPA is a Zn^{2+} dependent metallo-carboxypeptidase and functions best at weakly basic pHs.[118-120] CPA hydrolyzes most proteogenic amino acids from peptides but cannot hydrolyze C-terminal amino acids which contain ionizable or cyclic side chains[121,122] such as basic amino acids or proline residues.[123] To address this, treatment with a cocktail of complementary enzymes is often required when using CPA.[124] CPY is a serine carboxypeptidase which functions best at weakly acidic pHs.[125,126] CPY is able to hydrolyze all proteogenic amino acids from the C-terminus of peptides at different rates depending on the amino acid side chain.[127] Additionally, it was shown to cleave C-terminal amides and esters to release ammonia and alcohols respectively.[128-131]

The amidase and esterase activity of CPY broadens its applicability for hydrolyzing peptides and C-termini modified peptides. Consequently, CPY was often the enzyme of choice for peptide sequence analysis.[117,129] Modern proteomic methods can avoid this enzymatic process by performing an initial tryptic digest of target molecules and subsequently using LC high resolution mass spectrometry (MS) or MS-MS to identify fragments.[132] Such studies involving proteins and peptides assume that both are composed entirely of L-amino acids. However, the realization that D-amino acid containing epimer peptides may be more prevalent

and relevant in a variety of biological systems and certain diseases than previously thought, will require different analytical approaches since the exact masses of epimers are identical.[133,134] Further, locating and identifying the D-amino acid in the epimer sequence can be problematic. Despite existing methods such as ion mobility MS, which utilizes the differences in epimier conformation in the MS, a synthetic all L-amino acid standard is still needed for epimer differentiation.[135] More recently, enzymatic methods for chiral differentiation with aminopeptidases have achieved success in discovering new biological D-amino acid containing peptides (DAACP) in this manner.[136]

Despite carboxypeptidases having capabilities to hydrolyze most proteogenic amino acids from peptides, complete hydrolysis of underivatized substrate down to the N-terminal amino acid with these enzymes often is not possible.[117] To alleviate this problem N-derivatizing groups have been used to "enlarge" the short peptides and thereby enhancing enzymatic hydrolysis with CPY. Previous work on CPY ranked N-acetyl, N-furylacrylolyl, N-benzoyl, and N-carbobenzoxy (Cbz) functionalized peptides in order of increasing susceptibility to catalytic hydrolysis of peptide bonds.[117,136] Considering the nature of these N-blocking groups, it can be seen that increasing the size, aromaticity and/or hydrophobicity of the N-derivatization group improves the catalytic effectiveness of carboxypeptidases. When compared to the aforementioned N-terminus moieties, 6-aminoquinolyl-N-succimidyl-carbamate (AQC) supersedes them all in size, aromaticity and hydrophobicity making it a prime candidate for improving carboxypeptidase hydrolysis. AQC-derivatization is fast, reliable, and has a high percent yield.[40,42,138-140] Conversely, Cbz derivatization requires C-terminus protection and subsequent reflux at higher temperatures, but has poorer yields compared to AQC-derivatization.[139] It would be beneficial to have a faster and easier N-derivatization method, such as AQC, which also could improve

carboxypeptidase efficacy relative to those previously studied. However, no attempts have been made in investigating the compatibility of AQC as an N-terminus moiety with carboxypeptidases A and Y in improving hydrolysis.

As the standard N-terminal derivatization agent for amino acid quantitation,[42,140] the addition of an AQC group to amino acids and peptides can significantly improve limits of detection (LODs) across multiple modes of detection. In optical detection, AQC can function as a UV chromophore[141-143] and fluorophore.[138,140] In mass spectrometry it is an easily ionizable group in the positive ion mode which increases sensitivity in electrospray ionization (ESI)-MS,[50] MS/MS [53,54,144,145] and MALDI-ToF.[79] Further, substantial improvements in extractions and separations on reversed phase stationary phases are known to result from the addition of a hydrophobic AQC group.[40,140,143] It would be ideal if these beneficial attributes of AQC-derivatization could be transposed to the analysis of low abundance peptides.

The focus of this study was to investigate the possible benefits of AQC-derivatization on carboxypeptidase efficacy for peptides and to enhance the catalytic hydrolysis of peptide bonds. Further, enhanced detection and identification of peptide N-terminal amino acids and/or any unhydrolyzed peptides or epimers are considered. In order to test whether carboxypeptidases can be used to identify D-amino acids in peptides and proteins, the substrate specificity of carboxypeptidases A and Y also was examined using synthetic penta-peptides containing D-amino acid moieties. Such enzymatic techniques for identifying epimers across all proteinogenic amino acids may prove to be essential as our understanding of the biological relevance of D-amino acid containing peptides continues to evolve.

4.2 Experimental

4.2.1 Materials and Instrumentation

All peptides, enzymes and centrifugal filters (3 kDa) were from purchased from Sigma Aldrich (MilliporeSigma, Saint-Louis, MO, USA). The AminoTag and AccQ-Tag Ultra "3X" derivatization kits were obtained from AZYP LLC (Arlington, TX, USA) and Waters (Milford, MA, USA) respectively. A Shimadzu Prominence HPLC unit with an 8040 MS detector was used for all sample analyses.

4.2.2 AQC-derivatization for peptides

3.0 mM of the peptide sample was prepared from powder in 90:10% (v/v) water: methanol (CH_3OH) (sample solvent). The borate buffer and AQC-reagent were used at concentrations provided in the Waters kit and prepared according to the user manual. The borate buffer received should be 0.2 mM and the AQC-reagent 10 mM if reconstituted according to the user manual. Peptide samples were mixed with AQC reagent at a 10:20:70% (v/v/v) of sample: AQC reagent: borate buffer and a separate underivatized peptide control was mixed at the same ratio of sample: acetonitrile (CH_3CN): borate buffer. Blank controls consisted of sample solvent: CH_3CN: borate buffer, and AQC-blank controls consisted of sample solvent: AQC reagent: borate buffer, all at 10:20:70% (v/v/v). Both derivatized and underivative peptides will be at 300 μM following this procedure. All peptide samples were heated in the oven for 25 min at 55 °C. After heating, samples were left at room temperature for a minimum of 6 h before proceeding.

4.2.3 Carboxypeptidase-catalyzed hydrolysis and sample preparation

For CPY-catalyzed hydrolysis, separate solutions were prepared with 50 mM 2-(*N*-morpholino)ethanesulfonic acid hydrate (MES) and 0.1 M NaCl adjusted to pHs 4.5 or 5.5 with

HCl and to pH 6.8 with 1 M NaOH. Enzyme solutions were prepared with 1.6 mg of lyophilized CPY in 800 μL of MES solution. For CPA-catalyzed hydrolysis a solution of 25 mM Tris • HCl and 0.5 M NaCl was prepared and buffered to pH 7.5 with 1 M NaOH. 90 μL of CPA suspension was dissolved in 710 μL of 1 M NaCl to yield the CPA solution. 25 mM ammonium formate in CH_3OH was prepared as a post hydrolysis quenching solution to prevent microbial browth. When preparing the samples, 25 μL of 300 μM peptide solution was pipetted into 700 μL of MES buffer for CPY (Tris • HCl buffer for CPA) and topped off with 25 μL of enzyme solution 3.3:92.4:3.3% (v/v/v) in 1.5 mL Eppendorf tubes and vortexed well. All samples had respective no-enzyme controls with 25 μL of 300 μM peptide sample added into 725 μL of buffer. All of the peptides used in the stereoselective studies were assayed in pH 5.5 MES. All tubes were placed in 37°C water bath for 24 h. After 24 h the samples were removed from the water bath and 500 μL of the solution was pipetted into Amicon centrifugal filters (3 kDa). Enzyme removal was achieved by spinning down the solution at 14,000 rpm for 12 min at 4°C. Shorter time study samples were treated in identical fashion with hydrolysis time as the only variable. Sampling times were 0, 5, 10, 15, 20, 30, and 45 min. The filtrate was mixed with the 25 mM ammonium formate CH_3OH quenching solution at a 1:1 ratio in a sample vial and subsequently analyzed on LC-MS.

4.2.4 HPLC-MS separation conditions

The samples were separated into three groups and analyzed with three different mobile phase gradients. The first method was used for smaller and neutral peptides listed in Table 4.1, the second was used for larger neutral peptides shown in Table 4.2, Table 4.3 and the third was used for larger peptides with ionizable side chains shown in Table 4.3.

Table 4.1 CPA- and CPY-catalyzed hydrolysis results of dipeptides and their AQC derivatized counterparts. Confirmation of N-terminus amino acid indicates that the enzyme has traversed and hydrolyzed the entire length of the peptide.

Dipeptides	% hydrolysis of reactant		Appearance of N-terminal AA	
	CPA[a]	CPY[b]	CPA	CPY
Ala-Leu	0	0	No	No
AQC-Ala-Leu	100	100	Yes	Yes
Leu-Leu	53 ± 6	57 ± 7	Yes	Yes
AQC-Leu-Leu	100	100	Yes	Yes
Phe-Ala	7.0 ± 0.8	16 ± 2	Yes	Yes
AQC-Phe-Ala	100	100	Yes	Yes
Val-Met	1.4 ± 0.2	18 ± 2	Yes	Yes
AQC-Val-Met	100	100	Yes	Yes
Val-Tyr	50 ± 6	12 ± 1	Yes	Yes
AQC-Val-Tyr	100	100	Yes	Yes
Val-Pro	0	0	No	No
AQC-Val-Pro	0	100	No	Yes
Val-Ser	0	100	No	Yes
AQC-Val-Ser	68 ± 8	100	Yes	Yes
Gly-Tyr	88 ± 11	1.6 ± 0.2	Yes	No
AQC-Gly-Tyr	100	100	Yes	Yes
Asp-Asp	0	0	No	No
AQC-Asp-Asp	0	15 ± 2	No	Yes
Asp-Asp[c]	0	0	No	No
AQC-Asp-Asp[c]	0	85 ± 10	Yes	Yes
Asp-Asp[d]	0	0	No	No
AQC-Asp-Asp[d]	0	100	No	Yes

[a]: enzyme buffer pH 7.5, [b]: enzyme buffer pH 6.8, [c]: enzyme buffer pH 5.5, [d]: enzyme buffer pH 4.5
% of reactant hydrolyzed: 0% ≤ red < 50 % ≤ orange < 90% ≤ green ≤ 100%

Table 4.2 CPA- and CPY- catalyzed hydrolysis results of tripeptides and their AQC derivatized counterparts. Confirmation of N-terminus amino acid indicates that the enzyme has traversed and hydrolyzed the entire length of the peptide.

Tripeptides	% hydrolysis of reactant		Appearance of N-terminal AA	
	CPA[a]	CPY[b]	CPA	CPY
Ala-Gly-Gly	1.6 ± 0.2	1.0 ± 0.1	No	No
AQC-Ala-Gly-Gly	2.0 ± 0.2	17 ± 2	No	No
AQC-Ala-Gly-Gly[c]	0	100	No	Yes
Thr-Val-Leu	100	100	No	No
AQC-Thr-Val-Leu	100	100	Yes	Yes
Arg-Gly-Asp[d]	0	0	No	No
AQC-Arg-Gly-Asp[d]	0	100	No	Yes
AQC-Gly-Gly-His	0	30 ± 4	No	Yes
AQC-Gly-Gly-His[c]	0	15 ± 2	No	Yes
Lys-Tyr-Lys	25 ± 3	53 ± 6	No	No
AQC-Lys-Tyr-Lys	100	100	Yes	Yes
AQC-Lys-Tyr-Lys[c]	0	100	No	Yes

[a]: enzyme buffer pH 7.5, [b]: enzyme buffer pH 6.8, [c]: enzyme buffer pH 5.5, [d]: enzyme buffer pH 4.5
% of reactant hydrolyzed: 0% ≤ red < 50 % ≤ orange < 90% ≤ green ≤ 100%

Table 4.3 CPA- and CPY- catalyzed hydrolysis results of pentapeptides and their AQC derivatized counterparts. Confirmation of the N-terminus amino acid indicates that the enzyme has traversed and hydrolyzed the entire length of the peptide for that sample.

Larger Peptides	% hydrolysis of reactant		Appearance of N-terminal AA	
	CPA[a]	CPY[b]	CPA	CPY
$(Ala)_5$	100	100	No	No
AQC-$(Ala)_5$	100	100	Yes	Yes
Enkephalin	100	100	No	No
AQC-Enkephalin	10 ± 1	89 ± 11	No	Yes
AQC-Enkephalin[c]	0	100	No	Yes

[a]: enzyme buffer pH 7.5, [b]: enzyme buffer pH 6.8, [c]: enzyme buffer pH 5.5, [d]: enzyme buffer pH 4.5.
Enkephalin (Leu)-YGGFL pentapeptide
% hydrolysis of reactant: 0% ≤ red < 50 % ≤ orange < 90% ≤ green ≤ 100%

All three methods used the same mobile phases. Mobile phase A was 0.1% formic acid in water and mobile phase B was 0.1% formic acid in acetonitrile. Separation column used was a Supelco C-18 Ascentis 90 Å (150 mm × 3.0 mm, 2.7 μm superficially porous particles). Gradient conditions for the first method were: 0–5 min hold at 5%B, 5–20 min from 5 to 38%B, 20–25 min hold at 38%B, 25–30 min hold at 5%B. Gradient conditions for the second method were: 0–2 min hold at 5%B, 2–7 min hold at 12%B, 7–20 min from 12 to 40%B, 20–25 min hold at 40%B, 25–30 min hold at 5%B. Gradient conditions for the third method were: 0–3 min hold at 15%B, 3–12 min from 25 to 50%B, 12–14 min hold at 50%B, 14–20 min hold at 15%B. Flow rate was 0.4 mL/min for all gradients.

4.2.5 Detection and data analysis in MS

Each AQC group attached give a *m*/*z* increase of 170 from the underivatized peptide when singly charged in the positive ion mode. Single ion monitoring (SIM) in the positive ion mode on LC-MS was used to assess catalytic progress. The detector response for peptides will be affected by the charge acquired during the ESI process. All possible charge states for peptides with ionizable side chains were monitored and events that produced the strongest signals were selected to represent their respective peptides. Mass spectrometry conditions for the desolvation line temperature was 250 °C and heat block temperature was 400 °C. Nebulizing gas flow was 3 L/min and drying gas flow was 15 L/min.

Product and starting material peaks were confirmed with chromatographic standards. Identity of intermediates with positively charged side chains can be further confirmed by their multiple charged states with matching retention times. Peak areas of the reactant were integrated using Shimadzu LabSolutions Insight software. Percent of reactant hydrolyzed was calculated as

shown in equation (1) with *A* representing the integrated peak area. The results are reported in Table 4.1 as well as confirmation of N-terminus amino acid if detected. The criteria for appearance of N-terminal amino acid shown in Table 4.1, Table 4.2 is the appearance of a peak above 10σ where σ is the baseline noise of the MES control. Standard deviations in all tables are from experimental hydrolyses in triplicate. The mass spectrum average of events in the peak must also correspond to the mass of the expected N-terminal amino acid for confirmation in the tables.

$$\%\ hydrolysis = \left(1 - \frac{A_{control} - A_{CPY}}{A_{control}}\right) \times 100 \quad (1)$$

4.3 Results and discussion

4.3.1 CPA and CPY-catalyzed hydrolysis of peptides with aliphatic and polar amino acid side chains

Table 4.1 shows that comparable results are obtained for CPA and CPY which partially hydrolyzed the peptide bond of Ala-Leu, Leu-Leu, Phe-Ala and Val-Met. Results for these underivatized dipeptides with aliphatic side chains indicate low hydrolysis with only 57±7% as the highest amount of peptide starting material depleted. Susceptibility of peptides to enzyme catalyzed hydrolysis significantly improved with the addition of an AQC-N-terminus moiety, as compared to the underivatized peptide (Table 4.1). After CPY treatment, no starting material was detected for AQC-peptides with aliphatic side chain amino acids, and the N-terminal AQC-amino acid was easily and quantitatively detected. When hydrolyzing peptides with polar side chain amino acids, Table 4.1 also shows that CPY was able to completely hydrolyze the peptide bonds of Val-Ser and AQC-Val-Ser. In contrast, CPA had little hydrolase effect towards Val-Ser

and only depleted 68% of AQC-Val-Ser. CPA unexpectedly outperformed CPY in the cases of Gly-Tyr, and Val-Tyr. However, this advantage disappeared after AQC-derivatization which allowed for complete peptide bond hydrolysis with both enzymes. For AQC-Gly-Tyr and AQC-Val-Tyr, the amount of starting material depleted did not differ significantly between CPA and CPY.

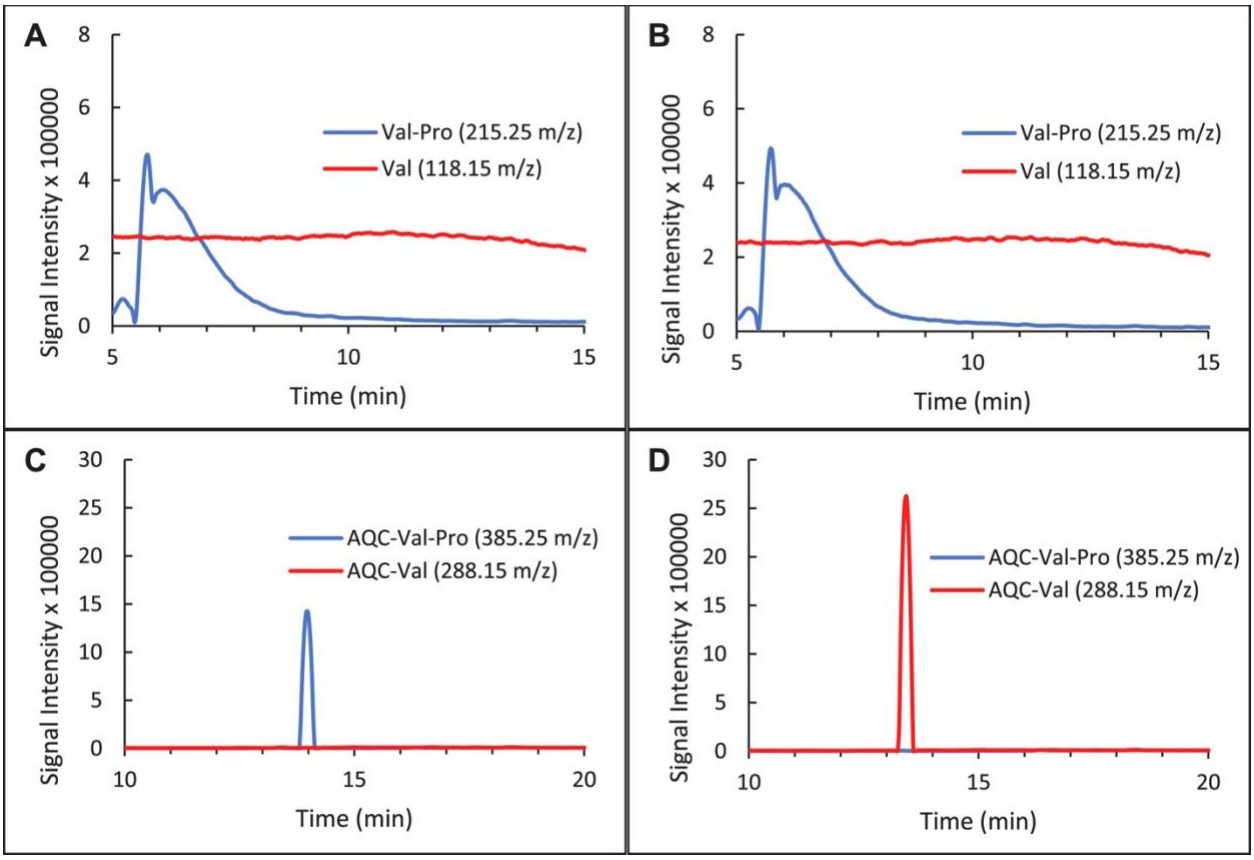

Fig. 4.1 HPLC-MS chromatograms of Val-Pro and AQC-Val-Pro after treatment with CPY at pH 5.5. No significant change in peak area was observed when monitoring for Val-Pro without (A) and with CPY treatment (B). The starting material peak for AQC-Val-Pro without enzyme addition (C) is not detected in the AQC-Val-Pro sample after hydrolysis with CPY (D). AQC-Val-Pro (RT: 13.99 min) is completely hydrolyzed to yield AQC-Val (RT: 13.43 min).

Negligible CPY-catalyzed peptide hydrolysis towards some underivatized dipeptides and greatly enhanced peptide hydrolysis towards AQC-peptides is depicted in Fig 4.1. Fig 4.1A shows the LC-MS chromatogram of a Val-Pro peptide that was not subjected to enzymatic hydrolysis with CPY. Fig 4.1A was indistinguishable from Fig 4.1B which shows Val-Pro that was subjected to CPY-catalyzed hydrolysis. This indicated that peptide hydrolysis with CPY towards this representative dipeptide was negligible. Fig 4.1C shows AQC-Val-Pro without the addition of CPY and Fig 4.1D shows AQC-Val-Pro that was subjected to CPY-catalyzed hydrolysis. When comparing Fig 4.1C with Fig 4.1D, the complete absence of the AQC-Val-Pro starting material in the sample and the quantitative appearance of AQC-Val indicates the successful enzymatic hydrolysis of the peptide bond. Further, note from Fig 4.1C, as compared to Fig 4.1A, that the chromatography (sharper peaks) and detectability of AQC derivatized peptides, is far superior to that of the underivatized peptide in MS. Since CPY also is able to remove C-terminus proline residues within peptides, the resistance to peptide bond hydrolysis seen in Fig 4.1 B is not due to limitation of enzyme specificity but rather the short length of the peptide [19]. It is well known that carboxypeptidases are often unable to hydrolyze the peptide bonds of short underivatized peptides, stopping at the dipeptide stage [7]. This highlights the beneficial effects of AQC-derivatization towards CPY hydrolysis by adding an additional moiety to the N-terminus and emphasizes the need for AQC-derivatization if complete peptide bond hydrolysis is desired across the entire length of the peptide. This specific example will be generalized subsequently (*vide infra*). CPA showed no hydrolysis towards Asp-Asp and AQC-Asp-Asp. The results for CPY hydrolysis of dipeptides with acidic amino acid residues will be discussed subsequently as a special case.

Table 4.2 provides the CPA and CPY-catalyzed hydrolysis results for tripeptides. Consider the enzymatic hydrolysis of Thr-Val-Leu. This tripeptide was incompletely hydrolyzed by both CPA and CPY as no Thr was detected. This was further confirmed as significant amounts of Thr-Val intermediate were detected in both the CPA and CPY enzyme runs. However, AQC derivatization circumvented this problem and quantitatively produced AQC-Thr after enzymatic treatment of AQC-Thr-Val-Leu (Table 4.2). As with the acidic dipeptides in Table 4.1, the tripeptides not mentioned here will be discussed as special cases.

Table 4.3 provides the CPA and CPY-catalyzed hydrolysis results for pentapeptides and larger. The complete peptide bond hydrolysis of underivatized penta-alanine can only be reliably determined by the absence of the Ala-Ala intermediate. This is due to the inability to chromatographically distinguish the N-terminal Ala from other Ala moieties, which can be avoided with any N-tagging reagents including AQC. Since the Ala-Ala dipeptide was detected after CPA and CPY-catalyzed hydrolysis reaction of penta-alanine, it is evident that the hydrolysis was incomplete (data not shown). This further demonstrates that important structural information can be obtained with AQC-derivatization and subsequent carboxypeptidase hydrolysis if identical amino acids appear within the peptide. Enkephalin peptide results also will be discussed subsequently as special cases due to the residues they contain.

4.3.2 Optimal pH for CPY-catalyzed hydrolysis

pH is an extremely important parameter when using any enzyme. Although the optimal pH of 5.5 was sufficient for the majority of peptides that were screened in this project, optimization within a pH range of 4.5–6.8 was needed for certain amino acid residues. CPY's active site includes a catalytic triad consisting of Ser^{146}, Asp^{338} and His^{397}.[127] With two ionizable residues in CPY's active site, pH optimization for enzymatic hydrolysis is beneficial when the target

peptide contains ionizable side chains. This was done to improve the degree of hydrolysis towards specific resistant residues. The peptide bonds of acidic amino acids and basic amino acids residues within peptides can be difficult for CPA to hydrolyze as shown in Table 4.1 for AQC-Asp-Asp and Table 4.2 for Lys-Tyr-Lys respectively.

4.3.3 CPY catalyzed hydrolysis of peptides with acidic amino acid residues

CPY-catalyzed hydrolysis under acidic conditions allows the acidic side chains to be protonated within the catalytic triad of the enzyme as well as acidic amino acids in the substrate.[128,130,131] Early work on CPY has shown that enzymatic activity towards peptides containing acidic residues can be improved by lowering the pH of the buffer matrix.[117] This was tested for AQC-Asp-Asp with acidic residues on the N-terminus and C-terminus positions. Fig 4.2A shows the AQC-Asp-Asp peptide with no enzyme addition. Fig 4.2 B shows AQC-Asp-Asp after exposure to CPY at pH 6.8. A comparison between Fig. 4.2A and B indicates that catalytic hydrolysis towards AQC-Asp-Asp was negligible at pH 6.8 where the side chains are mostly deprotonated. Fig. 4.2C shows AQC-Asp-Asp after treatment with CPY at pH 5.5. A significant decrease in the AQC-Asp-Asp peak area was observed as well as a significant increase in the product AQC-Asp peak area at this pH. Fig. 4.2D shows the CPY-catalyzed hydrolysis of AQC-Asp-Asp sample at pH 4.5. In this case, the starting material has been completely eliminated and the product AQC-Asp was quantitatively produced. This indicates that protonating aspartate residues either in the active site and/or the substrate dramatically improves the degree of hydrolysis towards acidic residues for AQC-peptides with CPY.

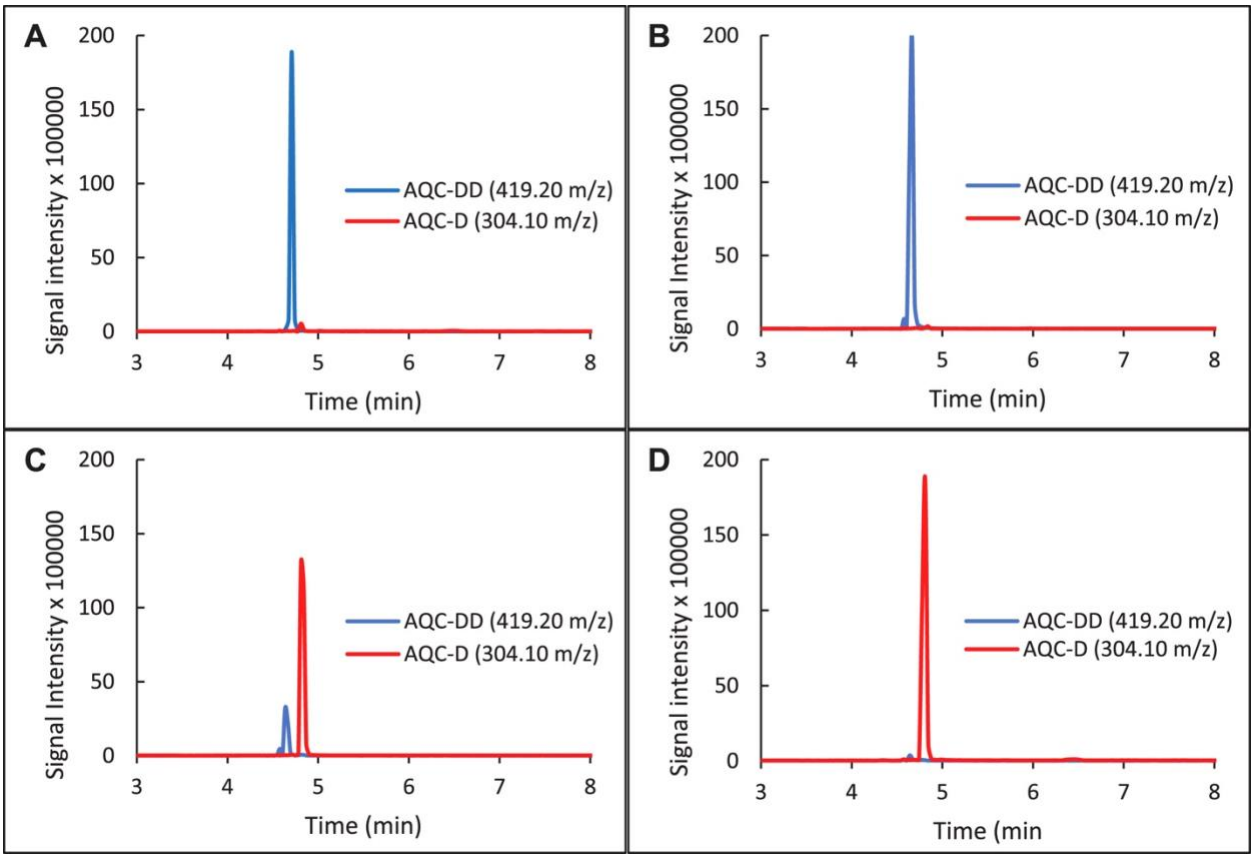

Fig 4.2 LC-MS chromatogram of AQC-Asp-Asp without CPY addition (A) and AQC-Asp-Asp with CPY at pH 6.8 (B), pH 5.5 (C), and pH 4.5 (D). Essentially no change in peak area had occurred under pH 6.8 when compared with the no-enzyme control. Some catalytic hydrolysis occurred at pH 5.5 as indicated by the appearance of the AQC-Asp peak and the decreased peak area in the intact peptide peak (Fig 3.2C. Near complete hydrolysis occurred at pH 4.5 as indicated by minimal amounts of reactant detected and the appearance of a strong AQC-Asp peak (D).

4.3.4 CPY-catalyzed hydrolysis of peptides with basic amino acid residues

Apart from amino acids with acidic side chains, ones with basic side chains (specifically lysine and arginine) also can be charged depending on the pH. The charge state on

the imidazole side chain of histidine may vary depending on the pH of the enzyme buffer. The AQC reagent will readily react with any free amines in the sample.[144] When lysine is present on the N-terminus of the peptide both the N-terminal amine and side chain amine will be derivatized with an AQC group, which is indicated as AQC_2-Lys. Early reports indicate that lysine was a poor substrate to CPY's active site.[117] For peptides with internal lysine groups, the addition of an AQC hydrophobic moiety and removal of the charged nature of the side chain can be advantageous in ways that we subsequently discuss. The effects of having lysine on the C-terminus and N-terminus in Lys-Tyr-Lys and AQC-Lys-Tyr-Lys is illustrated in Fig. 4.3. Fig. 4.3A shows that substantial Lys-Tyr-Lys starting material was detected after extended enzymatic hydrolysis with CPY. Also, the intermediate Lys-Tyr peak was detected. This indicates that the CPY was able to hydrolyze some of the C-terminus lysine but stopped at the dipeptide stage. Fig 4.3B shows AQC_2-Lys-Tyr-Lys-AQC after exposure to CPY. No intact peptide starting material was detected after CPY addition and only the N-terminal AQC_2-Lys peak was observed. The inset figure shows the AQC_2-Lys-Tyr-Lys-AQC standard at a higher concentration to confirm its retention time and its multiple charged states which were monitored for additional confirmation. Also note the greater retention, improved peak shape, and narrow peak width of the AQC-Lys-Tyr-Lys (Fig. 4.3B inset) versus the underivatized tripeptide (Fig. 4.3A). The complete peptide bond hydrolysis of AQC_2-Lys-Tyr-Lys-AQC down to the N-terminus amino acid also demonstrates that the hydrophobic pockets in CPY's active site can accommodate a large hydrophobic aminoquinoline carbamide group. The second AQC-group on the N-terminal lysine is a distinguishing characteristic in the chromatography and MS identification which could provide valuable structural information.

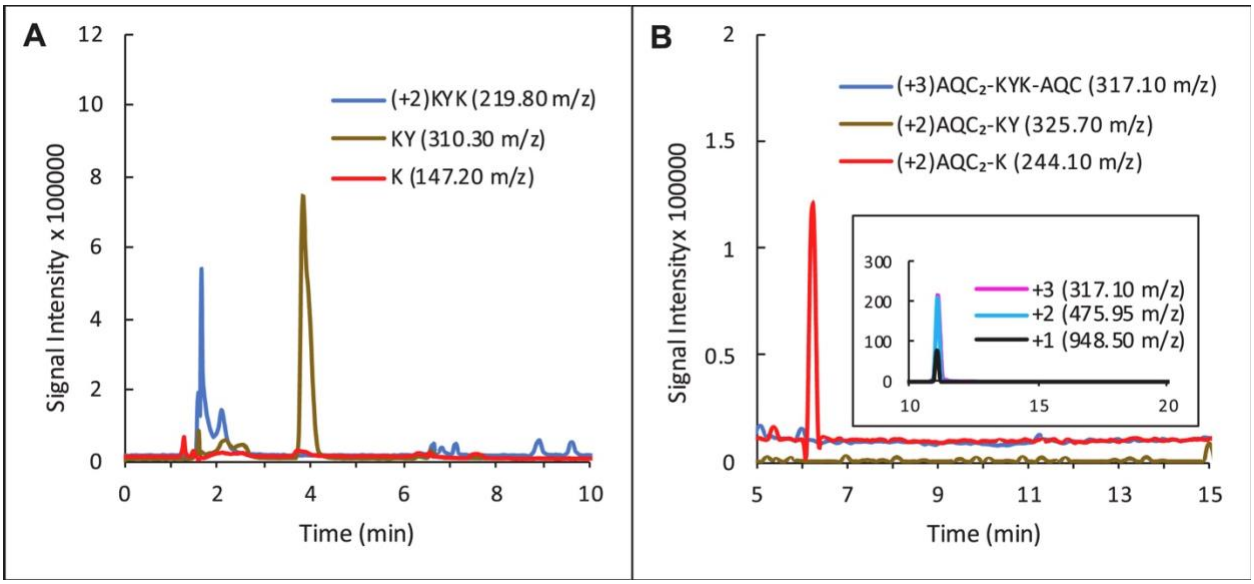

Fig. 4.3 LC-MS chromatograms of Lys-Tyr-Lys (A) versus AQC derivatized Lys-Tyr-Lys (B) after hydrolysis with CPY at pH 5.5. After 24 h of CPY-catalyzed hydrolysis of the underivatized tripeptide. Significant amounts of the dipeptide as well as unhydrolyzed tripeptide are seen (A). K-AQC denotes a lysine residue with an AQC-group on the side chain. AQC_2-K represents a lysine residue with both its N-terminus and side chain amines derivatized. CPY-catalyzed hydrolysis of the AQC derivatized tripeptide yielded AQC_2-K, indicating complete enzymatic hydrolysis of the peptide bonds (B). Removal of the C-terminal lysine with a derivatized side chain indicates that the AQC group on the amine side chain is a compatible substrate for the CPY enzyme.

CPY-catalyzed hydrolysis of arginine containing peptide AQC-Arg-Gly-Asp produced the N-terminal AQC-amino acid which is shown in Table 4.2. Starting material and intermediates were not detected in the sample after exposure to CPY for 24 h. Arginine's guanidino does not form a stable compound with AQC reagent likely due to the inherent resonance of its side chain.

Histidine residues in peptides creates a unique problem for CPY due to the close proximity of the optimal hydrolysis pH to its imidazole side chain pKa, resulting in situationally difficult, and sometimes incomplete peptide hydrolysis with CPY when glycine is involved, even with AQC-derivatization. This was shown in Fig 4.4A with a significant amount of AQC-Gly-Gly-His remaining after 24 h of exposure to CPY at pH 5.5. In the specific case of AQC-Gly-Gly-His, the problem of a charged imidazole at lower pH may be further compounded by the glycine on the penultimate position, which will be discussed in the subsequent section. A pH of 6.8 ensures that a large majority of imidazole side chain will be uncharged in the active site and on the substrate. A comparison of AQC-Gly-Gly-His enzymatically hydrolyzed at pH 6.8 and 5.5, showed greater % hydrolysis for the removal of histidine from the peptide at pH 6.8 than at 5.5. This correllated with the findings of Hayashi et al. in their work with N-Cbz peptides.[137] The CPY-catalyzed hydrolysis of AQC-Gly-Gly-His produced AQC-Gly (Table 3.2).

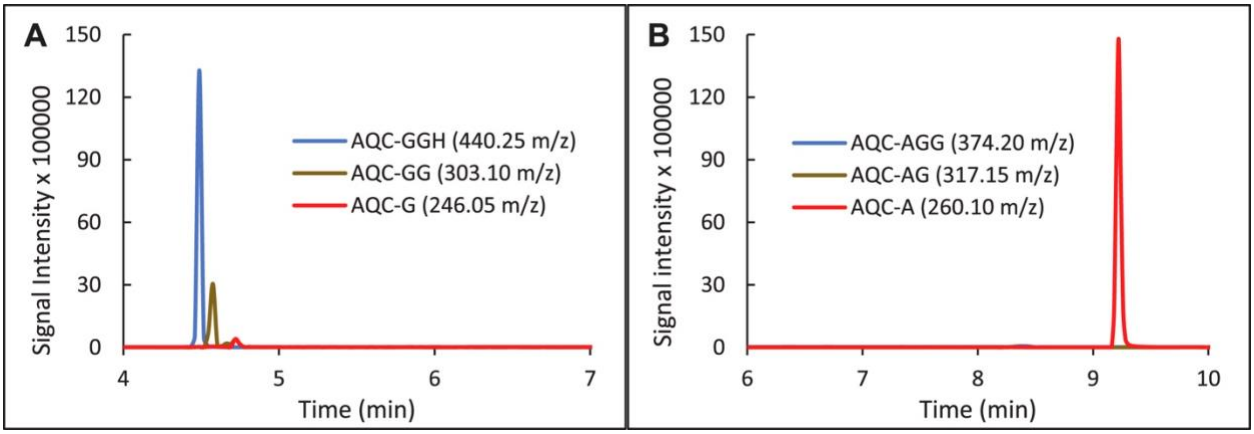

Fig 4.4 LC-MS chromatograms of the CPY-catalyzed hydrolysis products of AQC-GGH (A) and CPY-catalyzed hydrolysis of AQC-AGG (B). The positional effects of internal Gly-Gly relative to AQC-derivatized N-terminus Gly-Gly are shown after CPY-catalyzed hydrolysis at pH 5.5. The incomplete hydrolysis in A indicates that AQC-GG is a significant obstacle for CPY-catalyzed hydrolysis. AQC-AGG, where the Gly-Gly sequence is not situated on the N-terminus was completely hydrolyzed within 24 h by CPY. The combination of A and B indicates that the Gly-Gly sequence will only show incomplete CPY-catalyzed hydrolysis when positioned on the N-terminus.

4.3.5 The specific case of Gly-Gly resistance to CPY-catalyzed hydrolysis

The sequential pair Gly-Gly was previously suggested to be highly resistant to CPY-catalyzed hydrolysis which was determined to be negligible towards N-acetyl-Gly-Gly and Cbz-Gly-Gly.[117,137] This was further investigated, and the results shown in Fig. 4.4 where the positional effect of Gly-Gly was observed. Fig 4.4A shows the AQC-Gly-Gly-His peptide sample after it was subjected to CPY-catalyzed hydrolysis at pH 5.5. The dipeptide intermediate AQC-Gly-Gly also was monitored in SIM which occurs after the removal of the histidine from the C-terminus. The significant AQC-Gly-Gly peak indicates that its peptide bond remained

largely resistant to CPY-catalyzed hydrolysis at pH 5.5 after the removal of the histidine fragment. We concluded that N-terminus Gly-Gly was a major obstacle for CPY and prevents complete peptide bond hydrolysis of AQC-Gly-Gly-His under these conditions. However, a small peak in the AQC-Gly SIM event indicates that small amounts can be produced via enzymatic hydrolysis and detected, when derivatized with AQC. Results in Table 4.2 indicate that Gly-Gly sequences are poorly hydrolyzed at pH 6.8 and should always be hydrolyzed at pH 5.5 unless there are histidine residues in the peptide.

The case of an internal Gly-Gly sequence was investigated, and the results are shown in Fig 4.4B. The *m*/*z* of the intact AQC-peptide and its intermediate was not seen in significant amounts. The complete peptide bond hydrolysis of AQC-Ala-Gly-Gly at pH 5.5 is indicated by the appearance of a prominent peak for AQC-Ala. At pH 5.5 we find that internal sequential Gly-Gly pairs can be hydrolyzed at the peptide bond with CPY to the N-terminus amino acid with little resistance.

4.3.6 CPY-catalyzed hydrolysis of a biologically active peptide

The vast majority of the peptides screened in this work were biologically inactive. These were mainly selected to examine carboxypeptidase substrate compatibilities with AQC-peptides. Since this method was developed with the intention of interrogating endogenous peptides, an L-amino acid exclusive peptide of biological relevance was chosen as a model. Leucine enkephalin is an endogenous neuropeptide found in humans, a synthesized form of which was subjected to the method developed herein.

Leucine enkephalin (enk) has a sequential Gly-Gly pair on the 2nd and 3rd amino acid position. Further evidence for the resistance of sequential Gly-Gly is seen in Fig 4.5A, which shows the enkephalin after exposure to CPY. Peptide bond hydrolysis of the enkephalin was

observed to stop at the tripeptide stage as shown by the significant Tyr-Gly-Gly peak. Conversely, Fig 4.5B shows a significant improvement for the enzymatic hydrolysis of the AQC-enk with CPY. SIM for the intact starting material and all possible intermediate events showed only a small amount of AQC-Tyr-Gly intermediate. The lack of starting material and intermediates in Fig 4.5B shows that the AQC-enk starting material was catalytically cleaved down to the N-terminus AQC-Tyr.

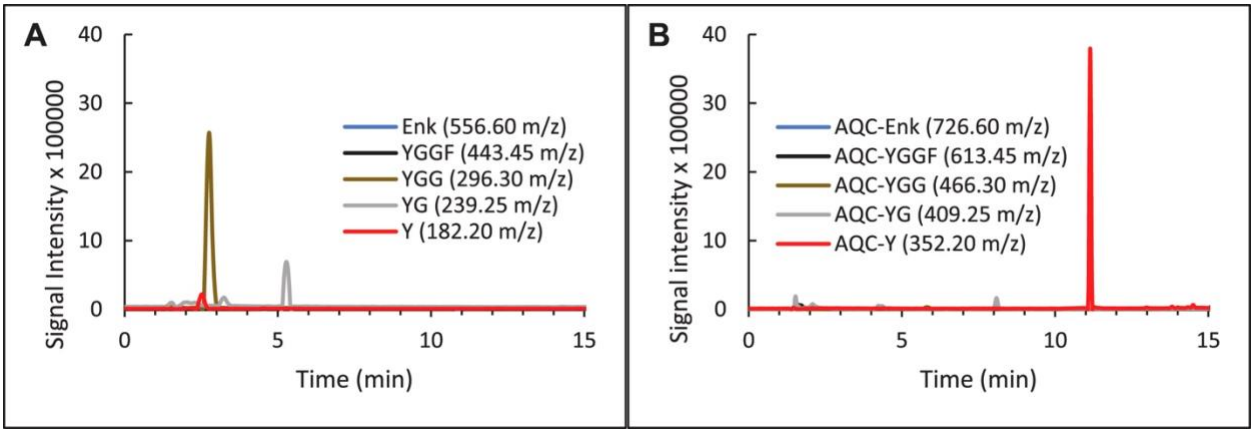

Fig 4.5 LC-MS chromatograms of enkephalin (A) hydrolyzed with CPY versus AQC-enkephalin hydrolyzed with CPY (B) at pH 6.8. After 24 h of CPY-catalyzed hydrolysis, the underivatized enkephalin yielded the tripeptide and dipeptide, but an insignificant amount of tyrosine. Under the same conditions, AQC-derivatized enkephalin yielded AQC-tyrosine with no significant intermediates remaining. With the addition of an AQC group, the internal Gly-Gly was easily hydrolyzed by CPY.

4.3.7 Stereochemistry effects about the ultimate and penultimate position of larger peptides

Varying the amino acid stereochemistry on the C-terminus also provides a more comprehensive look into the effects of different C-terminal amino acids on peptide bond

hydrolysis with CPY. Therefore, the peptide motif Tyr-Gly-Leu-Phe-X was used while varying the amino acid (i.e., "X") on the C-terminus of the peptide. Peptides with variations in the stereochemistry of the amino acids at the 4th and 5th positions were examined. These peptides were AQC-derivatized before a lengthy enzymatic (24 h) treatment and the % hydrolysis results are shown in Table 4.

After enzymatic treatment, all of the L-amino acid exclusive peptides were completely hydrolyzed at the peptide bond down to the AQC-N-terminal amino acid (Table 4.4, Column 1). Pentapeptide stereoisomers with sequential D-amino acids at the 4th and 5th positions were highly resistant to enzymatic hydrolysis (Table 4.4, Column 4). Even after a lengthy 24 h reaction time, some peptide epimers with carboxy-terminal D-amino acids remained intact, although some hydrolysis clearly occurred (Table 4.4, Column 3).

Table 4.4 CPY-catalyzed hydrolysis of AQC-derivatized YGLF-X peptide motifs with varying stereocenters on the penultimate and C-terminus position after 24 h at pH 5.5. No derivatized L-amino exclusive peptides remained intact and in detectable amounts after 24 h. AQC-peptides with a single D-amino acid showed varying percentages of catalytic hydrolysis. AQC-peptides with two sequential D-amino acids on the penultimate and C-terminus typically showed little or no catalytic hydrolysis.

	% hydrolysis of reactant[a]			
AQC-Tyr-Gly-Leu-	*-LL stereochemistry*	*-DL stereochemistry*	*-LD stereochemistry*	*-DD stereochemistry*
-Phe-Asp	100[b]	96 ± 4[c]	98 ± 1	0
-Phe-Glu	100[b]	83 ± 2[c]	94 ± 1	0
-Phe-Lys	100[b]	100[c]	82 ± 8	0
-Phe-Pro	100[b]	45 ± 4[c]	68 ± 2	0
-Phe-Tyr	100[b]	100[c]	85 ± 6	0
-Phe-Val	100[b]	100[c]	95 ± 2	12 ± 5
-Phe-Leu	100[b]	100[c]	100	24 ± 2
-Phe-Phe	100[b]	97 ± 2[c]	94 ± 2	51 ± 3

% hydrolysis of reactant: 0% ≤ red < 50 % ≤ orange < 90% ≤ green ≤ 100%
[a]: complete depletion of the AQC-pentapeptide starting material
[b]: complete peptide bond hydrolysis to yield AQC-N-terminal amino acid
[c]: observed tetrapeptide resistance to hydrolysis

DAACPs with the highest % hydrolysis of reactant in Table 4.4 and their L-amino acid exclusive counterparts were reexamined using shorter reaction times. Fig. 4.6 shows a time curve in which AQC derivatized YGLFE peptide epimers with different stereocenters on the C-terminus position was subjected to CPY-catalyzed hydrolysis and sampled at 0, 5, 10, 15, 20, 30, and 45 min. AQC-YGLFE (green curve, Fig 4.6) was quickly hydrolyzed by CPY, asymptotically approaching 100% in 20 min. The C-terminus D-epimer clearly was more

resistant to CPY-catalyzed hydrolysis (red curve, Fig. 4.6) at this time scale. Thus, the L-exclusive amino acid peptide could be distinguished from the C-terminal D-epimer within 5 min. Other peptides examined under these conditions include the AQC derivatized YGLFD and YGLFF motifs.

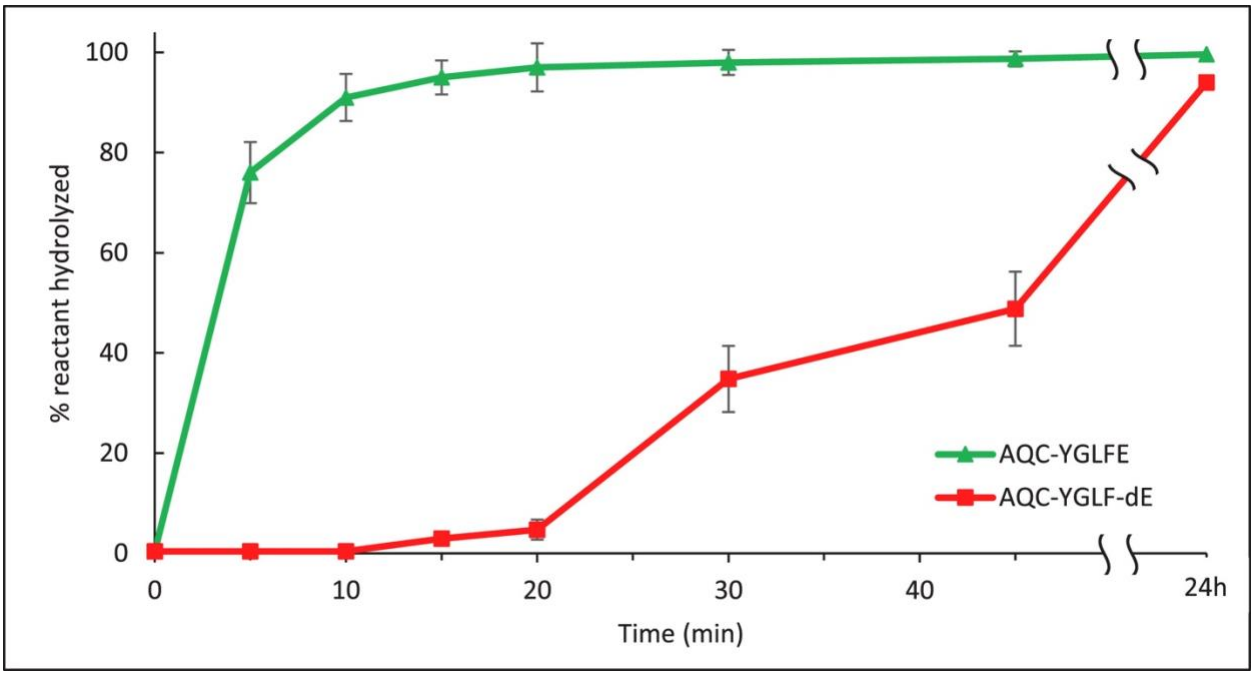

Fig. 4.6 Time curves of AQC-derivatized YGLFE epimers with chiral variation on the C-terminus position that were subjected to CPY-catalyzed hydrolysis. A significant difference in % reactant hydrolyzed by CPY is observed within 5 min between AQC-YGLFE versus AQC-YGLF-dE. AQC-YGLF-dE is significantly less susceptible to catalytic hydrolysis by CPY than the L-AA exclusive peptide. The time curves asymptotically approach their respective values at 24 h, established in Table 4.4.

Peptide epimers with a penultimate D-amino acid might initially appear to have near identical hydrolysis as the L-amino acid pentapeptide. However, this is not the case (see footnote "c" in Table 4.4). Note that the values given in Table 4.4 are for the disappearance of the

pentapeptide starting material, the final hydrolysis product is not observed in significant amounts except in the L-amino acid pentapeptide (see footnote "b" in Table 4.4).

Fig. 4.7 further examines the case of peptides containing penultimate D-amino acids after the C-terminal L-amino acid is removed. The carboxy-terminal D-Phe tetrapeptide (red line, Fig. 4.7) shows similar enzymatic resistance to the C-terminal D-Phe pentapeptide, this intermediate is produced and accumulates with time. The L-amino acid exclusive tetrapeptide intermediate (green line, Fig 4.7) did not accumulate significantly over time in contrast to the DAACP intermediate.

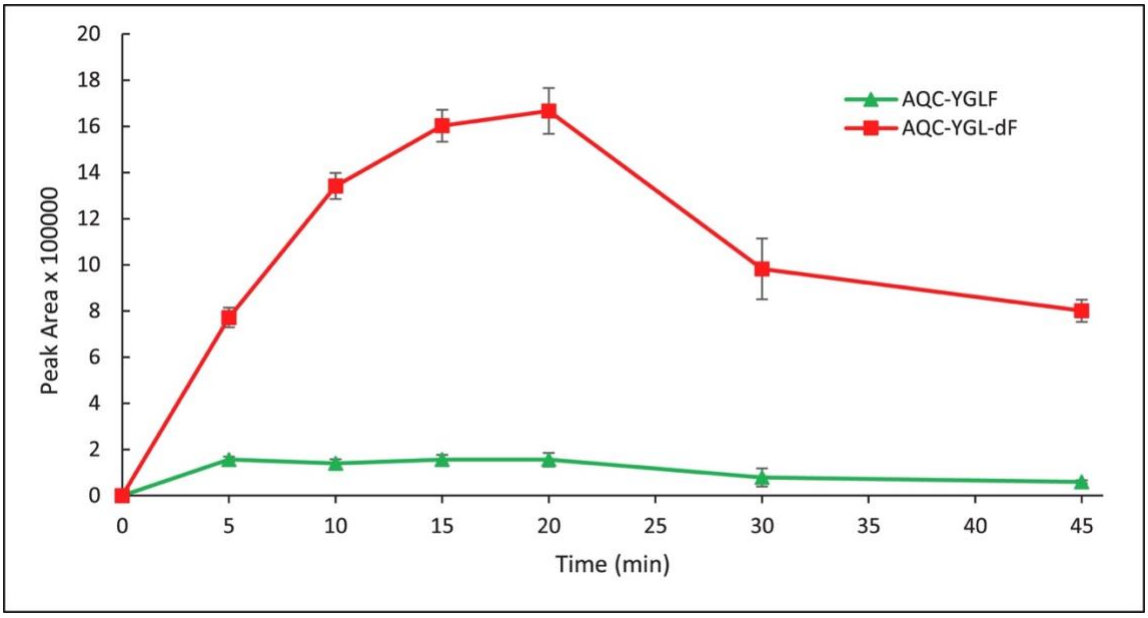

Fig 4.7 Time curve of tetrapeptide intermediates from CPY-catalyzed hydrolysis of AQC-YGLFF motif. DAACP accumulates up to 20 min before slowly decreasing as a result of CPY catalysis. The levels of the L-amino acid exclusive tetrapeptide did not change significantly after 5 min. This data suggests that the majority of the L-amino acid exclusive peptide was hydrolyzed quickly by CPY whereas the C-terminal DAACP intermediate required more time to remove the D-amino acid.

4.4 Conclusions

All AQC-derivatized peptides comprised of L-amino acids and hydrolyzed by CPY in this study produced an N-terminus AQC tagged amino acid product, indicating that the enzyme was able to traverse and hydrolyze the peptide bonds across the entire length of the peptide. The CPY enzyme was able to hydrolyze peptides that CPA could not, such as those containing proline and aspartic acid. In the majority of cases, regarding AQC-peptides, CPY was significantly more effective than CPA in terms of having broader substrate compatibility, with the exception of tyrosine containing peptides. The specificity of CPY towards AQC-derivatized peptides was similar or superior to reported N-Cbz-peptides. However, the ease and speed of the AQC derivatization was highly beneficial. It was shown that both carboxypeptidases can hydrolyze the peptide bond of lysine with an AQC-derivatized side chain. Furthermore, it was demonstrated that this method can be applied towards an endogenous peptide such as leucine enkephalin. Cbz-Gly-Gly residues are known to be resistant to CPY-catalyzed hydrolysis. However, such AQC-derivatized peptides, particularly internal Gly-Gly residues, were hydrolyzed at the peptide bond in the tested samples. Further AQC derivatized peptides and amino acids have significantly better chromatographic peak shapes and higher sensitivity in contrast to their underivatized counterparts, making this method ideal for LC-MS analysis. The presence of the AQC group also is crucial to ensure that the entire length of the peptide can be interrogated for variations in stereochemistry. Peptides with C-terminal D-amino acids are resistant to peptide bond hydrolysis with CPY. Peptides containing sequential D-amino acids are nearly impervious to enzymatic hydrolysis as compared to those comprised exclusively of L-amino acids. The ability of CPY to differentiate between the L-amino acid exclusive peptides and

single DAACPs was demonstrated with shorter catalysis times. This concise method would be a useful addition to the tools and methodologies that are available for detecting and identifying where D-amino acid are located within peptides.

Chapter 5 Teicoplanin aglucone media and carboxypeptidase Y: Tools for finding low-abundance D-amino acids and epimeric peptides

Abstract

D-amino acids and epimeric peptides/proteins can play crucial biological roles and adversely affect protein folding and oligopeptide aggregation in age-related pathologies in humans. This has ignited interest in free D-amino acids as well as those incorporated in peptides/proteins and their effects in humans. However, such stereoisomeric analytes are often elusive and in low abundance with few existing methodologies capable of scouting for and identifying them. In this work, we examine the feasibility of using teicoplanin aglycone, a macrocyclic antibiotic, which has been reported to strongly retain D-amino acids and peptides with a D-amino acid on the C-terminus, for use as a solid phase extraction (SPE) medium. The HPLC retention factors of L-/D-amino acids and C-terminus modified D-amino acid-containing peptides and their L-amino acid exclusive counterparts on teicoplanin aglycone are presented. Retention curve differences between amino acids and peptides highlight regions of solvent composition that can be utilized for their separation. This approach is particularly useful when coupled with enzymatic hydrolysis via carboxypeptidase Y to eliminate all L-amino acid exclusive peptides. The remaining peptides with carboxy-terminal D-amino acids are then more easily concentrated and identified.

5.1 Introduction

The study of biological sources of D-amino acids (D-AAs) and D-amino acid-containing peptides (DAACP) has intensified due to their occurrence in pathologies such as cancer,[53,54,146,147] age-related pathologies such as cataracts (α-crystalline)[147-150] and various neurological conditions including epilepsy, and Alzheimer's disease.[151-156] With the resurgence in interest involving biological roles and impacts of free D-AAs as well as those incorporated in peptides/proteins, there is an increasing demand for sequence-dependent stereospecific methodologies to aid in the search for these low-abundance analytes in complex biological matrices.[136,157,158] Traditional methods of isolating and characterizing D-AAs and DAACPs have analytical impediments including partial racemization during acid hydrolysis, and they are isobaric to dominant L-amino acids (L-AAs) and all L-AA peptides.[136,157-165] A selective solid-phase extraction (SPE) type of format would be ideal if it could facilitate the extraction of D-AAs and D-AA-containing peptides from complex biological samples.

Teicoplanin is a macrocyclic glycopeptide antibiotic that was first isolated from the soil bacterium *Actinoplanes teichomyceticus*.[166,167] Aside from its use as an antibiotic, teicoplanin has also found success as a chiral stationary phase (CSP) for enantiomeric separations.[168-170] First utilized as a silica-based stationary phase in 1995, one of its first uses was for the enantioseparation of both unmodified and *N*-derivatized L- and D-AAs.[100] It was found that D-AAs were significantly retained on teicoplanin when compared to L-AAs.[171] Teicoplanin aglycone (TAG) is a product of synthetically modified teicoplanin in which all three carbohydrate groups of the precursor compound were removed.[172-174] The end product was found to have decreased solubility in water but increased specificity toward D-AAs.[175] Thus, the TAG CSP appeared to be an ideal choice when considered as a SPE approach targeting D-AAs and DAACPs.

TAG selectively interacts with the carboxylate functionality of amino acids and the carboxy-terminal D-AAs of peptides. Such a TAG stationary phase could selectively retain DAACPs that contain a carboxy-terminal amino acid. Presumably, this would be quite rare in biological matrices. Recently, we reported an enzymatic method using carboxypeptidase Y (CPY) that was capable of eliminating L-AA exclusive peptides and creating C-terminal DAACPs from embedded DAACPs.[37] This would allow the natural affinity of immobilized TAG to be used in either a chromatographic or SPE format. CPY is a serine carboxypeptidase that sequentially hydrolyzes amino acids at the peptide bond from the C-terminus of peptides.[111-113,117] This enzyme has been shown to have decreased enzymatic activity when cleaving D-AAs from peptide chains, sometimes by two or more orders of magnitude.[37] It has been previously shown that enzymatic screening with CPY is capable of eliminating L-AA exclusive peptides while possessing low activity toward DAACPs.[37,113,117]

Herein we provide screening results for amino acids, dipeptides, and longer peptides on TAG stationary phase under reversed phase conditions. The combination of a streamlined and targeted enzymatic methodology can potentially eliminate L-amino acid exclusive peptides while being largely inactive towards low-abundance DAACPs. This stereospecific enzymatic methodology when combined with the TAG stationary phase's natural affinity toward D-AAs/C-terminal DAACPs is potentially a powerful tool for selectively identifying such low-abundance species.

5.2 Experimental

5.2.1 Materials

Solvent sourcing for LC separations was as follows: methanol was purchased from Fischer Chemical (Fair Lawn, NJ, USA), anhydrous ethanol 200 proof from Decon Labs Inc. (King of Prussia, PA, USA), and DI water was obtained through a Barnstead GenPure Pro UV water purification system. The mobile phase additives ammonium formate and formic acid were purchased from Sigma Aldrich (St. Louis, MO, USA). Buffers such as 2-*N*-(morpholino)-ethanesulfonic acid hydrate (MES hydrate) and boric acid were also purchased from Sigma to make the enzyme buffer and 6-aminoquinoline-*N*-hydroxysuccinimidyl carbamate (AQC) derivatization buffer, respectively. Carboxypeptidase Y was purchased from Worthington Biochemical Corporation (Lakewood, NJ, USA). All amino acid standards were sourced from Sigma Aldrich. All dipeptides were sourced from either Sigma-Aldrich or Tokyo Chemical Industry America (TCI) (Portland, OR, USA), whereas all tetra- and pentapeptides were purchased from Peptide 2.0 except for enkephalin analogues, which were obtained from Sigma Aldrich. AQC derivatization reagent was provided by AZYP LLC (Arlington, TX, USA).

5.2.2 HPLC instrumentation and methods

Initial screening of peptides was performed on a 1200 Agilent series HPLC and data analyzed with ChemStation. LC–MS analysis of enzymatic hydrolysis products was conducted on a Shimadzu 8040 LC–MS and the data analyzed using LabSolutions software. Screening separations were conducted using a 4.6 × 100 and 250 mm, 5 μm FPP Astec Chirobiotic TAG from Supelco, which utilizes a TAG stationary phase. The column used for LC–MS analysis of hydrolysis products was a 3 × 150 mm 2.7 μm SPP TeicoShell from AZYP LLC, which utilizes a teicoplanin stationary phase.

All HPLC separations were performed using a flow rate of 1 mL/min and LC–MS with 0.4 mL/min. Screening samples were prepared in 50:50 water methanol (v/v) at a concentration of 100 ppm. Retention factors (*k*) and optimal separation of amino acids were obtained using a mobile phase composition of 80:20 methanol: water with a sample injection volume of 1 μL on a 4.6 × 100 mm Chirobiotic TAG and detected at 220 nm. The retention factor curves were obtained by varying mobile phase percentages of water and methanol with identical conditions to the amino acid analysis. The optimal separation for glycyl- and alanyl-dipeptides was obtained using a mobile phase composition of 80:20 methanol: water with a sample injection volume of 1 μL on a 4.6 × 250 mm Chirobiotic TAG and detected at 220 nm.

5.2.3 AQC-derivatization of peptides

The AQC derivatization procedure was as follows. A 3 mM peptide sample was mixed with AQC reagent at a 10:20:70%(v/v) of sample: AQC reagent: borate buffer. Peptide samples were then heated in the oven for 25 min at 55 °C. After heating, the 300 μM samples were left at room temperature for a minimum of 6 h before proceeding.

5.2.4 CPY hydrolysis conditions

In the CPY-catalyzed hydrolysis, the solution was prepared with 50 mM 2-(*N*-morpholino)ethanesulfonic acid hydrate (MES) and 0.1 M NaCl adjusted to pH 5.5 with 1 M HCl to make the MES solution. Enzyme solutions were prepared with 1.6 mg of lyophilized CPY in 800 μL of MES solution. 25 mM ammonium formate in CH_3OH was prepared as a post hydrolysis quenching solution to prevent microbial growth and halt enzymatic activity. When preparing the samples, 60 μL of the DAACP AQC-enkephalin was mixed with 140 μL of the L-amino acid exclusive enkephalin. 50 μL of 300 μM of the mixed enkephalin peptide solution was

pipetted into 1400 μL of MES buffer for CPY (or tris • HCl buffer for CPA) and topped off with 50 μL of enzyme solution 3.3:92.4:3.3% (v/v) in 15 mL Eppendorf tubes and vortexed well. All samples had respective no-enzyme controls with 50 μL of 300 μM peptide sample added into 1450 μL of buffer. All tubes were placed in 37°C water bath and sampled at 5-, 15-, and 25-min intervals. 450 μL of the sampled solution was pipetted into Amicon centrifugal filters (3 kDa).

5.2.5 Sample treatment and subsequent LC-MS/MS analysis

Enzyme removal was achieved by spinning down the solution at 14,000 rpm for 12 min at 25°C. The filtrate was mixed with the 25 mM ammonium formate CH_3OH quenching solution at a 1:1 ratio in a sample vial and subsequently analyzed on LC–MS with a flow rate of 0.4 mL/min.

5.3 Results and discussion

The difference in retention factor between representative D,L-amino acid enantiomeric pairs: alanine, serine, glutamine, and asparagine, is plotted in Fig. 5.1 against varying concentrations of methanol in the mobile phase when screened on a TAG stationary phase support. An increase in $k_{D\text{-}AA}$-$k_{L\text{-}AA}$ (Δk) as well as enantiomeric selectivity (α) was observed with increasing methanol concentration in the mobile phase. As small zwitterionic analytes, amino acids are better solubilized in water while having limited solubility in higher % organic solutions under reversed phase conditions. Discrimination between D-AA and L-AA enantiomers is shown to be greatest at high methanol concentrations (Fig. 5.1). This behavior can vary somewhat by changing the nature of the organic modifier, the concentration of buffer salts in the mobile phase, and the pH of the aqueous portion of the mobile phase. All proteinogenic amino acids were screened, and all their behaviors followed this trend (Table 5.1). However, the

hydrophobic or charged nature of the amino acid side chains affected the shape and steepness (slope) of the curves. The effects of adding 50 mM ammonium formate buffered to pH 4 as the aqueous portion of the mobile phase under the optimized conditions of 90:10 methanol: water is detailed in Table 5.2. Consequently, some of the most retained L-enantiomer amino acids were retained longer than the D-enantiomer of the least retained amino acids under these particular conditions. The overlaid chromatographic separations of eight glycyl-dipeptides is depicted in Figure 5.2 and is offset for clarity. As a result of glycine's achiral nature, the number of stereocenters in this group of peptides is limited to one. Thus, all variations in stereochemistry are situated at the C-terminus and retention differences due to side-chain characteristics were less apparent when screening glycyl-dipeptides.

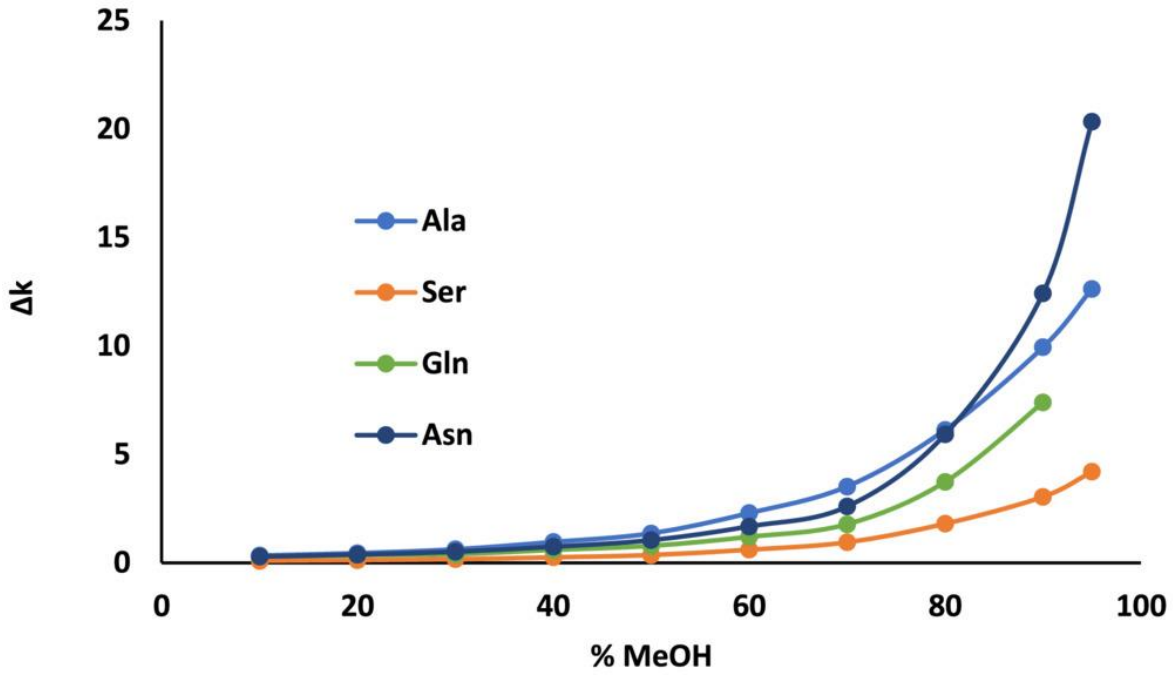

Figure 5.1 Difference in retention values ($k_2 - k_1$) for enantiomers of Ala, Ser, Gln, and Asn with varying ratios of methanol:water; 1 mL/min on Chirobiotic TAG, 5 µm particles and detected at 220 nm.

Table 5.1 *k* values for different mobile phase concentrations of methanol:water

AAs / %MeOH	Ala		Phe		Ile		Leu		Met		Asn	
	k_L	k_D	k_L	k_D	k_L	k_D	k_L	k_D	k_L	k_D	k_L	k_D
95	3.98	16.6	2.79	7.10	1.34	13.1	1.78	9.16	2.86	14.5	7.62	28.0
90	3.07	13.0	2.38	5.93	1.22	10.8	1.52	7.94	2.35	12.2	4.99	17.4
80	1.83	7.96	1.55	3.79	0.870	7.60	1.04	5.57	1.45	7.38	2.57	8.49
70	1.03	4.55	1.17	2.74	x	x	0.732	3.87	0.968	4.66	1.23	3.83
60	0.687	2.98	1.05	2.38	x	x	0.637	3.26	0.825	3.78	0.797	2.48
50	0.572	1.93	1.15	2.36	0.603	3.37	0.694	2.70	0.792	2.98	0.577	1.62
40	0.403	1.36	1.21	2.30	0.571	2.81	0.637	2.11	0.716	2.46	0.431	1.17
30	0.306	0.930	1.17	2.06	0.503	2.13	0.559	1.75	0.636	1.90	0.331	0.841
20	0.258	0.703	1.18	1.89	0.487	1.68	0.537	1.46	0.603	1.56	0.289	0.669
10	0.238	0.574	1.18	1.73	0.474	1.36	0.501	1.23	0.551	1.29	0.243	0.527
AAs / %MeOH	Gln		Ser		Thr		Val		Trp		Tyr	
	k_L	k_D	k_L	k_D	k_L	k_D	k_L	k_D	k_L	k_D	k_L	k_D
95	x	x	3.08	7.28	1.75	5.03	1.71	9.02	3.27	10.1	2.50	6.53
90	4.38	11.8	2.18	5.22	1.34	3.64	1.41	7.71	2.75	8.01	2.02	5.16
80	2.39	6.12	1.22	3.02	0.726	2.16	0.957	5.00	1.93	5.34	1.30	3.29
70	1.24	3.02	0.634	1.58	0.387	1.18	0.630	3.27	1.58	4.12	0.928	2.34
60	0.850	2.05	0.405	1.01	0.271	0.800	0.535	2.48	1.64	3.90	0.861	2.07
50	0.649	1.43	0.316	0.676	0.253	0.590	0.554	1.90	1.88	3.78	0.871	1.85
40	0.507	1.10	0.215	0.468	0.176	0.424	0.424	1.44	2.07	4.00	0.851	1.75
30	0.445	0.843	0.165	0.336	0.145	0.322	0.367	1.07	2.32	4.06	0.857	1.61
20	0.374	0.728	0.146	0.271	0.134	0.267	0.338	0.837	2.61	4.15	0.903	1.56
10	0.330	0.618	0.110	0.205	0.105	0.210	0.297	0.658	2.76	4.11	0.891	1.43

Table 5.2 Comparison of k for 90:10 methanol:water with and without buffer

AA	90:10 without buffer		90:10 with buffer	
	k_L	k_D	k_L	k_D
Ala	3.07	13.0	2.50	10.4
Cys	3.02	14.1	2.62	8.50
Asp	1.21	2.71	2.22	5.35
Glu	1.24	4.04	1.77	6.85

Phe	2.38	5.93	1.96	5.13
His	x	x	x	x
Ile	1.22	10.8	0.937	8.87
Lys	x	x	21.1	x
Leu	1.52	7.94	1.17	6.39
Met	2.35	12.2	1.85	10.5
Asn	4.99	17.4	4.34	15.5
Pro	2.40	x	9.86	49.0
Gln	4.38	11.8	3.87	11.0
Arg	x	x	22.1	x
Ser	2.18	5.22	1.82	4.40
Thr	1.34	3.64	1.08	3.10
Val	1.41	7.71	1.14	6.38
Trp	2.75	8.01	2.20	6.46
Tyr	2.02	5.16	1.71	4.38

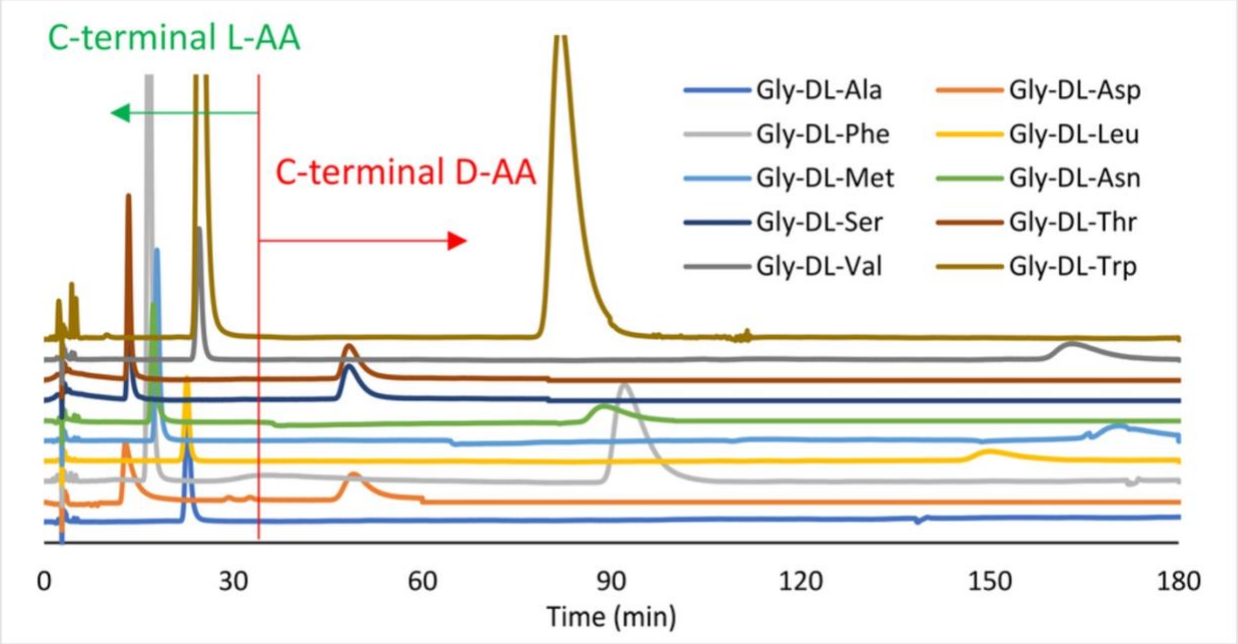

Fig. 5.2 Enantiomeric separation of glycyl-dipeptides with all C-terminal L-amino acid peptides eluting prior to the 33 min cutoff; 1 mL/min 80:20 MeOH:water, 4.6 × 250 mm, Chirobiotic TAG 5 μm detected at 220 nm.

Under these separation conditions, all screened glycyl-peptides with a C-terminal D-amino acid were highly retained, with all of the L-enantiomer peptides eluting prior to the cutoff time of 33 min, or a k of 18.4. The dipeptides with C-terminal D-AAs eluted in the order as listed: Gly-D-Thr, Gly-D-Asp, Gly-D-Trp, Gly-D-Ser, Gly-D-Phe, Gly-D-Leu, Gly-D-Val, Gly-D-Met, and Gly-D-Ala. Peak identities were confirmed via pure standards.

In similar fashion, Fig. 5.3 shows the overlaid chromatographic separations of alanyl-dipeptides offset for clarity. The additional chiral center results in four possible stereoisomers in the form of LL, DL, LD, and DD that must be separated. The alanyl-dipeptides were separated under identical conditions as the glycyl-dipeptides. The solvent "cutoff" composition for glycyl-dipeptides was also acceptable for separating alanyl-dipeptides on TAG stationary phase with all C-terminal L-AA peptides eluting prior to all C-terminal D-AAs. The four possible stereoisomers of each peptide were classified into two groups, those with an L-AA on the C-terminus in contrast to those with a D-AA on the C-terminus. The majority of peptide stereoisomers followed the elution order of LL, DL, LD, and DD. All alanyl-dipeptides with a C-terminal L-amino acid were found to elute prior to the cutoff time of 33 min, or *k* of 18.4. The notable exception being the four stereoisomers of DL-Ala-DL-Met. These separation conditions were unable to provide chromatographic resolution between the pairs L-Ala-L-Met, D-Ala-L-Met and L-Ala-D-Met, D-Ala-D-Met. Hence, only two peaks were observed in this chromatogram.

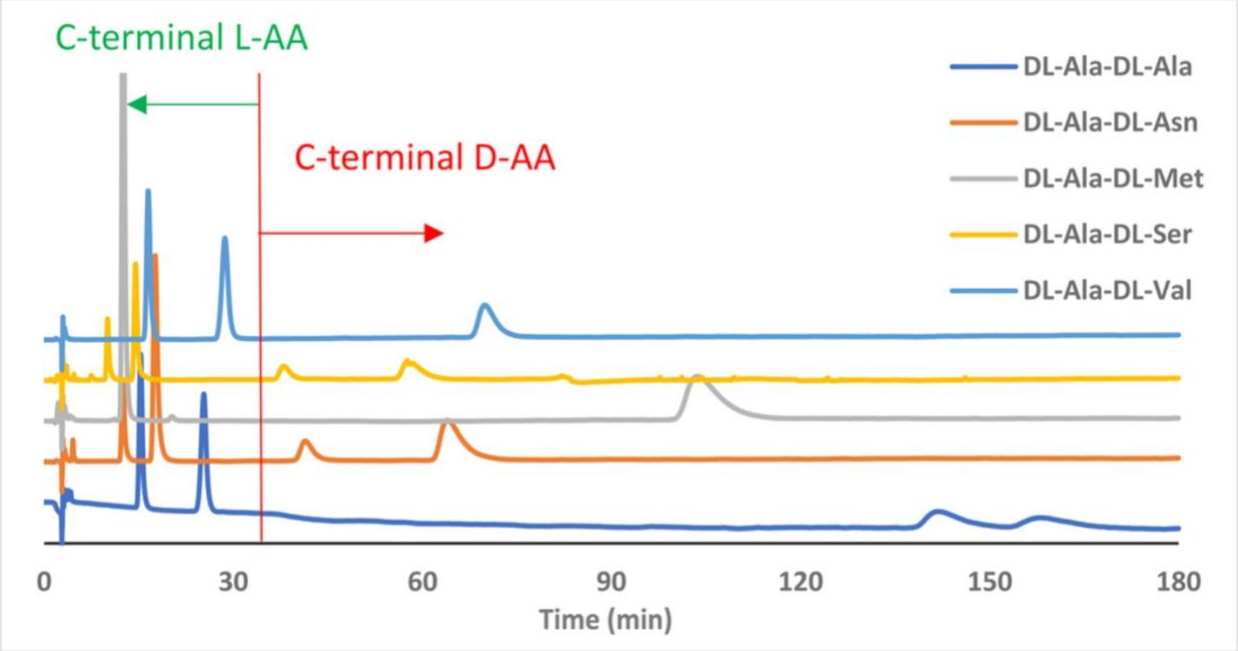

Fig 5.3 Separation of alanyl-dipeptides with all C-terminal L-amino acid peptides eluting prior to the 33 min cutoff. 1 mL/min 80:20 MeOH:water, 4.6 × 250 mm, Chirobiotic TAG, 5 µm, detected at 220 nm.

The general amino acid elution order of peptides was Ala-Ser, Ala-Asn, Ala-Val, Ala-Met, and Ala-Ala. Peak identity was confirmed with separate standards of the epimers. Notably D-Ala-D-Val was not detected within the 3-h method run time. This very highly retained dipeptide only eluted when the pH of the aqueous part of the mobile phase was lowered to pH 4. When the side chain of the N-terminal amino acid was kept constant, the elution order trend was dependent on the side chain characteristics of the C-terminus amino acid. The general amino acid elution order was acidic side chains<polar side chains<aromatic side chains<aliphatic side chains. The higher retention of peptides with aliphatic side chains compared to those with aromatic side chains, despite the presence of five aromatic rings on TAG, can be explained by the hydrophobic effect in reversed phase solvent systems as well as weakened pi–pi interactions

in the same solvents. The aliphatic side chains of alanine, methionine, and valine interact more strongly with the hydrophobic pocket of the aglycone, hence their increased retention.

The chromatogram of an epimeric mixture of insulin B fragment 22–25 with the sequence L-Arg-Gly-L-Phe-L-Phe and a synthesized epimer with the sequence L-Arg-Gly-L-Phe-D-Phe is shown in Figure 5.4A. The terminal D-epimer was significantly more retained. In similar fashion, Figure 5.4B depicts the chromatogram of an epimeric mixture of bovine pineal antireproductive peptide with the sequence L-Thr-L-Ser-L-Lys-L-Tyr and its synthesized epimeric counterpart with the sequence L-Thr-L-Ser-L-Lys-D-Tyr. Higher retention was again observed for the terminal D-epimer. Both chromatograms shown in Figure 5.4 were optimized for maximum α within a reasonable time frame.

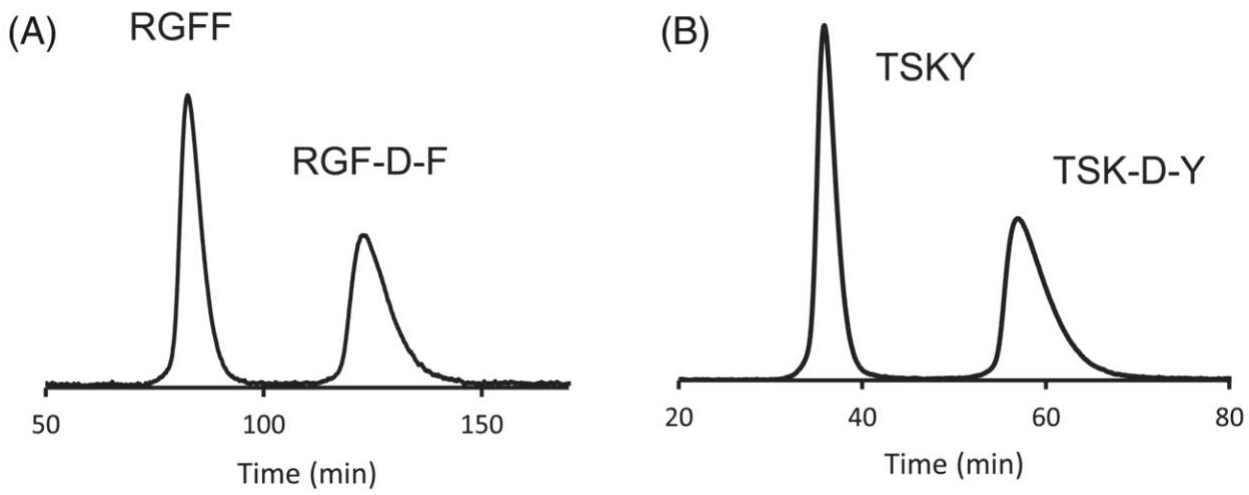

Fig. 5.4 (A) Separation of Insulin B fragment (22-25) RGFF and synthesized RGF-D-F peptide on Chirobiotic TAG 4.6 × 100 mm, 5 μm. 1 mL/min, 80/20 MeOH/50 mM ammonium formate pH = 4.0. (B) Separation of bovine pineal antireproductive peptide TSKY and synthetic TSK-D-Y peptide on Chirobiotic TAG 4.6 × 100 mm, 5 μm. 1 mL/min, 80/20 MeOH/50 mM ammonium formate pH = 4.0. Both were detected at 220 nm.

The retention behavior of selected peptides were investigated. Figure 5.5 is a plot of the retention factor of L-Arg-Gly-L-Phe-L-Phe and its C-terminus D-epimer at varying percentages of methanol: water. The C-terminal D-amino acid epimer is more retained than all the L-amino acid peptides at all ratios of methanol: water tested. Although both curves diverge (increase in α) when approaching solvent extremes, a larger Δk was observed at higher organic mobile phase compositions. These synthetic peptides with biological activity and their C-terminus D-epimers, which were screened at different methanol: water concentrations serve to demonstrate the preference of TAG toward C-terminal DAACPs at all solvent compositions.

Despite having screened many peptides with α's both large and small, differences in side-chain characteristics still play a significant role in their retention behavior. As a result, the data show that despite achieving high α's and resolutions, no all-inclusive cutoff could be determined for a wide array of peptide epimers. This, in part, was why a streamlined enzymatic method capable of eliminating most, if not all L-amino acid exclusive peptides while preserving the DAACPs, should be utilized. It should be noted that the AQC derivatization technique coupled with the enzymatic method aids in but is not required for detection. However, AQC derivatization is imperative if the second position from the N-terminus is to be interrogated for D-AAs as CPY has been largely found to be inactive toward native dipeptides.[37,111,112,117,175] The retention differences between peptides and amino acids become more apparent at low % organic mobile phases and may be exploited. This can be seen when comparing the *k* values in Table 5.1 with the U-shaped curves shown in Figures 5.5 under identical conditions.

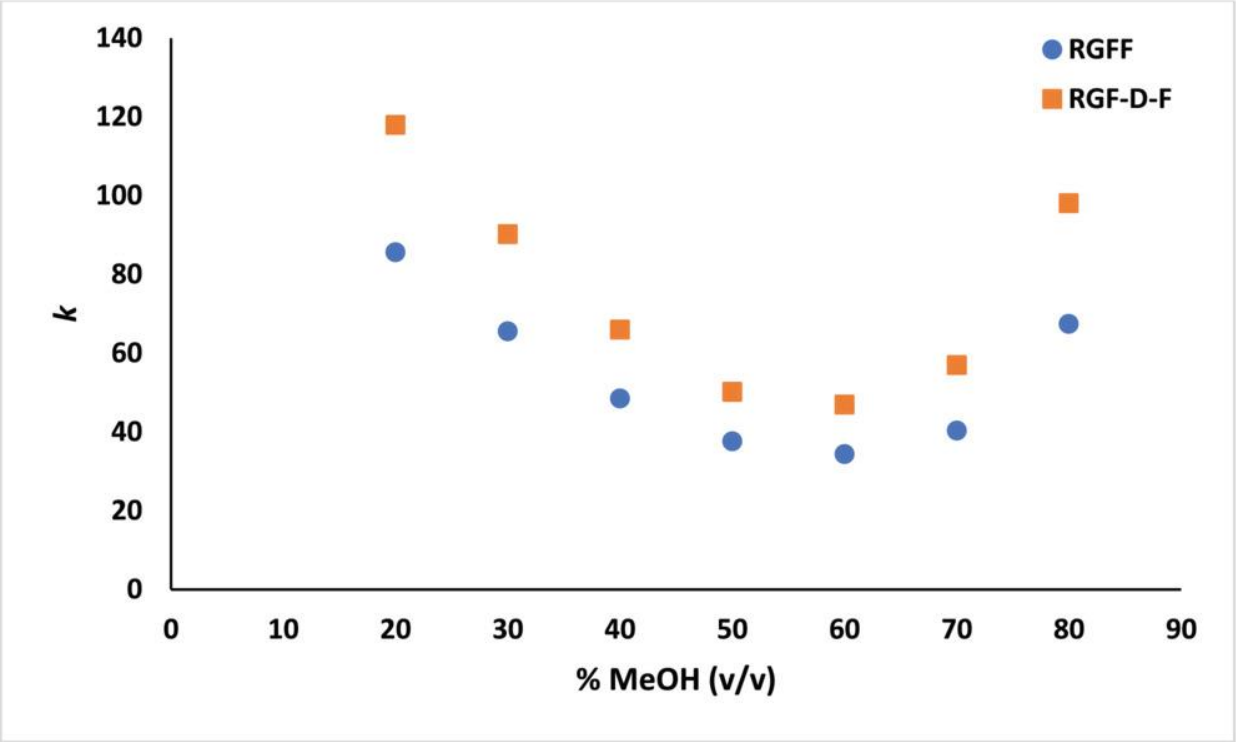

Fig 5.5 U-shaped retention curve of RGFF and synthetic RGF-D-F at varying ratios of methanol in 50 mM ammonium formate pH 4.0 mobile phases on Chirobiotic TAG 5 μm 4.6 × 100 mm at 1 mL/min and detected at 220 nm.

Additionally, AQC derivatization increases the hydrophobic character of the peptide. The hydrophobic AQC-peptide's preference for the hydrophobic pocket of the aglycone combined with the specificity of TAG toward C-terminal D-AAs is rare complimentary combination in stationary phases when targeting DAACPs. This streamlined methodology is capable of producing C-terminal DAACPs using enzymatic hydrolysis while fully hydrolyzing all L-amino acid exclusive peptides can now be combined with purification and preconcentration on a TAG stationary phase. Although a larger α was observed at higher % organic, a lower % organic would ensure the fast elution of endemic amino acids as well as hydrolyzed amino acids from the

CPY enzymatic method. Under the same conditions that elute amino acids, intact AQC-peptides would be strongly retained on the stationary phase.

The CPY-catalyzed hydrolysis of a mixture of AQC-Tyr-Ala-Gly-Phe-Leu and AQC-Tyr-D-Ala-Gly-Phe-D-Leu in 70:30 and 90:10 molar ratios sampled at 5-, 10-, and 25 min over a period of 25 min of enzymatic hydrolysis is shown (Figure 5.6). The L-amino acid exclusive peptide shown in black was below the limit of detection after 5 min of the enzymatic hydrolysis. The D-amino acid terminal peptide peak area is shown in green did not change significantly over the course of the hydrolysis reaction, compared to the control. The levels of the expected hydrolysis end product of the all L-AA containing peptide (i.e., AQC-tyrosine) spiked sharply after 5 min and remained throughout the hydrolysis experiment. The appearance of AQC-tyrosine and the unchanged peak area of the DAACP suggest that the AQC-tyrosine observed was solely from the L-AA exclusive peptide proving that the all L-AA peptide was fully hydrolyzed by the 5-min sampling interval despite being present in 9 and 2.3 times excess in two separate experiments.

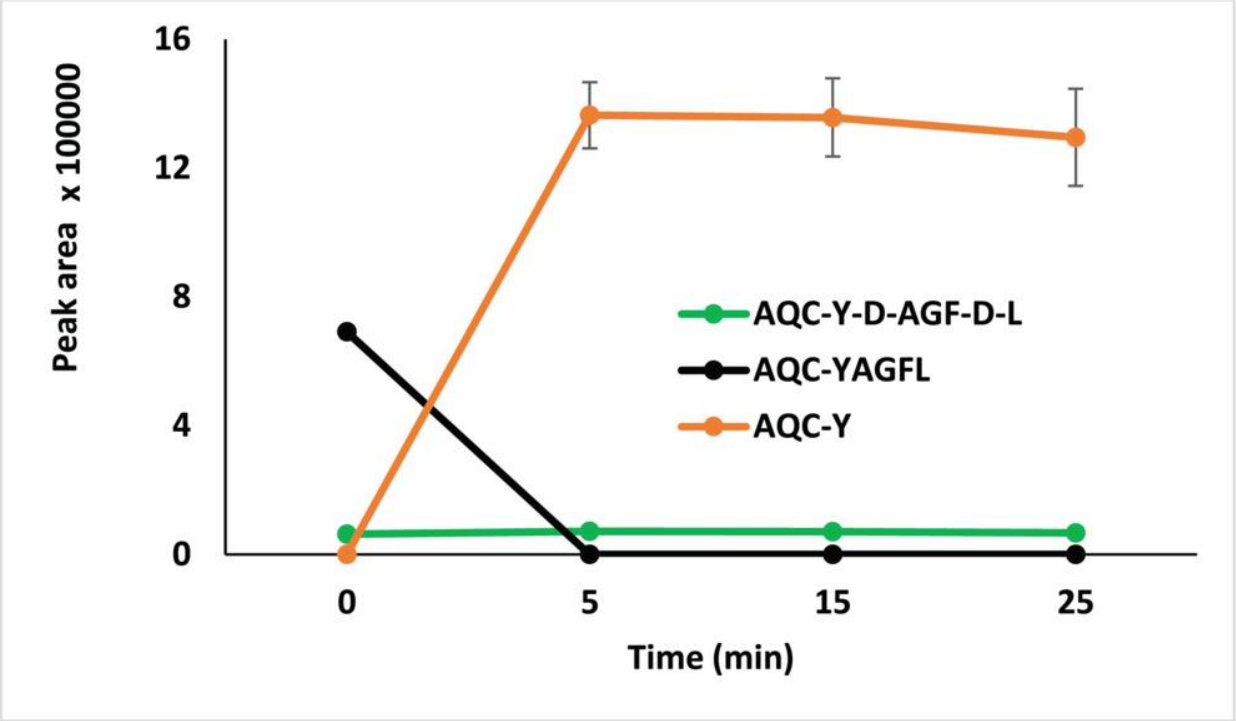

Fig 5.6 LC-MS peak area analysis of 70:30 (v/v) equimolar solutions of AQC-YAGFL:AQC-Y-D-A-GF-D-L hydrolyzed with CPY over time. Both starting materials were monitored at 5, 15, and 25 min as well as the final expected product. The separation was conducted on TeicoShell 2.7 μm SPP 3 × 150 mm column at 0.4 mL/min.

This proof of concept could be translated to biological samples where CPY is capable of fully eliminating non-DAACPs while not degrading DAACPs, which would remain intact for extraction and subsequent analysis.

5.4 Conclusions

The TAG CSP was able to establish a L- and D-amino acid (C-terminus) cutoff for most amino acids and short peptides. This may be useful in a SPE format for the purpose of

preconcentrating D-AAs and short C-terminal DAACPs while removing all L-AAs in a wash step. Amino acids with basic side chains were highly retained on TAG; amino acids with acidic side chains were much less retained. This resulted in some L-AAs eluting after D-AAs, only for these specific groups of amino acids. Addition of ammonium buffer hastened the elution of amino acids and decreased the selectivity between D- and L-AAs. In the case of peptides, the TAG media can be used to retain peptides with D-AAs on the C-terminus while eluting their all L-amino acid analogues. A usable solvent "cutoff" composition was established for both glycyl- and alanyl-dipeptides on the TAG stationary phase with all C-terminal L-AA peptides eluting prior to peptides with C-terminal D-AAs. TAG also excels at retaining peptides in general at high and low % organic mobile phase compositions as the U-shaped retention curves demonstrate. A CPY enzymatic hydrolysis was performed on a mixture of AQC-derivatized synthetic DAACP and its L-amino acid counterpart. It was demonstrated that the L-amino acid exclusive enkephalin peptide was eliminated, whereas the DAACP enkephalin epimer remained intact for subsequent extraction and analysis by LC–MS with a TeicoShell CSP.

Chapter 6 Comprehensive chiral GC-MS/MS and LC-MS/MS methods for identification and determination of N-acyl homoserine lactones

Abstract

N-acyl homoserine lactones (*N*-HLs) are signalling molecules synthesized by gram-negative bacteria to communicate in a process called quorum sensing. Most reported methods for the analysis of *N*-HLs, which are chiral molecules, do not distinguish between enantiomers. Typical examples include biosensors, liquid chromatography with UV detection, gas chromatography coupled with a mass spectrometer (GC-MS) and liquid chromatography coupled with mass spectrometer (LC-MS). Recently, the production of both D,L-*N*-HLs have been reported

in *Vibrio fischeri* and *Burkholderia cepacia*. Concentrations of the D-*N*-HLs were found at the limit of quantification for the employed method. Therefore, for further studies of the role of the D-*N*-HLs in bacterial physiology, more sensitive, reliable, and selective analytical methods are necessary. In this work, such comprehensive chiral analytical methods for the identification and determination of 18 *N*-HLs using solid phase extraction followed by GC-MS/MS and LC-MS/MS analyses were developed. Extraction recoveries for the more hydrophillic C4 *N*-HLs were <10% of all other *N*-HLs, thus offering a possible explanation as to their lack of detection in previous studies. The chiral separations of all 18 *N*-HLs derivatives were accomplished by the complementary GC-MS/MS and LC-MS/MS methods. The limit of detection for LC-MS/MS method was as low as 1 ppb. The limit of detection for the GC-MS/MS method was found to be one to three orders of magnitude higher than the LC-MS/MS method. Due to the high extraction recovery and a preconcentration factor of 100, concentrations as low as 10 ppt can be detected by LC-MS/MS in biological samples. The LC-MS/MS approach provided greater enantioselectivity for the larger, more hydrophobic *N*-HLs while GC-MS/MS provided better enantioselectivity for the smaller *N*-HLs.

6.1 Introduction

N-acyl homoserine lactones (*N*-HLs) (Fig 6.1) are communication/signaling molecules synthesized by gram-negative bacteria for a process known as quorum sensing. *N*-HLs are biosynthesized from *S*-adenosyl-L-methionine.[176] It was shown previously that different bacteria, e.g., *Vibrio fischeri*,[177] *Burkholderia cepacia*,[178] *Pseudomonas aeruginosa*,[179-181] etc. produce specific *N*-HLs. *N*-HLs differ in the acyl chain length and in the substitution on the third position of the acyl chain, which can be unsubstituted (AHLs), oxo-substituted (OHLs) or hydroxy-substituted (HHLs), see Fig. 6.1. *N*-HLs are chiral due to the stereogenic center located on the α-

position of the γ-butyrolactone ring. Since *N*-HLs are closely related to the amino acid, homoserine, D, L-stereochemical nomenclature is used. HHLs possess another stereogenic center resulting from the hydroxy-group located at the third carbon of the acyl chain, yielding two sets of enantiomers.

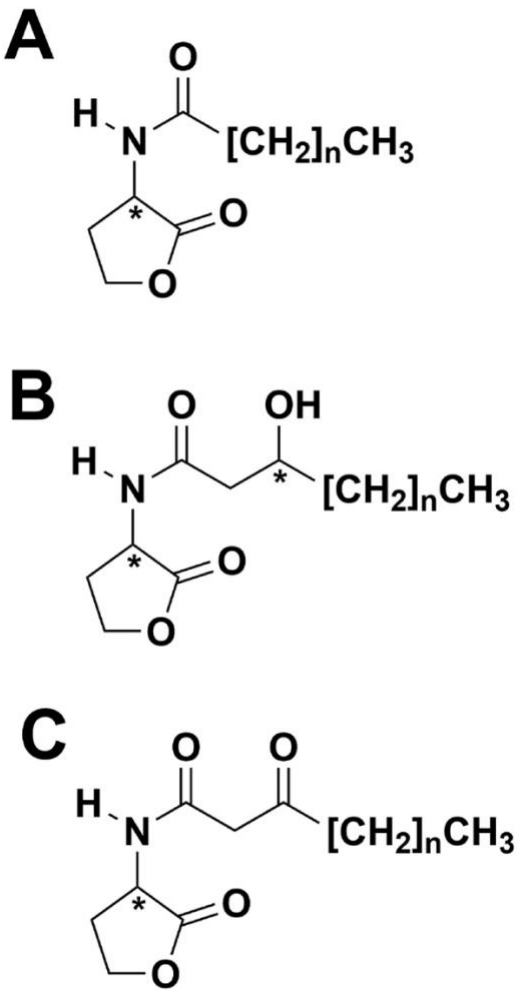

Fig 6.1 **A.** D,L-*N*-acyl homoserine lactones, **B.** D,L-*N*-3-hydroxyacyl homoserine lactones and **C.** D,L-*N*-3-oxoacyl homoserine lactones. Asterisks (*) correspond to chiral centers. For the D,L-*N*-acyl homoserine lactone structures **n** = 2,4,6,8,10 and 12. For the D,L-*N*-3-hydroxyacyl and D,L-N-3-oxoacyl homoserine lactone structures **n** = 2,4,6,8 and 10.

Although quorum sensing pathways employing *N*-HLs have been well known for more than 40 years, the general assumption was that only L-*N*-HLs were biosynthesized by bacteria. Therefore, predominantly achiral methods including biosensors,[182,183] GC-MS,[184] HPLC-UV,[185] LC-MS/MS,[186] MALDI-MS,[187] SFC-MS,[188] and LC-ESI-LTQ-FTICR-MS[189]were developed for their identification and determination. Nevertheless, a few and limited chiral methods for the analysis of D-enantiomers of *N*-HLs have been developed using GC-MS[190-192] and LC-MS.[193] Some chiral separations of *N*-HLs have recently been reported employing GC-MS and LC-MS on standards[194] and to detect and quantify D-*N*-HLs in bacterial cultures.[195] These methods had moderate sensitivity, at best.

Considering the important role of D-amino acids in bacterial metabolism,[196] it is not surprising that D-enantiomers of *N*-HLs have been reported recently in bacteria.[195] It has become clear that methods to detect trace amounts of enantiomeric *N*-HLs (e.g., in the ppb to ppt range) are necessary. To achieve this sensitivity, sample preconcentration with very sensitive detection must be utilized.

Previously single drop microextraction,[191] liquid-liquid extraction[191] and solid phase extraction (SPE)[195,197] were used to purify and preconcentrate *N*-HLs from different matrices. Generally, liquid-liquid extraction is considered unsuitable for trace analysis due to the high volume of the extraction solvents, repeated extractions needed to increase extraction recoveries, and the lack of a high throughput sample processing procedure. In contrast, SPE cartridges with higher loadability (e.g., 1 g of extraction sorbent) can preconcentrate large volumes of sample in a single extraction with high throughput for sample processing.

Highly sensitive detection of *N*-HLs can be achieved by biosensors, LC-MS/MS, and GC-MS/MS. The advantages of using biosensors are their affordable price, fast analysis time, and high sensitivity, which makes them ideal for routine testing and screening of samples. However, biosensors cannot yet compete with the combination of SPE and LC-MS/MS methods in accuracy, reproducibility, reliability of results and the capacity for multi-analyte determination.[198] Furthermore, each bacterium used as a biosensor has different receptor proteins (e.g., *Chromobacterium violaceum*,[199] *Agrobacterium tumefaciens* (TraR)[200] and *Pseudomonas aeruginosa* (LasR)[201] each responding to a distinct range of *N*-HLs. Hence the occurrence of false positive results are possible thereby rendering the comprehensive determination of *N*-HLs with biosensors, unreliable.[184] In contrast, LC or GC coupled in tandem to a triple quadrupole MS using selected reaction monitoring (SRM) is a highly selective and sensitive approach for the detection and quantification of *N*-HLs in complex matrices. Another advantage of using chromatographic techniques coupled with MS/MS is the possibility of comprehensive chiral separations that enable detection and quantification of all D, L-*N*-HL in one analysis.

The aim of this paper is to develop the most sensitive and comprehensive chiral methods for the detection and quantification of trace amounts of six AHLs, six OHLs, and six HHLs using SPE LC-MS/MS and SPE GC-MS/MS. The recovery of the SPE method will be investigated and chromatographic techniques compared in terms of enantioselectivity, enantioresolution, limit of detection (LOD), limit of quantification (LOQ), linearity of calibration curves, and reproducibility. The investigated methods will enable further research on the role of D-*N*-HLs in quorum sensing.

6.2 Experimental

6.2.1 Materials

ZORBAX SB-C18 (4.6 × 150 mm, 5 μm particle size) columns were purchased from Agilent Technologies, Inc. (Santa Clara, CA). CHIRALPAK® IC-3 (250 × 4.6 mm, 3 μm particle size) columns were purchased from Chiral Technologies, Inc. (Ann Arbor, MI). β-DEX™ 225 (30 m × 0.25 mm, 0.25 μm film thickness) and Supel™-Select HLB SPE cartridges were provided by MilliporeSigma (Supelco, Bellefonte, PA). LCMS grade acetonitrile (ACN), LCMS grade methanol (MeOH), LCMS grade water, ACS grade dichloromethane (DCM) and ACS grade ethyl acetate (EtOAc) were purchased from Fisher Chemical (Fischer Scientific, Hampton, NH) High purity formic acid (FA) was purchased from VWR (Randor, PA). Racemic standards of *N*-butanoyl homoserine lactone (A-C4), *N*-hexanoyl homoserine lactone (A-C6), *N*-heptanoyl homoserine lactone (A-C7) *N*-octanoyl homoserine lactone (A-C8), *N*-decanoyl homoserine lactone (A-C10), *N*-dodecanoyl homoserine lactone (A-C12), *N*-tetradecanoyl homoserine lactone (A-C14), *N*-3-oxohexanoyl homoserine lactone (O–C6), *N*-3-oxooctanoyl homoserine lactone (O–C8), *N*-3-oxotetradecanoyl homoserine lactone (O–C14), *N*-3-hydroxyoctanoyl homoserine lactone (H–C8), *N*-3-hydroxydecanoyl homoserine lactone (H–C10), and *N*-3-hydroxytetradecanoyl homoserine lactone (H–C14) were obtained from MilliporeSigma (St. Louis, MO). Racemic standards of *N*-3-oxobutanoyl homoserine lactone (O–C4), *N*-3-oxodecanoyl homoserine lactone (O–C10), *N*-3-hydroxybutanoyl homoserine lactone (H–C4), *N*-3-hydroxy hexanoyl homoserine lactone (H–C6), and *N*-3-hydroxy dodecanoyl homoserine lactone (H–C12) and L-*N*-3-oxododecanoyl homoserine lactone (O–C12) were purchased from Chemodex Ltd. (St. Gallen, Switzerland). All solvents (HPLC and LC-MS grade methanol and acetonitrile, and reagent grade dichloromethane), M9 medium, D-

(+)-glucose, and magnesium sulfate were purchased from MilliporeSigma (St. Louis, MO). A Thermo Scientific™ Barnstead™ GenPure™ Pro water purification system was used for the preparation of deionized (DI) water.

6.2.2 Preparation of stock solutions and full M9 medium

Samples of 2 mg of racemic *N*-HLs were weighed with an analytical balance into 5 mL volumetric flasks. The flasks were filled with acetonitrile to the volume line to yield 400-ppm solutions for each racemic *N*-HLs, except for 3-oxododecanoyl-homoserine lactone which was a 400-ppm solution for the L-enantiomer. From the 400-ppm *N*-HL stock solutions, 1-ppm and 4 ppm working solutions were prepared for standards and the internal standard, respectively. M9 medium was prepared according to instructions and autoclaved to sterilize. Full M9 medium was completed with filter sterilized 20% (w/w) glucose and 1 M magnesium sulfate.

6.2.3 Sample preparation

A 100 µL aliquot of a 1-ppm working solution of AHLs, OHLs and HHLs in acetonitrile (C4–C14 AHLs; C4–C12 OHLs; C4–C14 HHLs) was used for the LC-MS/MS method development. The same working solution was used for the method development in GC-MS/MS with aliquots placed in 2 mL sample vials, dried with a gentle stream of ultrahigh purity N_2, and derivatized with the method described below.

The samples for quantification and extraction recovery were prepared using an SPE manifold coupled to a vacuum pump. The SPE cartridges were conditioned with 10 mL each of acetonitrile, methanol, and water respectively. Then, 10 mL of full M9 medium spiked with internal standard (A-C7) working solution and *N*-HLs working solution was loaded on the SPE cartridge and processed. Subsequently, the cartridge was washed with 10 mL of 95:5 methanol: water and eluted with 11 mL of acetonitrile. The extracts were then evaporated using a rotatory

evaporator and transferred in 2 mL of dichloromethane. Transferred samples were evaporated using a gentle stream of ultrahigh purity N_2. The evaporated samples were either reconstituted with 100 μL of methanol for the analysis in LC-MS/MS or further derivatized for GC-MS/MS.

6.2.4 Derivatization for GC-MS/MS analysis

Derivatization of OHLs and HHLs was conducted by adding a 75 μL of BSTFA with 1% TMCS and a 25 μL aliquot of acetonitrile as a co-solvent to the dried standard solution or biological sample and sealed with a PTFE lined cap. The solution was then mixed for 10 s and placed into a 130 °C preheated sand bath for 45 min.

6.2.5 LC-MS/MS

A Shimadzu LC-MS 8040 system (Shimadzu Scientific Instruments, Columbia MD) with electrospray ionization and a triple quadrupole mass spectrometer was used in the positive ion mode for the LC-MS/MS analysis. The analysis was done in SRM with optimized transitions and collision energies for each enantiomeric standard. All SRM transitions used in this study are given in Table S1 in the Supplemental Materials. The nebulizing gas flow and drying gas flow were 3.0 and 15.0 L/min respectively. The interface voltage was 4.5 kV and the heat block temperature was 400 °C. A ZORBAX SB-C18 column was used in tandem with a CHIRALPAK IC-3. A flow rate of 0.4 mL/min was used with a gradient method starting at water (0.1% FA):methanol (0.1% FA): (40:60) from 0 to 25 min, with a ramp from (40:60) to (10:90) from 25 to 37.5 min. Then a step gradient from (10:90) to (5:95) from 37.50 to 37.51 min and held at (5:95) from 37.51 to 50 min was implemented.

6.2.6 GC-MS/MS

Samples were run on a Shimadzu GCMS-TQ 8040 (Shimadzu Scientific Instruments, Columbia, MD, USA) equipped with a β-DEX 225™ column (30 m × 0.25 mm x 0.25 μm film

thickness) (25% 2,3-di-*O*-acetyl-6-*O*-TBDMS-β-cyclodextrin in SPB-20 poly [20% phenyl/80% dimethylsiloxane]) (Millipore-Sigma, Burlington, MA, USA). A split-less injection of 1 μL with 2-min split-time, ending at a split ratio of 20:1 was delivered (220 °C). The constant flow of carrier gas (He) was 1.1 mL/min (40 cm/s), with an oven temperature program starting at 160 °C (10-min hold) increased at a rate of 1 °C/min to 230 °C (50-min hold). A GC-MS interface temperature and MS ion source temperature were set to 230 °C and 280 °C, respectively. EI was adjusted to 70 eV and the mass spectrometer was operated in SRM mode with optimized collision energies and quadrupole one and quadrupole three voltages.

6.2.7 Extraction recovery

The extraction recovery was assessed in quintuplicate for a final concentration of 100 ppb. Firstly, a 10 mL amount of full M9 medium was spiked with 10 μL of working solution (1 ppm) ("pre-spike") and subsequently processed as outlined in the Sample Preparation section above. A 7.5 μL internal standard working solution (4 ppm) was added to the reconstituted sample (2 mL of dichloromethane) before the last evaporation step. Secondly, a blank 10 mL amount of full M9 medium was processed as outlined in the Sample Preparation section above. Then, 10 μL of working solution (1 ppm) and 7.5 μL of internal standard working solution (4 ppm) were spiked ("post-spike") into the reconstituted sample (2 mL of dichloromethane). As indicated in the previous "Sample Preparation" section, the dichloromethane was evaporated using a gentle stream of ultra-high purity N_2 and then reconstituted in 100 μL of methanol. All samples were analyzed using LC-MS/MS. Extraction recovery was calculated as the ratio of area corrected with internal standard in "pre-spike" and "post-spike" samples.

6.2.8 Quantitation

The calibration curves were measured in quintuplicate. For LC-MS/MS, a 10 mL of full M9 medium was spiked with 1, 2.5, 5, 10, 25, 50, 100 and 200 μL of *N*-HL working solution (1 ppm) and 7.5 μL of internal standard working solution (4 ppm). For GC-MS/MS, a 10 mL of full M9 medium was spiked with 50, 75, 100, 150 and 200 μL of *N*-HLs working solution (1 ppm) and 100 μL of internal standard working solution (4 ppm).

6.3 Results and discussion

The *N*-HLs have widely varying alkyl chain lengths (i.e., from C4 to C14 in this study). Thus, the shorter alkyl chain length *N*-HLs are more hydrophillic and the longer chain length ones are more hydrophobic. Consequently, both the extraction/preconcentration steps and the chromatographic approach must be optimized to take these variables into account.

6.3.1 Solid-phase extraction

In a previous study, the extraction recovery of 13 AHLs was tested on polyamidic, ion exchange, primary-secondary amine, end capped octadecyl silica-bonded, and hydrophilic-lipophilic balanced (HLB) SPE cartridges.[197] The highest recoveries were observed for the HLB sorbent. However, the most hydrophilic *N*-HLs; H–C4-homoserine lactone, O–C4-homoserine lactone and H–C6-homoserine lactone were not tested. Therefore, a more comprehensive recovery study using the HLB sorbent has been carried out for the 18 *N*-HLs in this study, including the more challenging polar derivatives.

N-HLs are produced in trace amounts by individual bacterial species, thus a preconcentration factor of 100 is considered optimal during extraction. It is clear that

preconcentration will increase the sensitivity of the method, however, the drawback of this approach is the preconcentration of other compounds present in the sample matrix, possible impurities in organic solvents and leachable compounds from the laboratory consumables. The presence of these substances in the electrospray ion source concurrently with *N*-HLs can cause suppression or enhancement of analyte ionization. If the presence of these compounds in samples varies over time, the reproducibility of method is diminished.

It was found that the initial extractions of standard samples spiked in M9 growth medium were not reproducible (%RSD >20), with multiple matrix peaks observed throughout the chromatogram. Several experiments were carried out to find the source of these unwanted contaminants, including blanks of preconcentrated organic solvents used during sample preparation and extraction blanks of 10 mL of pure M9 medium. The source of the contaminants was identified as leachable polymers from the SPE cartridge itself. Pretreatment of the cartridge with the elution solvent was applied as an extra step before the conditioning of HLB cartridges to limit leaching during the elution step.

The extraction of polar compounds from polar matrices is known to be challenging. In this case, polar matrix compounds affected the extraction recovery and reproducibility of the early eluting polar *N*-HLs. To limit or prevent the presence of polar matrix molecules in the final sample, the evaporated extracts were reconstituted in organic solvent, transferred to another vial, evaporated again and finally reconstituted in the sample solvent. Three different organic solvents were tested (i.e., DCM, EtOAc, and MeOH). In the case of DCM and EtOAc, the matrix molecules eluting near the dead volume were substantially reduced compared to MeOH with the highest recoveries achieved using DCM.

Introducing the pretreatment of SPE cartridges with the elution solvent, together with using DCM as the transferring solvent, significantly increased the reproducibility of the extraction recovery and reduced the number of matrix peaks. The final extraction recoveries for all *N*-HLs in the study ranged from 80% to 105% except for H–C4, O–C4, and A-C14 which were 4%, 10%, and 70%, respectively (Fig 6.2). The low recoveries of H–C4 and O–C4 are the likely reason why these compounds were rarely detected or reported in previous real bacterial samples.

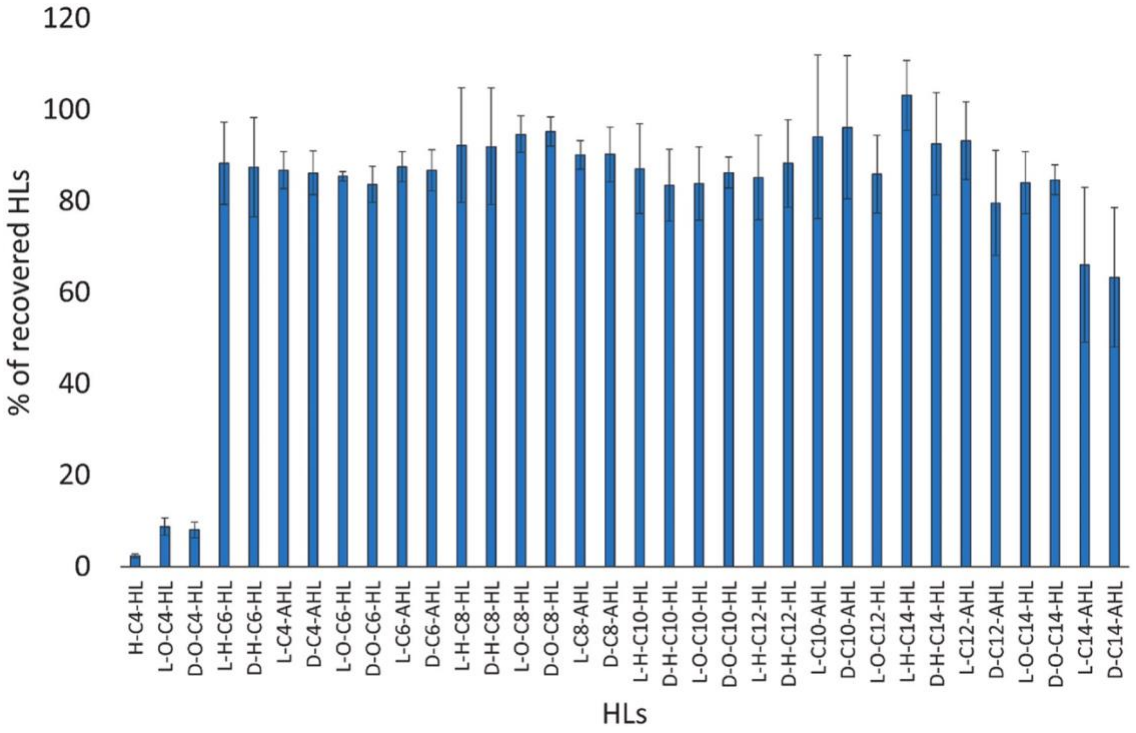

Fig 6.2 Acquired percent Recovery for 100 ppb D,L-*N*-acyl homoserine lactones, D,L-*N*-3-hydroxyacyl homoserine lactones and D,L-*N*-3-oxoacyl homoserine lactones. Standards processed by SPE in quintuplicate and analyzed by LC-MS/MS. Method described in Extraction Recovery under the Experimental section.

6.3.2 LC-MS/MS method

The chiral separations of all compounds were achieved using immobilized cellulose *tris*(3,5-dichlorophenylcarbamate). However, the retention of all *N*-HLs on this stationary phase is very low, resulting in co-elution of all peaks just after the dead volume of the column. This co-elution leads to inevitable ionization suppression and inaccurate quantification. To overcome this issue, a stationary phase with a different selectivity is needed. A similar problem was encountered and solved earlier by connecting, in-tandem, a C18 column with the chiral column**.** This approach was briefly presented for the chiral separation of 6 AHLs,[194] not including OHLs and HHLs. However, peaks for A-C6, A-C8, and A-C10 still co-eluted and A-C4 was omitted. The connection of the C18 column with cellulose *tris*(3,5-dichlorophenylcarbamate) allowed the separation of all homologous compounds along with the enantio-separation of seven AHLs, six OHLs, and six HHLs (Fig. 6.3). All OHLs and AHLs were baseline separated with L-enantiomers always eluting before D-enantiomers (Table 6.1). These results could not be confirmed for the analyte O–C12 due to the lack of a racemic standard or the pure D-enantiomer. In the case of the HHLs, four peaks were obtained for the C10 and C14 compounds, three peaks for the C6, C8, and C12 compounds, and two peaks were observed for the C4 analytes, respectively. The chiral elution order of HHLs followed the same trend as for other *N*-HLs derivatives, i.e., L-enantiomers are eluted before D-enantiomers.

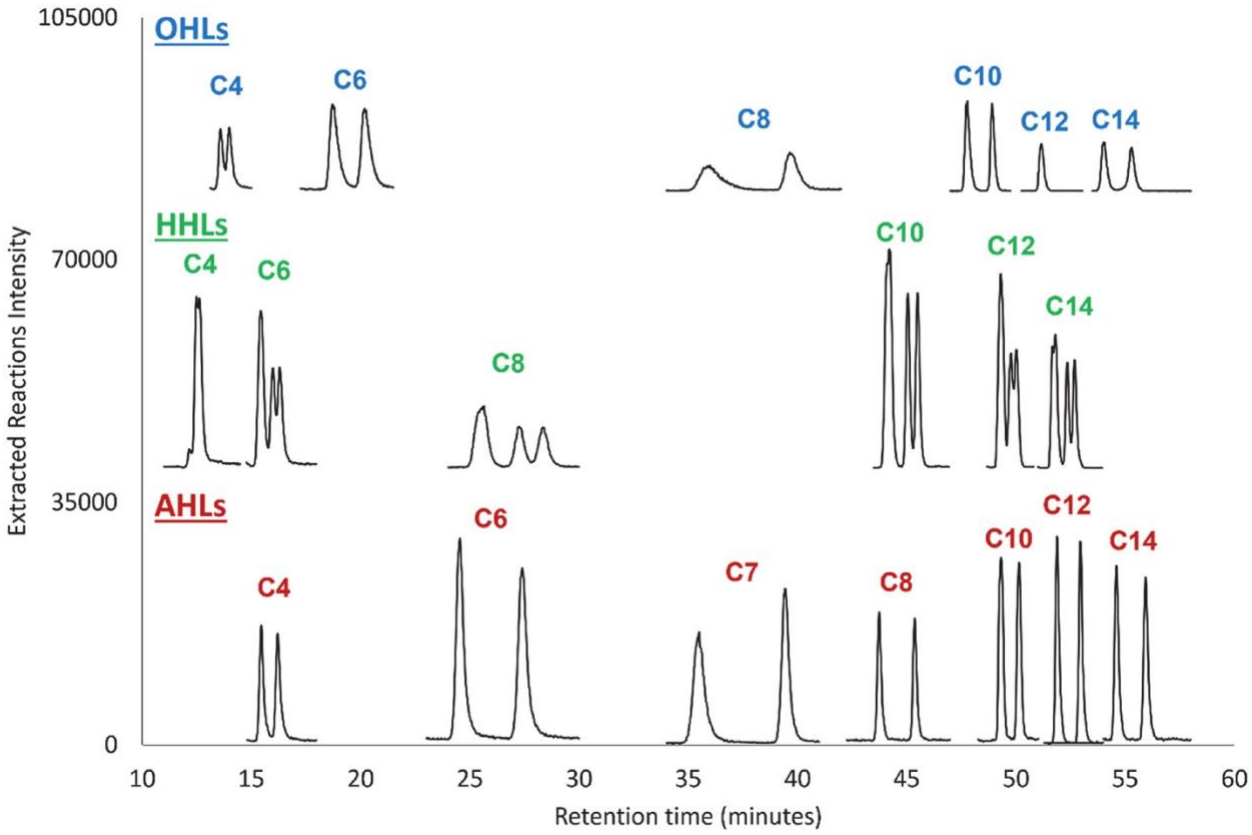

Fig 6.3 LC SRM chromatogram for $[M+H]^+$ to 102 *m/z* for D,L-*N*-acyl homoserine lactones (AHLs), D,L-*N*-3-hydroxyacyl homoserine lactones (HHLs) and D,L-*N*-3-oxoacyl homoserine lactones (OHLs). Chromatographic conditions are outlined in the Chromatographic and MS Conditions. Chromatograms are offset for visual clarity. LC SRM transition are detailed in Supplementary information.

The identification of *N*-HLs was carried out by the conformity of retention time, and three different SRM transitions. To increase the certainty of identification, the ratios of the SRM transitions can be calculated and compared. This identification can be carried out only for peaks that are over the LOD of the chromatographic method (see Section 6.3.4). A previously reported

LC-MS method had approximately two orders of magnitude higher LODs which was insufficient for many biological studies.[194] Therefore, this more sensitive LC-MS/MS analysis can be readily used as the scouting method for the identification of D-*N*-HLs in various matrices, e.g., bacterial medium, nasal lavages, earwashes, wastewater, etc.

The LOQs for all the compounds is below 10 ppb excluding A-C10 and O–C14. The quantitation was carried out using calibration curves for analytes with 6–8 concentration levels of pentaplicate standards spiked into full M9 bacterial medium and processed by the sample preparation method described herein (see Experimental). The linearity of calibration curves was higher than 0.99 in all cases. The precision was calculated as the relative standard deviation and was consistently lower than 20% for AHLs and HHLs and 30% for OHLs. The calculated LODs and LOQs are discussed in Section 6.3.4. The real lower limit of quantification (LLOQ); i.e., the lowest point on the calibration curve was as low as 5 ppb.

6.3.3 GC-MS/MS method

A previously developed chiral method using GC coupled with a single quadrupole MS[194] was used for the analysis of 17 *N*-HLs). The chromatographic method presented herein was coupled with a triple quadrupole MS system allowing for a more sensitive and specific technique compared to the aforementioned method. The enantioseparation of the *N*-HLs in this study was carried out using a β-DEX 225 GC column (Table 6.2, Fig. 6.4).

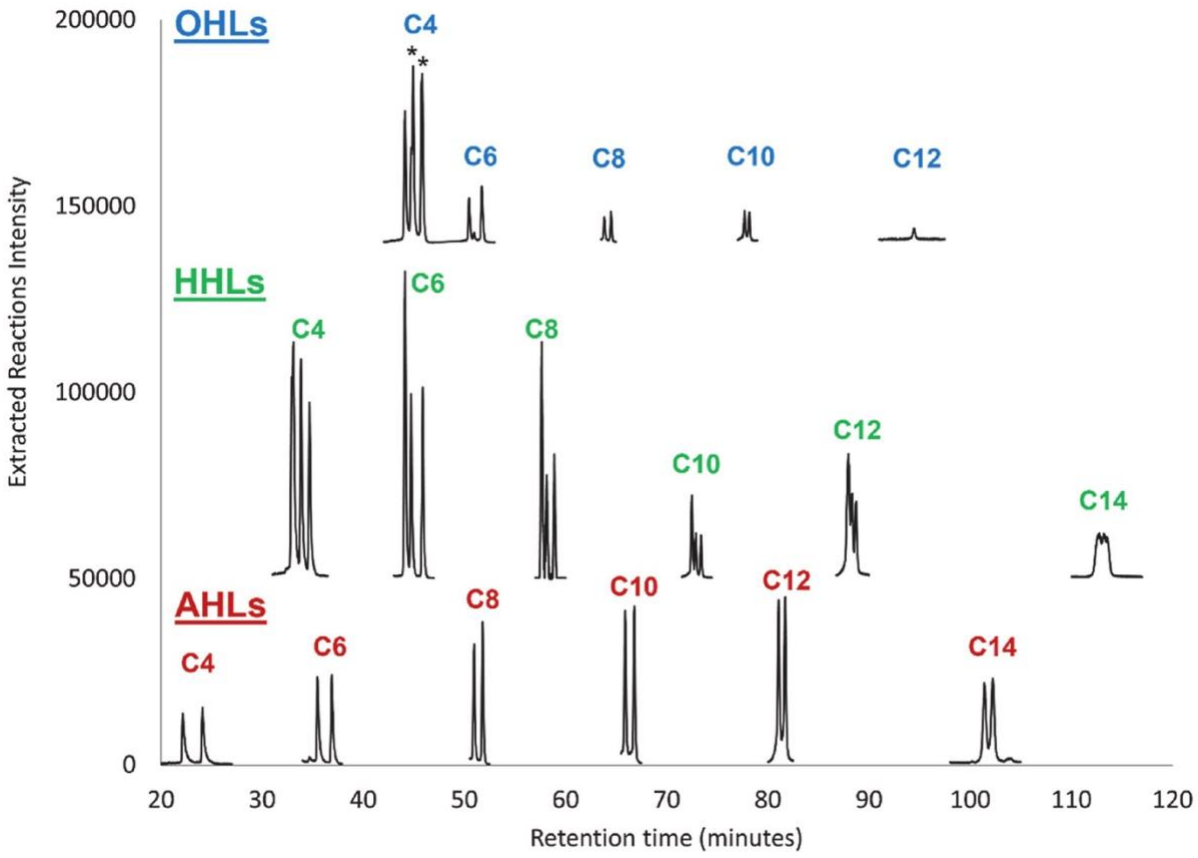

Fig. 6.4 GC SRM chromatogram for D,L-*N*-acyl homoserine lactones (AHLs), D,L-*N*-3-hydroxyacyl homoserine lactones (HHLs) and D,L-*N*-3-oxoacyl homoserine lactones (OHLs). Chromatographic conditions are outlined in the Chromatographic and MS Conditions. Chromatograms are offset for visual clarity.

This particular stationary phase has an advantage when it comes to separating chiral homologous series due to the presence of both an achiral stationary phase and chiral selector. The 75% of SPB-20 (20 poly [20% phenyl/80% dimethylsiloxane]) enabled the separation of the homologous *N*-HLs, while concurrently the 25% of 2,3-di-*O*-acetyl-6-*O*-TBDMS-β-cyclodextrin, that is dissolved in SPB-20, provided chiral resolution for the *N*-HLs

enantiomers (Table 6.2). The AHLs can be analyzed by GC without derivatization. Due to their decomposition at high temperatures and low sensitivity, respectively, derivatization of OHLs and HHLs is required. The oxidized carbon on the acyl chain is derivatized by using BSTFA with 1% TMCS as a trimethylsilyl (TMS) donor to the oxygen atom (see Experimental). When OHLs are derivatized, the carbonyl reacts with the TMS, with an unsaturated bond forming between carbons 2 and 3 on the acyl chain, no new stereogenic center is created in this process. When HHLs are derivatized, the hydroxyl- moiety is derivatized with TMS and no change in chirality occurs.

For the six *N*-HLs, the best resolution between enantiomers is observed for the A-C4 which is baseline separated in 25 min. GC resolution between enantiomeric pairs decreases as the alkyl chain length increases with partial coelution apparent for A-C12 and A-C14 (Table 6.2, Figure 6.4). For the five TMS-OHLs the best resolution is observed for TMS-*O*-C4. A decrease in resolution with increasing chain length is again apparent with partial coelution starting with TMS-*O*-C10. Separation between enantiomers of TMS-*O*-C12 was inconclusive because of the unavailability of a racemic standard. HHLs retain their two chiral centers, after derivatized with TMS, thus four possible stereoisomers may be present. Four distinct peaks are visible for racemic TMS-H-C4. The first two peaks being L-HHLs, which are only partially separated and the last two peaks being D-*N*-HLs which are baseline separated. The chiral retention order for L- and D-*N*-HLs remains for TMS-H-C6 through TMS-H-C14, however, the partial separation of the L-enantiomers is lost from C6 onward. Resolution between L- and D-TMS-HHLs decreases with increasing chain length with partial coelution apparent at TMS-H-C10 (Fig. 6.4).

6.3.4 Comparison of chiral separation methods of N-HLs

Until now, all comprehensive chiral analytical methods involving *N*-HLs were carried out with GC-MS (single quadrupole). The limit of detection for these methods was around 1 ppm.[191,194,195] However, the concentrations of *N*-HLs in nasal lavages, wastewater, and bacterial medium can be 10 to 1000 times lower. GC coupled with triple-quadrupole was employed and LODs as low as 63 ppb were obtained (Table 6.3). Even lower LOD and LOQ were obtained using LC-MS/MS. Therefore, both GC-MS/MS (QqQ) and LC-MS/MS (QqQ) methods can be used as complementary approaches for the chiral separation of *N*-HLs in biological samples. Deciding which technique to use depends on the available instrumentation and the application of the analytical method. The main advantage of LC-MS/MS over GC-MS/MS is the lack of derivatization of HHLs and OHLs, two times faster analysis time, higher sensitivity, and a lower number of artificial peaks from the matrix. Despite these drawbacks, higher resolution of the smaller more hydrophilic *N*-HLs was obtained in GC-MS/MS. In contrast, higher resolution for more hydrophobic *N*-HLs was achieved in LC-MS/MS.

The use of the chiral LC-MS/MS method is suggested for scouting and quantification methods. Chiral GC-MS/MS methods developed herein should be used preferably for confirmation of the results obtained by LC-MS/MS. The double confirmation increases specificity towards *N*-HLs and will ameliorate the sensitivity and reproducibility issue of the results obtained by previous chiral and achiral analytical methods.[191,194,195]

Table 6.1 Optimized chiral separations of L/D-homoserine lactones by LC-MS/MS.

Analyte	***No. of isomers***	$t_{R1\ (min)}$[a]	$t_{R2\ (min)}$[b]	R_s[c]
L, D C4-HSL	2	15.33	16.06	2.00
L, D C6-HSL	2	24.07	26.78	4.12
L, D C8-HSL	2	43.40	45.04	4.87
L, D C10-HSL	2	49.14	50.00	2.20
L, D C12-HSL	2	51.76	52.76	2.62
L, D C14-HSL	2	54.38	55.68	3.44
P_1, P_2, P_3, P_4 [d] 3-hydroxy-C4-HSL[e]	4	12.45	not separated	0.00
P_1, P_2 3-hydroxy-C6-HSL	2	15.32	not separated	0.00
P_2, P_3 3-hydroxy-C6-HSL	2	15.32	15.84	1.10
P_3, P_4 3-hydroxy-C6-HSL	2	15.84	16.15	0.65
P_1, P_2 3-hydroxy-C8-HSL	2	25.03	not separated	0.00
P_2, P_3 3-hydroxy-C8-HSL	2	25.03	27.66	2.82

P_3, P_4 3-hydroxy-C8-HSL	2	27.66	28.85	1.53
P_1, P_2 3-hydroxy-C10-HSL	2	43.77	43.91	0.30
P_2, P_3 3-hydroxy-C10-HSL	2	43.91	44.75	1.37
P_3, P_4 3-hydroxy-C10-HSL	2	44.75	45.18	1.20
P_1, P_2 3-hydroxy-C12-HSL	2	49.17	not separated	0.00
P_2, P_3 3-hydroxy-C12-HSL	2	49.17	49.61	0.81
P_3, P_4 3-hydroxy-C12-HSL	2	49.61	49.88	0.43
P_1, P_2 3-hydroxy-C14-HSL	2	51.50	51.69	0.30
P_2, P_3 3-hydroxy-C14-HSL	2	51.69	52.18	1.18
P_3, P_4 3-hydroxy-C14-HSL	2	52.18	52.50	0.91
L, D 3-oxo-C4-HSL	2	13.52	13.91	1.00
L, D 3-oxo-C6-HSL	2	18.44	19.87	1.96

L, D 3-oxo-C8-HSL	2	34.90	38.93	3.02
L, D 3-oxo-C10-HSL	2	47.47	48.64	2.98
L, D 3-oxo-C14-HSL	2	53.77	55.02	2.60

[a] Retention time of first peak.
[b] Retention time of second peak.
[c] Resolution between indicated peaks.
[d] P_1, P_2, P_3, P_4 stands for first, second, third, and fourth eluted peak of HHLs, respectively.
[e] 3-hydroxy-C4-HSL is eluted as one peak.

Table 6.2 Optimized chiral separations of L/D-homoserine lactones by GC-MS/MS.

Analyte	*No. of isomers*	t_{R1} *(min)*[a]	t_{R2} *(min)*[b]	R_S[c]
L, D C4-HSL	2	22.16	24.11	4.65
L, D C6-HSL	2	35.30	36.93	3.44
L, D C8-HSL	2	50.95	51.72	2.48
L, D C10-HSL	2	65.89	66.80	3.17
L, D C12-HSL	2	81.06	81.70	2.03
L, D C14-HSL	2	101.40	102.23	1.45
P_1, P_2 3-hydroxy-C4-HSL[d]	2	33.08	not separated	0.00
P_2, P_3 3-hydroxy-C4-HSL[d]	2	33.08	33.85	1.81
P_3, P_4 3-hydroxy-C4-HSL[d]	2	33.85	34.68	2.52
P_1, P_2 3-hydroxy-C6-HSL[d]	2	44.13	not separated	0.00
P_2, P_3 3-hydroxy-C6-HSL[d]	2	44.13	44.73	1.49

P3, P4 3-hydroxy-C6-HSL[d]	2	44.73	45.87	4.03
P1, P2 3-hydroxy-C8-HSL[d]	2	58.53	not separated	0.00
P2, P3 3-hydroxy-C8-HSL[d]	2	58.53	58.85	1.62
P3, P4 3-hydroxy-C8-HSL[d]	2	58.85	59.88	3.86
P1, P2 3-hydroxy-C10-HSL[d]	2	72.49	not separated	0.00
P2, P3 3-hydroxy-C10-HSL[d]	2	72.49	72.88	1.37
P3, P4 3-hydroxy-C10-HSL[d]	2	72.88	73.41	2.01
P1, P2 3-hydroxy-C12-HSL[d]	2	87.97	not separated	0.00
P2, P3 3-hydroxy-C12-HSL[d]	2	87.97	88.29	0.66
P3, P4 3-hydroxy-C12-HSL[d]	2	88.29	88.71	0.93
P1, P2 3-hydroxy-C14-HSL[d]	2	112.74	not separated	0.00
P2, P3 3-hydroxy-C14-HSL[d]	2	112.74	113.24	0.14
P3, P4 3-hydroxy-C14-HSL[d]	2	113.24	113.54	0.11
L, D 3-oxo-C4-HSL	2	44.91	45.81	1.64
L, D 3-oxo-C6-HSL	2	50.68	51.76	3.57
L, D 3-oxo-C8-HSL	2	63.84	64.52	2.83
L, D 3-oxo-C10-HSL	2	77.70	78.16	2.21

[a] Retention time of first peak.

[b] Retention time of second peak.

[c] Resolution between indicated peaks.

[d] P1, P2, P3, P4 stands for first, second, third, and fourth eluted peak of HHLs, respectively

Table 6.3 Comparison of enantiomeric quantification of homoserine lactones using LC-MS/MS and GC-MS/MS. Samples extracted by SPE.

Analyte	**LC -MS/MS**			**GC – MS/MS**		
	LOD (ppb)	**LOQ (ppb)**	**R^2**	**LOD (ppb)**	**LOQ (ppb)**	**R^2**
L C4-HSL	4	13	0.9981	<LOD	<LOD	<LOD
D C4-HSL	2	7	0.9964	<LOD	<LOD	<LOD
L C6-HSL	2	7	0.9993	382	1160	0.9730
D C6-HSL	3	11	0.9992	242	735	0.9890
L C8-HSL	3	9	0.9994	307	932	0.9824
D C8-HSL	3	9	0.9998	566	1716	0.9426
L C10-HSL	7	23	0.9991	336	1018	0.9635
D C10-HSL	8	27	0.9992	880	2667	0.9425
L C12-HSL	5	16	0.9995	210	637	0.9854
D C12-HSL	2	8	0.9918	63	192	0.9987
L C14-HSL	4	13	0.9979	418	1268	0.9444
D C14-HSL	6	19	0.9965	366	1109	0.9569
3-hydroxy-C4-HSL	Quantitation was not possible because of low extraction recovery.					
P_1 + **P_2** [a] 3-hydroxy-C6-HSL	4	13	0.9972	221	671	0.9838
P_3 + **P_4** [a] 3-hydroxy-C6-HSL	5	15	0.9977	209	632	0.9586
P_1 + **P_2** 3-hydroxy-C8-HSL	5	16	0.9976	123	374	0.9949

P₃ + **P₄** 3-hydroxy-C8-HSL	5	15	0.9980	3588	10,872	0.8443
P₁ + **P₂** 3-hydroxy-C10-HSL	4	14	0.9996	1296	3926	0.8833
P₃ + **P₄** 3-hydroxy-C10-HSL	3	11	0.9989	1180	3575	0.9725
P₁ + **P₂** 3-hydroxy-C12-HSL	4	12	0.9982	83	251	0.9977
P₃ + **P₄** 3-hydroxy-C12-HSL	5	15	0.9951	535	1621	0.9744
P₁ + **P₂** 3-hydroxy-C14-HSL	2	7	0.9908	417	1264	0.9448
P₃ + **P₄** 3-hydroxy-C14-HSL	1	5	0.9986	137	414	0.9872
L 3-oxo-C4-HSL	Quantitation was not possible because of low extraction recovery.					
D 3-oxo-C4-HSL	Quantitation was not possible because of low extraction recovery.					
L 3-oxo-C6-HSL	2	8	0.9905	678	2057	0.9159
D 3-oxo-C6-HSL	4	13	0.9900	515	1561	0.9498
L 3-oxo-C8-HSL	2	7	0.9911	<LOD	<LOD	<LOD
D 3-oxo-C8-HSL	2	6	0.9905	<LOD	<LOD	<LOD
L 3-oxo-C10-HSL	4	13	0.9917	<LOD	<LOD	<LOD
D 3-oxo-C10-HSL	2	6	0.9911	446	1338	0.9625
L 3-oxo-C12-HSL	2	7	0.9891	742	2250	0.9081
L 3-oxo-C14-HSL	15	50	0.9917	n.a.	n.a.	n.a.
D 3-oxo-C14-HSL	15	51	0.9866	n.a.	n.a.	n.a.

n.a. = not applicable (this analyte was not analyzed with GC-MS/MS).

[a] P_1, P_2, P_3, P_4 stands for first, second, third, and fourth eluted peak of HHLs, respectively.

6.4 Conclusions

Comprehensive analytical approaches for the analysis of *N*-HLs including sample preparation (SPE), chiral LC-MS/MS and chiral GC-MS/MS were developed. The extraction recovery for the majority of *N*-HLs ranged from 80% to 105%. The LC-MS/MS method outperforms GC-MS/MS in sensitivity, time of the analysis, and ease of use. Therefore, it is the method of choice with GC-MS/MS being used preferably for the confirmation of results. However, GC-MS/MS provided better stereoisomeric resolution of the smaller, more hydrophilic *N*-HLs. These newly developed, sensitive methods will aid to unveil the role of not only D-*N*-HLs in bacteria *in vitro* but subsequently *in vivo*.

Chapter 7 General summary

Chapter 2 details the achiral separation of AQC-derivatized amino acids across 4 commonly used detection modes. This is the first LOD study to encompass UV, fluorescence, single quadrupole and MRM detection modes for AQC-amino acids. UV detection yielded the highest LODs for the majority of AQC-amino acids. Single quadrupole, or essentially SIM, yielded comparable results to UV. Fluorescence detection was highly sensitive with most LODs <0.1 pmol. MRM detection was comparable with fluorescence in LOD ranges for roughly half of the AQC-amino acids that were screened. LODs for AQC-Asn and AQC-Gln were reported as without incident in contrast to contemporary reports which often omitted the LODs of these analytes. An explanation for the low LODs for AQC-cysteine across multiple detection modes were presented. Additionally, the low fluorescence response of AQC-Trp was addressed and causes for this were discussed.

Chapter 3 reported the intracellular and extracellular profiles for L- and D-amino acids in human breast cancer (MCF-7) vs non-tumorigenic breast cells (MCF-10A) for the first time. The

tumorous cells always had elevated levels of L-amino acids with the exception of L-Asn. Interestingly, the levels of D-Ser and D-Asp were significantly higher in the cancerous cells when compared to the normal cells and could be possible oncometabolites. The effect of D-amino acid agonists on blockaded NMDA receptors was investigated as well. It was suggested that cancer cells may be producing an increased amount of NMDA receptor agonists to resuscitate blockaded channels. This study also featured a chiral method on a modified quinine stationary phase that was able to enantiomerically separate the derivatized analytes with the D-enantiomer as the first eluting analyte.

Chapter 4 introduced the enzymatic method of using carboxypeptidase Y as a scouting enzyme for peptides containing D-amino acids. This is based on the stereospecificity of hydrolytic enzymes, most of which are designed to hydrolyze peptides and proteins comprised solely of L-amino acids. CPA and CPY were investigated in this study. AQC-derivatization of peptides greatly increased their susceptibility to hydrolysis with both enzymes. It was determined that CPA was too limited in substrate compatibility with the peptides used in this study. CPY was found to be more suitable as a scouting enzyme for D-amino acids in peptides due to its lack of substrate specificity. Additionally, CPY fully hydrolyzed all AQC-peptides that were screened to the N-terminus amino acid residue. Optimal conditions for hydrolyzing acidic and basic residues are discussed. D-amino acids within peptides were found to be hydrolyzed at a significantly slower rate whereas the L-amino acid residues were rapidly hydrolyzed from the polypeptide chain. This enzymatic methodology would be a useful tool for locating and detecting D-amino acids within primary structures.

Chapter 5 investigates the feasibility of using teicoplanin aglycone as a solid phase extraction media due to the stronger retentions of D-amino acids and C-terminal D-amino acid

containing peptides on the stationary phase. Retention curves plotting retention factor versus varying ratios of methanol:water were reported for all enantiomeric separations of amino acids on TAG. The addition of ammonium formate was found to lower retention time and decrease the enantioselectivity for amino acids. A mutual cutoff between C-terminal D-amino acid containing peptides and peptides with L-amino acids on the C-terminus was achieved for all glycyl- and alanyl- dipeptides screened using TAG stationary phase. In these two peptide groups, all C-terminal L-amino acid peptides eluted prior to the cutoff and all C-terminal D-amino acid peptides eluted after the cutoff under these chromatographic conditions. Retention curves plotting retention factor versus different ratios of methanol:water were also constructed for synthetic peptides. This U-shaped curve suggested that mobile phases with higher methanol:water ratios yielded greater selectivity and increased retention of D-amino acid containing peptides on TAG. An epimeric mixture of enkephalins was hydrolyzed with CPY at a 90:10 and 70:30 ratio of the L-amino acid exclusive containing peptide to the D-amino acid containing peptide. The C-terminal D-amino acid containing peptide intermediate persisted in solution whereas the L-amino acid exclusive peptide was fully hydrolyzed.

Chapter 6 features the most comprehensive analytical LC-MS/MS and complimentary GC-MS/MS methods for the quantitation of N-homoserine lactone homologues. The percent recoveries from extraction studies were within an acceptable range. The LC-MS/MS was significantly more sensitive than the GC-MS/MS method. However, hydrophilic homoserine lactones with shorter acyl chains that lack resolution in LC could be resolved by GC. Confirming the identity of novel homoserine lactones could also be done with GC-MS/MS. It is the development of these sensitive methods that will aid in uncovering the role of not only D-*N*-HLs in bacteria *in vitro* but subsequently *in vivo*.

References

(1) Ilisz, I.; Berkecz, R.; Péter, A. HPLC separation of amino acid enantiomers and small peptides on macrocyclic antibiotic-based chiral stationary phases: A review. *J. Sep. Sci.* **2006**, *29* (10), 1305-1321. DOI: https://doi.org/10.1002/jssc.200600046.

(2) Jeschke, P. Current status of chirality in agrochemicals. *Pest Manag. Sci.* **2018**, *74* (11), 2389-2404. DOI: https://doi.org/10.1002/ps.5052.

(3) Silvestri, I. P.; Colbon, P. J. J. The Growing Importance of Chirality in 3D Chemical Space Exploration and Modern Drug Discovery Approaches for Hit-ID. *ACS Med. Schem. Lett.* **2021**, *12* (8), 1220-1229. DOI: 10.1021/acsmedchemlett.1c00251.

(4) Church, D. D.; Hirsch, K. R.; Park, S.; Kim, I.-Y.; Gwin, J. A.; Pasiakos, S. M.; Wolfe, R. R.; Ferrando, A. A. Essential Amino Acids and Protein Synthesis: Insights into Maximizing the Muscle and Whole-Body Response to Feeding. *Nutrients.* **2020**, *12* (12), 3717.

(5) Bröer, S.; Bröer, A. Amino acid homeostasis and signalling in mammalian cells and organisms. *Biochem.* **2017**, *474* (12), 1935-1963. DOI: 10.1042/bcj20160822

(6) Pappa, K. I.; Vlachos, G.; Theodora, M.; Roubelaki, M.; Angelidou, K.; Antsaklis, A. Intermediate metabolism in association with the amino acid profile during the third trimester of normal pregnancy and diet-controlled gestational diabetes. *AJOG.* **2007**, *196* (1), 65.e61-65.e65. DOI: https://doi.org/10.1016/j.ajog.2006.06.094.

(7) Kogl, F.; Erxleben, H. The glutamic acid of tumour proteins. *Nature.* **1939**, 144: 111-111.

(8) Konikova, A. Glutamic Acid of Proteins. *Nature.* **1940**, *145* (3669), 312-312. DOI: 10.1038/145312a0.

(9) Konikova, A.S., Dobbert, N.N. *Biokhimiya* **1948**, 13:115-123.

(10) Stevens, C.M.; Halpern, P.E.; Gigger, R.P. Occurrence of D-amino acids in some natural materials. *J. Biol. Chem.* **1951**, 190(2): 705-710.

(11) Park, J.T.; Strominger, J.L. Mode of Action of Penicillin. Biochemical Basis for the Mechanism of Action of Penicillin and for Its Selective Toxicity. *Science.* **1957**, 125(3238):99-101.

(12) Aliashkevich, A.; Alvarez, L.; Cava, F. New Insights Into the Mechanisms and Biological Roles of D-Amino Acids in Complex Eco-Systems. *Frontiers in Microbiology.* **2018**, *9*, Review. DOI: 10.3389/fmicb.2018.00683.

(13) Lu, J.; Xu, H.; Xia, J.; Ma, J.; Xu, J.; Li, Y.; Feng, J. D- and Unnatural Amino Acid Substituted Antimicrobial Peptides With Improved Proteolytic Resistance and Their Proteolytic Degradation Characteristics. *Frontiers in Microbiology.* **2020**, *11*, Original Research. DOI: 10.3389/fmicb.2020.563030.

(14) Kolodkin-Gal, I.; Romero, D.; Cao, S.; Clardy, J.; Kolter, R.; Losick, R. D-Amino Acids Trigger Biofilm Disassembly. *Science.* **2010**, *328* (5978), 627-629. DOI: doi:10.1126/science.1188628.

(15) Genchi, G. An overview on D-amino acids. *Amino Acids.* **2017**, 49:1521-1533.

(16) Wolosker, H.; Sheth, K.N.; Takahashi, M. Purification of serine racemase: biosynthesis of the neuromodulator D-serine. *Proc. Natl. Acad. Sci. USA.* **1999**, 96(2):721-725.

(17) Yoshimura, T.; Esak, N. Amino acid racemases: functions and mechanisms. *J. Biosci. Bioeng.* **2003**, 96(2):103-109.

(18) Thorne, C.D.; Gomez, C.G.,;Housewright, R.D. Transamination of D-amino acids by *Bacillus subtilis. J. Bacteriol.* **1955**, 69(3):357-362.

(19) Tanner, M.E. Understanding nature's strategies for enzyme-catalyzed racemization and epimerization. *Acc. Chem. Res.* **2002**, 35(4):237-246.

(20) Kim, P.M.; Duan, X.; Huang, A.S.; Snyder, S.H. Aspartate racemase, generating neuronal D-aspartate, regulates adult neurogenesis. *Proc. Nat. Acad. Sci.* **2010**, 107(7):3175-3179.

(21) Semenza, E. R.; Harraz, M. M.; Abramson, E.; Malla, A. P.; Vasavda, C.; Gadalla, M. M.; Kornberg, M. D.; Snyder, S. H.; Roychaudhuri, R. D-cysteine is an endogenous regulator of neural progenitor cell dynamics in the mammalian brain. *Proc. Nat. Acad. Sci*. **2021**, *118* (39), e2110610118. DOI: doi:10.1073/pnas.2110610118.

(22) Shleper, M.; Kartvelishvily, E.; Wolosker, H. D-Serine Is the Dominant Endogenous Coagonist for NMDA Receptor Neurotoxicity in Organotypic Hippocampal Slices. *J. Neurosci.* **2005**, *25* (41), 9413-9417. DOI: 10.1523/jneurosci.3190-05.2005.

(23) Newcomer, J. W.; Farber, N. B.; Olney, J. W. NMDA receptor function, memory, and brain aging. *Dialogues Clin. Neurosci.* **2000**, *2* (3), 219-232. DOI: 10.31887/DCNS.2000.2.3/jnewcomer.

(24) Hashimoto, A.; Nishikawa, T.; Hayashi, T.; Fujii, N.; Harada, K.; Oka, T.; Takahashi, K. The presence of free D-serine in rat brain. *FEBS Lett.* **1992**, *296* (1), 33-36. DOI: https://doi.org/10.1016/0014-5793(92)80397-Y.

(25) Du, S.; Sung, Y.-S.; Wey, M.; Wang, Y.; Alatrash, N.; Berthod, A.; MacDonnell, F. M.; Armstrong, D. W. Roles of N-methyl-D-aspartate receptors and D-amino acids in cancer cell viability. *Mol. Biol. Rep.* **2020**, *47* (9), 6749-6758. DOI: 10.1007/s11033-020-05733-8.

(26) Kimura, T.; Hesaka, A.; Isaka, Y. D-Amino acids and kidney diseases. *Clin. Exp. Nephrol.* **2020**, *24* (5), 404-410. DOI: 10.1007/s10157-020-01862-3.

(27) Piubelli, L.; Murtas, G.; Rabattoni, V.; Pollegioni, L. The Role of D-Amino Acids in Alzheimer's Disease. *J. Alzheimer's Dis.* **2021**, *80*, 475-492. DOI: 10.3233/JAD-201217.

(28) Madeira, C.; Freitas, M. E.; Vargas-Lopes, C.; Wolosker, H.; Panizzutti, R. Increased brain d-amino acid oxidase (DAAO) activity in schizophrenia. *Schizophr, Res.* **2008**, *101* (1), 76-83. DOI: https://doi.org/10.1016/j.schres.2008.02.002.

(29) Hartman, A.L.; Santos, P.; O'Riordan, K.J.; Stafstrom, C.E.; Hardwick, J.M. Potent anti-seizure effects of D-leucine. *Neurobiol. Dis.* **2015**, 82:46-53.

(30) Davankov, V. A.; Rogozhin, S. V. Ligand chromatography as a novel method for the investigation of mixed complexes: stereoselective effects in α-amino acid copper(II) complexes. *J. Chromatogr. A.* **1971**, *60*, 280-283. DOI: https://doi.org/10.1016/S0021-9673(00)95566-3.

(31) Armstrong, D. W.; Tang, Y.; Chen, S.; Zhou, Y.; Bagwill, C.; Chen, J.-R. Macrocyclic Antibiotics as a New Class of Chiral Selectors for Liquid Chromatography. *Anal. Chem.* **1994**, *66* (9), 1473-1484. DOI: 10.1021/ac00081a019.

(32) Armstrong, D. W.; Kullman, J. P.; Chen, X.; Rowe, M. Composition and chirality of amino acids in aerosol/dust from laboratory and residential enclosures. *Chirality.* **2001**, *13* (3), 153-158. DOI: https://doi.org/10.1002/1520-636X(2001)13:3<153::AID-CHIR1013>3.0.CO;2-8.

(33) Simpson, R. J.; Neuberger, M. R.; Liu, T. Y. Complete amino acid analysis of proteins from a single hydrolysate. *JBC.* **1976**, *251* (7), 1936-1940. DOI: https://doi.org/10.1016/S0021-9258(17)33637-2.

(34) Miyamoto, T.; Sekine, M.; Ogawa, T.; Hidaka, M.; Homma, H.; Masaki, H. Generation of Enantiomeric Amino Acids during Acid Hydrolysis of Peptides Detected by the Liquid Chromatography/Tandem Mass Spectroscopy. *Chem. Biodivers.* **2010**, *7* (6), 1644-1650. DOI: https://doi.org/10.1002/cbdv.200900309.

(35) Berthias, F.; Baird, M. A.; Shvartsburg, A. A. Differential Ion Mobility Separations of D/L Peptide Epimers. *Anal. Chem.* **2021**, *93* (8), 4015-4022. DOI: 10.1021/acs.analchem.0c05023.

(36) Sung, Y.-S.; Berthod, A.; Roy, D.; Armstrong, D. W. A Closer Examination of 6-Aminoquinolyl-N-Hydroxysuccinimidyl Carbamate Amino Acid Derivatization in HPLC with Multiple Detection Modes. *Chromatographia*. **2021**, *84* (8), 719-727. DOI: 10.1007/s10337-021-04051-w.

(37) Sung, Y.-S.; Putman, J.; Du, S.; Armstrong, D. W. Enhanced carboxypeptidase efficacies and differentiation of peptide epimers. *Anal. Biochem.* **2022**, *642*, 114451. DOI: https://doi.org/10.1016/j.ab.2021.114451.

(38) Sung, Y.-S.; Khvalbota, L.; Dhaubhadel, U.; Špánik, I.; Armstrong, D. W. Teicoplanin aglycone media and carboxypeptidase Y: Tools for finding low-abundance D-amino acids and epimeric peptides. *Chirality*. DOI: https://doi.org/10.1002/chir.23543.

(39) Horáček, O.; Portillo, A. E.; Dhaubhadel, U.; Sung, Y.-S.; Readel, E. R.; Kučera, R.; Armstrong, D. W. Comprehensive chiral GC-MS/MS and LC-MS/MS methods for identification and determination of N-acyl homoserine lactones. *Talanta.* **2023**, *253*, 123957. DOI: https://doi.org/10.1016/j.talanta.2022.123957.

(40) Cohen S. A.; Michaud D. P. Synthesis of a fluorescent derivatizing reagent, 6-aminoquinolyl-*N*-hydroxysuccinimidyl carbamate, and its application for the analysis of hydrolysate amino acids via HPLC. *Anal. Biochem.* **1993**, 211:279–287. https://doi.org/10.1006/abio.1993.1270

(41) Cohen S.A.; Michaud D.P. Preparation and use of novel *N*-hydroxysuccinimidyl heterocyclo-carbamates. Eur. Patent EP 0533200 B1 and US Patent 5,296,599 by Waters. **1993**.

(42) Pawlowska M.; Chen S.; Armstrong D. W. Enantiomeric separation of fluorescent, 6-aminoquinolyl-*N*-hydroxysuccinimidyl carbamate, tagged amino acids. *J. Chromatogr. A.* **1993**, 641:257–265. https://doi.org/10.1016/0021-9673(93)80142-U

(43) Deantonis K. M.; Brown P. R.; Cohen S. A. HPLC analysis of synthetic peptides using derivatization with 6-aminoquinolyl-*N*-hydroxysuccinimidyl carbamate. *Anal. Biochem.* **1994**, 223:191–197. https://doi.org/10.1006/abio.1994.1572

(44) Liu H. J. Determination of amino acids by precolumn derivatization with AQC and HPLC with ultraviolet detection. *J. Chromatogr. A.* **1994**, 670:59–66. https://doi.org/10.1016/0021-9673(94)00111-L

(45) Wang H.; McNeil Y. R.; Yeo T. W.; Anstey N. M. Simultaneous determination of multiple amino acids in plasma in critical illness by HPLC with UV and fluorescence detection. *J. Chromatogr. B.* **2013**, 940:53–58. https://doi.org/10.1016/j.jchromb.2013.09.016

(46) Petritis K.; Chaimbault P.; Elfakir C.; Dreux M. Parameter optimization for the analysis of underivatized protein amino acids by LC and ion spray tandem MS. *J. Chromatogr. A.* **2000**, 896:253–263. https://doi.org/10.1016/0021-9673(00)00582-3

(47) Qu J.; Wang Y.; Luo G.; Wu Z.; Yang C. Validated quantitation of underivatized amino acids in human blood samples by volatile ion-pair RPLC coupled to isotope dilution tandem MS. *Anal. Chem.* **2002**, 74:2034–2040. https://doi.org/10.1021/ac0111917

(48) Hou S.; He H.; Zhang W.; Xie H.; Zhang X. Determination of soil amino acids by HPLC-ESI-MS derivatized with AQC. *Talanta*. **2009**. 80:440–447. https://doi.org/10.1016/j.talanta.2009.07.013

(49) Fiechter G; Mayers H. K. Characterization of amino acid profiles of culture media via pre-column 6-aminoquinolyl-*N*-hydroxysuccinimidyl carbamate derivatization and UHPLC. *J. Chromatogr. A.* **2011**, 879:1353–1360. https://doi.org/10.1016/j.jchromb.2011.02.003

(50) Gornischeff A.; Kruve A.; Rebane R. Characterization of wines with LC-ESI-MS: quantification of amino acids via ionization efficiency values. *J. Chromatogr. A.* **2020**, 1620:461012. https://doi.org/10.1016/j.jchroma.2020.461012

(51) Ferre S.; Gonzalez-Ruiz V.; Guillarme D.; Rudaz S. Analytical strategies for the determination of amino acids: past, present and future trends. *J. Chromatogr. A.* **2019**, 1132:121819. https://doi.org/10.1016/j.jchromb.2019.121819

(52) Du S.; Wang Y.; Weatherly C. A.; Holden K.; Armstrong D. W. Variations of L- and D-amino acid levels in the brain of wild-type and mutant mice lacking D-amino acid oxidase activity. *Anal. Bioanal. Chem.* **2018**, 410:2971–2979. https://doi.org/10.1007/s00216-018-0979-9

(53) Du S.; Wang Y.; Alatrash N.; Weatherly C. A.; Daipayan R.; MacDonnell F. M.; Armstrong D. W. Altered profiles and metabolism of L- and D-amino acids in cultured human breast cancer cells vs. non-tumorigenic human breast epithelial cells. *J. Pharm. Biomed. Anal.* **2019**, 164:421–429. https://doi.org/10.1016/j.jpba.2018.10.047

(54) Du S.; Sung Y. S.; Wey M.; Wang Y.; Alatrash N.; Berthod A.; MacDonnell F. M.; Armstrong D. W. Roles of N-methyl-D-aspartate receptors and D-amino acids in cancer cell viability. *Mol. Biol. Rep.* **2020**, 47:6749–6758. https://doi.org/10.1007/s11033-020-05733-8

(55) Naffa R.; Holmes G.; Zhang W.; Maidment C.; Shehadi I.; Norris G. Comparison of LC with fluorescence detection for amino acid analysis with derivatization by AQC: applications for analysis of amino acids in skin. *Arab. J. Chem.* **2020**, 13:3997–4008. https://doi.org/10.1016/j.arabjc.2019.05.002

(56) Zhou P.; Zhao F.; Chen M.; Ye N.; Lin Q.; Ouyang L.; Cai X.; Meng P.; Gong X.; Wang Y. Determination of 21 free amino acids in 5 types of tea by UHPLC–MS/MS using a modified AQC method. *J. Food Comp. Anal.* **2019**, 81:46–54. https://doi.org/10.1016/j.jfca.2019.05.007

(57) Tsugita A.; Schefler J. J. A rapid method for acid hydrolysis of protein with a mixture of trifluoroacetic acid and hydrochloric acid. *Eur. J. Biochem.* **1982**, 124:585–588. https://doi.org/10.1111/j.1432-1033.1982.tb06634.x

(58) Peter A.; Laus G.; Tourwe D.; Gerlo E.; van Binst G. An evaluation of microwave heating for the rapid hydrolysis of peptide samples for chiral amino acid analysis. *Peptide Res.* **1993**, 6:48–52. https://europepmc.org/article/med/8439736

(59) Askretkov A. D.; Klishin A. A.; Zybin D. I.; Orlova N. V.; Kholodova A. V.; Lobanova N. V.; Seregin Y. A. Determination of twenty proteinogenic amino acids and additives in cultural liquid by HPLC. *J. Anal. Chem.* **2020**, 75:1038–1045. https://doi.org/10.1134/s1061934820080031

(60) Petritis K.; Elfakir C.; Dreux M. A comparative study of commercial liquid chromatographic detectors for the analysis of underivatized amino acids. *J. Chromatogr. A.* **2002**, 961:9–21. https://doi.org/10.1016/S0021-9673(02)00377-1

(61) Fernandez-Ramos A.; Cabaleiro-Lago E.; Hermida-Ramón J. M.; Marinez-Nuñez E.; Peña-Gallego A. DFT conformational study of cysteine in gas phase and aqueous

solution. *J. Mol. Struct. Theochem*. **2000**, 498:191–200. https://doi.org/10.1016/S0166-1280(99)00261-4

(62) Routh J. The decomposition of cysteine in aqueous solution. *J. Biol. Chem.* **1939**, 130:297–304. http://www.jbc.org/content/130/1/297.citation

(63) Chipinda I.; Stetson A. J.; Depree G. J.; Simoyi R. H.; Siegel P. D. Kinetics and mechanistic studies of the hydrolysis of diisocyanate-derived bis-thiocarbamates of cysteine methyl ester. *Chem. Res. Tox.* **2006**, 19:341–350. https://doi.org/10.1021/tx050311t

(64) Dexter D. L. A theory of sensitized luminescence in solids. *J. Chem. Phys.* **1953**, 21:836–850. https://doi.org/10.1063/1.1699044

(65) Vogel M.; Rettig W. Efficient intramolecular fluorescence quenching in triphenylmethane dyes involving excited states with charge separation and twisted conformations. *Ber. Buns. Phys. Chem.* **1985**, 89:962–968. https://doi.org/10.1002/bbpc.19850890908

(66) Adams P. D.; Chen Y.; Ma K.; Zagorski M. G.; Soennichsen F. D.; McLaughlin M. L.; Barkley M. D. Intramolecular quenching of tryptophan fluorescence by the peptide bond in cyclic hexapeptides. *J. Am. Chem. Soc.* **2002**, 124:9278–9286. https://doi.org/10.1021/ja0167710

(67) Chen J.; Shannon L. F.; Callis P. R.; King J. Mechanism of the highly efficient quenching of tryptophan fluorescence in human γ-D-crystallin. *Biochem.* **2002**, 45:11552–11563. https://doi.org/10.1021/bi060988v

(68) Zhu S.; Stein R. A.; Yoshioka C.; Lee C. H.; Goehring A.; Mchaourab H. S.; Gouaux E. Mechanism of NMDA receptor inhibition and activation. *Cell.* **2016**, 165:704–714

(69) Watkins J. C. Pharmacology of excitatory amino acid transmitters. *Adv. Biochem. Psychopharmacol.* 2016, 29:205–212

(70) Hogan-Cann A. D.; Anderson C. M. Physiological roles of non-neuronal NMDA receptors. *Trends Pharmacol. Sci.* **2016**, 37:750–767

(71) Traynelis S. F.; Wollmuth L. P.; McBain C. J.; Menniti F. S.; Vance K. M.; Ogden K. K.; Hansen K. B.; Yuan H.; Myers S. J.; Dingledine R. Glutamate receptor ion channels: structure, regulation, and function. *Pharmacol. Rev.* **2010**, 62:405–496

(72) Paoletti P.; Bellone C.; Zhou Q. NMDA receptor subunit diversity: impact on receptor properties, synaptic plasticity and disease. *Nat. Rev. Neurosci.* 2013, 14:383–400

(73) Cull-Candy S. G.; Leszkiewicz D. N. Role of distinct NMDA receptor subtypes at central synapses. *Science's STKE.* **2004,** re16

(74) Johnson J. W.; Ascher P. Glycine potentiates the NMDA response in cultured mouse brain neurons. *Nature.* **1987**, 325:529–531

(75) Kleckner N. W.; Dingledine R. Requirement for glycine in activation of NMDA-receptors expressed in Xenopus oocytes. *Science.* **1988**, 241:835–837

(76) Hashimoto A.; Oka T.; Nishikawa T. Extracellular concentration of endogenous free D-serine in the rat brain as revealed by in vivo microdialysis. *Neuroscience.* **1995**, 66:635–643

(77) Wolosker H.; Blackshaw S.; Snyder S. H. Serine racemase: a glial enzyme synthesizing D-serine to regulate glutamate-N-methyl-D-aspartate neurotransmission. *Proc. Natl. Acad. Sci. USA.* **1999**, 96:13409–13414

(78) Wolosker H.; Sheth K. N.; Takahashi M.; Mothet J. P.; Brady R. O. Jr; Ferris C. D.; Snyder S. H. Purification of serine racemase: biosynthesis of the neuromodulator D-serine. *Proc. Natl. Acad. Sci. USA.* **1999**, 96:721–725

(79) Matsui T.; Sekiguchi M.; Hashimoto A.; Tomita U.; Nishikawa T.;Wada K. Functional comparison of D-serine and glycine in rodents: the effect on cloned NMDA receptors and the extracellular concentration. *J. Neurochem.* **1995**, 65:454–458

(80) Schell M. J.; Brady R. O. Jr; Molliver M. E.; Snyder S. H. D-serine as a neuromodulator: regional and developmental localizations in rat brain glia resemble NMDA receptors. *J. Neurosci.* **1997**, 17:1604–1615

(81) Mothet J. P.; Parent A. T.; Wolosker H.; Brady R. O. Jr; Linden D. J.; Ferris C. D.; Rogawski M. A.; Snyder S. H. D-serine is an endogenous ligand for the glycine site of the N-methyl-D-aspartate receptor. *Proc. Natl. Acad. Sci. USA.* **2000**, 97:4926–4931

(82) McBain C. J.; Kleckner N. W.; Wyrick S.; Dingledine R. Structural requirements for activation of the glycine coagonist site of N-methyl-D-aspartate receptors expressed in Xenopus oocytes. *Mol. Pharmacol.* **1989**, 36:556–565

(83) D'Aniello A.; Fiore M. M. D.; Fisher G. H.; Milone A.; Seleni A.; D'Aniello S.; Perna A. F.; Ingrosso D. Occurrence of D-aspartic acid and N-methyl-D-aspartic acid in rat neuroendocrine tissues and their role in the modulation of luteinizing hormone and growth hormone release. *FASEB J.* **2000**, 14:699–714

(84) Erreger K.; Geballe M. T.; Kristensen A.; Chen P. E.; Hansen K. B.; Lee C. J.; Yuan H.; Le P.; Lyuboslavsky P. N.; Micale N.; Jorgensen L.; Clausen R. P.; Wyllie D. J. A.; Snyder J. P.; Traynelis S. F. Subunit-specific agonist activity at NR2A-, NR2B-, NR2C-,

and NR2D-containing N-methyl-D-aspartate glutamate receptors. *Mol. Pharmacol.* **2007**, 72:907–920

(85) Kim P. M.; Duan X.; Huang A. S.; Liu C. Y.; Ming G. L.; Song H.; Snyder S. H. Aspartate racemase, generating neuronal D-aspartate, regulates adult neurogenesis. *Proc. Natl. Acad. Sci. USA.* **2010**, 107:3175–3179

(86) Malinow R. New developments on the role of NMDA receptors in Alzheimer's disease. *Curr. Opin. Neurobiol.* 2012, 22:559–563

(87) Heng M. Y.; Detloff P. J.; Wang P. L.; Tsien J. Z.; Albin R. L. In vivo evidence for NMDA receptor-mediated excitotoxicity in a murine genetic model of Huntington disease. *J. Neurosci.* **2009**, 29:3200–3205

(88) Milnerwood A. J.; Gladding C. M.; Pouladi M. A.; Kaufman A. M.; Hines R. M.; Boyd J. D.; Ko R. W.; Vasuta O. C.; Graham R. K.; Hayden M. R.; Murphy T. H.; Raymond L. A. Early increase in extrasynaptic NMDA receptor signaling and expression contributes to phenotype onset in Huntington's disease mice. *Neuron.* **2010**, 65:178–190

(89) Balu D. T. The NMDA receptor and schizophrenia: from pathophysiology to treatment. *Adv. Pharmacol.* **2016**, 76:351–382

(90) Stepulak A.; Luksch H.; Gebhardt C.; Uckermann O.; Marzahn J.; Sifringer M.; Rzeski W.; Staufner C.; Brocke K. S.; Turski L.; Ikonomidou C. Expression of glutamate receptor subunits in human cancers. *Histochem. Cell Biol.* **2009**, 132:435–445

(91) Deutsch S. I.; Tang A. H.; Burket J. A.; Benson A. D. NMDA receptors on the surface of cancer cells: target for chemotherapy? *Biomed. Pharmacother.* **2014**, 68:493–496

(92) Stepulak A.; Rola R.; Polberg K.; Ikonomidou C. Glutamate and its receptors in cancer. *J. Neural. Transm.* **2014**, 121:933–944

(93) Abdul M.; Hoosein N. N-methyl-D-aspartate receptor in human prostate cancer. *J. Membr. Biol.* **2005**, 205:125–128

(94) Genever P. G.; Maxfield S. J.; Kennovin G. D.; Maltman J.; Bowgen C. J.; Raxworthy M. J.; Skerry T. M. Evidence for a novel glutamate-mediated signaling pathway in keratinocytes. *J. Investig. Dermatol.* **1999**, 112:337–342

(95) Nahm W. K.; Philpot B. D.; Adams M. M.; Badiavas E. V.; Zhou L. H.; Butmarc J.; Bear M. F.; Falanga V. Significance of N-methyl-d-aspartate (NMDA) receptor-mediated signaling in human keratinocytes. *J. Cell Physiol.* **2004**, 200:309–317

(96) North W. G.; Gao G.; Memoli V.; Pang R. H. L.; Lynch L. Breast cancer expresses functional NMDA receptors. *Breast Cancer Res. Treat.* **2010**, 122:307–314

(97) North W. G.; Liu F.; Lin L. Z.; Tian R.; Akerman B. NMDA receptors are important regulators of pancreatic cancer and are potential targets for treatment. *Clin. Pharmacol.* **2017**, 9:79–86

(98) Pfaffl M. W. A new mathematical model for relative quantification in real-time RT–PCR. *Nucleic Acids Res.* **2001**, 29:e45

(99) Patel D. C.; Breitbach Z. S.; Yu J.; Nguyen K. A.; Armstrong D. W. Quinine bonded to superficially porous particles for high-efficiency and ultrafast liquid and supercritical fluid chromatography. *Anal. Chim. Acta.* **2017**, 963:164–174

(100) Armstrong D. W.; Liu Y.; Ekborgott K. H. A covalently bonded teicoplanin chiral stationary phase for HPLC enantioseparations. *Chirality.* **1995**, 7:474–497

(101) Ahmed S. A.; Gogal R. M. Jr; Walsh J. E. A new rapid and simple non-radioactive assay to monitor and determine the proliferation of lymphocytes: an alternative to [3H] thymidine incorporation assay. *J. Immunol. Methods.* **1994**, 170:211–224

(102) Cull-Candy S.; Brickley S.; Farrant M. NMDA receptor subunits: diversity, development and disease. *Curr. Opin. Neurobiol.* **2001**, 11:327–335

(103) Monyer H.; Burnashev N.; Laurie D. J.; Sakmann B.; Seeburg P. H. Developmental and regional expression in the rat brain and functional properties of four NMDA receptors. *Neuron.* **1994**, 12:529–540

(104) Sheng M.; Cummings J.; Roldan L. A.; Jan Y. N.; Jan L. Y. Changing subunit composition of heteromeric NMDA receptors during development of rat cortex. *Nature*. **1994**, 368:144–147

(105) Rzeski W.; Turski L.; Ikonomidou C. Glutamate antagonists limit tumor growth. *Proc. Natl. Acad. Sci. USA.* **2001**, 98:6372–6377

(106) Duan W.; Hu J.; Liu Y. Ketamine inhibits colorectal cancer cells malignant potential via blockage of NMDA receptor. *Exp. Mol. Pathol.* **2019**, 107:171–178

(107) Stepulak A.; Sifringer M.; Rzeski W.; Endesfelder S.; Gratopp A.; Pohl E. E.; Bittigau P.; Felderhoff-Mueser U.; Kaindl A. M.; Bührer C.; Hansen H. H.; Stryjecka-Zimmer M.; Turski L.; Ikonomidou C. NMDA antagonist inhibits the extracellular signal-regulated kinase pathway and suppresses cancer growth. *Proc. Natl. Acad. Sci. USA.* **2005**, 102:15605–15610

(108) Santillo A.; Falvo S.; Chieffi P.; Burrone L.; Baccari G. C.; Longobardi S.; Di Fiore M. M. D-aspartate affects NMDA receptor-extracellular signal–regulated kinase pathway and upregulates androgen receptor expression in the rat testis. *Theriogenology.* **2014**, 81:744–751

(109) Santillo A.; Falvo S.; Chieffi P.; Di Fiore M. M.; Senese R.; Chieffi B. G. D-Aspartate induces proliferative pathways in spermatogonial GC-1 cells. *J. Cell Phsiol.* **2016**, 231:490–495

(110) McKay S.; Bengtson C. P.; Bading H.; Wyllie D. J.; Hardingham G. E. Recovery of NMDA receptor currents from MK-801 blockade is accelerated by Mg^{2+} and memantine under conditions of agonist exposure. *Neuropharmacology.* **2013**, 74:119–125

(111) Hata T.; Hayashi R.; Doi E. Purification of yeast proteinases: Part 1. Fractionation and some properties of the proteinases, *Agric. Biol. Chem.* **1967**, 31:150-159, https://doi.org/10.1080/00021369.1967.10858787.

(112) Hata T.; Hayashi R.; Doi E. Purification of yeast proteinases: Part 2. Purification and some properties of yeast proteinase C, *Agric. Biol. Chem.* **1967**, 31:160-169, https://doi.org/10.1080/00021369.1967.10858787.

(113) Hata T.; Hayashi R.; Doi E. Purification of Yeast proteinases: Part 3. Isolation and physiochemical properties of yeast proteinase A and C, *Agric. Biol. Chem.* **1967**, 31: 357-367, https://doi.org /10.1080/00021369.1967.10858812.

(114) Matsumoto A.; Itoh K.; Matsumoto R. A novel carboxypeptidase B that processes native β- amyloid precursor protein that is present in human hippocampus, *Eur. J. Neurosci.* **2000**, 12: 227-238, https://doi.org/10.1046/j.1460-9568.2000.00908.

(115) Davidson H. W.; Hutton J. C. The insulin-secretory-granule carboxypeptidase H. Purification and demonstration of involvement in proinsulin processing, *Biochem. J.* **1987**, 245 () 575-582, https://doi.org/10.1042/bj2450575.

(116) Chen H.; Jawahar S.; Qian Y.; Duong Q.; Chan G.; Parker A.; Meyer J. M.; Moore K. J.; Chayen S.; Gross D. J.; Glaser B.; Permutt M. A.; Fricker L. D. Missense polymorphism

in the human carboxypeptidase E gene alters enzymatic activity, *Hum. Mutat.* **2001**, 18 (2) 120-131, https://doi.org/10.1002/humu.1161.

(117) Breddam K. Serine carboxypeptidases. A review, *Carlsberg Res. Commun.* **1986**, 51: 81-128, https://doi.org/10.1007/BF02907561.

(118) Anson M. L. I. Carboxypeptidase, The preparation of crystalline carboxypeptidase, *J. Gen. Physiol.* 1937, 20: 663-669, https://doi.org/10.1085/jgp.20.5.663.

(119) Valle B.; Neurath H. Carboxypeptidase, a zinc metalloprotein, *J. Am. Chem. Soc.* **1954**, 76: 5006-5007, https://doi.org/10.1021/ja01648a088.

(120) Williams R. Binding of zinc in Carboxypeptidase, *Nature.* **1960**, 188 () 332, https://doi.org/10.1038/188322a0.

(121) Christianson D. W.; Lipscomb W. N.; A. Carboxypeptidase, *Acc. Chem. Res.* 1989, 22: 62-69, https://doi.org/10.1021/ar00158a003.

(122) Wu S.; Zhang C.; Xu D.; Hua G. Catalysis of carboxypeptidase A: promoted- Water versus nucleophilic pathways, *J. Phys. Chem. B.* **2010**, 114 () 9259-9267, https://doi.org/10.1021/jp101448j.

(123) Smith M. B., Biochemistry: an Organic Chemistry Approach, first ed., CRC Press, Boca Raton, **2020**, p. 284.

(124) Ambler R. P. Enzymatic hydrolysis with carboxypeptidases, *Methods Enzymol.* **1967**, 11: 155-166, https://doi.org/10.1016/S0076-6879(67)11016-1.

(125) Kuhn R., Walsh K.; Neurath H. Isolation and partial characterization of an acid carboxypeptidase from yeast, *Biochem.* **1974**, 13: 3871-3877, https://doi.org/10.1021/bi00716a008.

(126) Hayashi R.; Moore S.; Stein W. Carboxypeptidase from yeast. Large scale preparation and application to COOH- terminal analysis of peptides and proteins, *J. Biol. Chem.* **1973**, 248: 2296-2302, https://doi.org/10.1016/S0021-9258(19)44109-4.

(127) Jung G.; Ueno R.; Hayashi R. Y. Carboxypeptidase, Structural basis for protein sorting and catalytic triad, *J. Biochem.* **1999**, 126: 1-6, https://doi.org/10.1093/oxfordjournals.jbchem.a022408

(128) Nakase H.; Murata S.; Ueno H,; Hayashi R. Substrate recognition mechanism of carboxypeptidase Y. *Biosci. Biotechnol. Biochem.* **2001**, 65: 2465-2471. https://doi.org/10.1271/bbb.65.2465

(129) Walker J. M.; Winder J. S.; Enzymes in molecular biology, Volume 16, M.M. Burrell (Eds.), Humana Press, Totowa, NJ, **1993** pp. 313-318

(130) Stennicke H.; Mortensen U.; Breddam K. Studies on the hydrolytic properties of (Serine) carboxypeptidase Y. *Biochem*. **1996**, 35: 7131-7141. https://doi.org/10.1021/bi952758e

(131) Rawlings N. D.; Salvesen G. Handbook of Proteolytic Enzymes, Volume 1, 3rd edition, Oxford, Academic **2012** pp. 3408-3412

(132) Li M.; Zheng H.; Lin M.; Zhu W.; Zhang J. Characterization of the protein and peptide of excipient zein by the multi enzyme digestion with nano-LC-MS/MS. *Food Chem.* **2015**, 321:126712.https://doi.org/10.1016/j.foodchem.2020.126712

(133) Feng Z.; Xu B. Inspiration from the mirror: D-amino acid containing peptides in biomedical approaches. *Biomol. Concepts.* **2016**, 7: 179-187.https://doi.org/10.1515/bmc-2015-0035

(134) Du S.; Readel E. R.; Wey M.; Armstrong D. W. Complete identification of all 20 relevant epimeric peptides in -amyloid: A new HPLC-MS based analytical strategy for

Alzheimer's research. *Chem. Comm.* **2020**, 56: 1537-1540.https://doi.org/10.1039/C9CC09080K

(135) Jia C.; Lietz C. B.; Yu Q.; Li L. Site-specific characterization of D-amino acid containing epimers by ion mobility spectrometry, *Anal. Chem.* 2014, 86: 2972-2981. https://doi.org/10.1021/ac4033824

(136) Livnat I.; Tai H-C.; Jansson E. T.; Bai L.; Romanova E. V.; Chen T-T.; Yu K.; Chen S-A.; Zhang Y.; Wang Z-Y.; Liu D-D.; Weiss K. R.; Jing J.; Sweedler J. V. A D-Amino Acid-Containing Neuropeptide Discovery Funnel. *Anal. Chem.* **2016**, 88 () 11868-11876. https://10.1021/acs.analchem.6b03658

(137) Hayashi R.; Bai Y.; Hata T. Kinetic studies for carboxypeptidase Y: I. Kinetic parameters for the hydrolysis of synthetic substrates. *J. Biol. Chem.* **1975**, 77 () 69-79. https://doi.org/10.1093/oxfordjournals.jbchem.a130720

(138) Cohen S.; DeAntonis A. Applications of amino acid derivatization with 6-aminoquinolyl-N-hydroxysuccinimidyl carbamate: Analysis of feed grains, intravenous solutions and glycoproteins. *J. Chromatogr. A.* **1994**, 661: 25-34. https://doi.org/10.1016/0021-9673(93)E0821-B

(139) Dymicky M. Preparation of carbobenzoxy-L-tyrosine methyl and ethyl esters and of the corresponding carbobenzoxy hydrazides. *Org. Prep. Proced. Inl.* 1989, 21: 83-90.https://doi.org/10.1080/00304948909356350

(140) Sung Y.S.; Berthod A.; Roy D.; Armstrong D. W. A closer examination of 6-aminoquinolyl-N-hydroxysuccimidyl carbamate amino acid derivatization in HPLC with multiple detection modes. *Chromatographia*. **2021**, 84: 719-727.https://doi.org/10.1007/s10337-021-04051-w

(141) Mayer H.; Feichter G. Application of UHPLC for the determination of free amino acids in different cheese varieties. *Anal. Bioanal. Chem.* **2013**, 405: 8053-8061.https://doi.org/10.1007/s00216-013-6974-2

(142) Hong J. Determination of amino acids by precolumn derivatization with 6-aminoquinolyl-N-hydroxysuccimidyl carbamate and high performance liquid chromatography with ultraviolet detection. *J. Chromatogr. A.* **1994**, 670: 59-66.https://doi.org/10.1016/0021-9673(94)80280-7

(143) Sharma G. ; Attri S.; Behra B.; Bhisikar S.; Kumar P.; Tageja M.; Sharda S.; Singhi P.; Singhi S. Analysis of 26 amino acids in human plasma by HPLC using AQC as derivatizing agent and its application in metabolic laboratory. *Amino Acids.* **2014**, 46: 1253-1263. https://doi.org/10.1007/s00726-014-1682-6

(144) Salazar C.; Armenta J.; Shulaev V.; An UPLC-ESI MS/MS assay using 6-aminoquinolyl-N-hydroxysuccimidyl carbamate derivatization for targeted amino acid analysis: application to screening of Arabidopsis thaliana mutants. *Metabolites*. **2012**, 2 () 389-428. https://doi.org/10.3390/metabo2030398

(145) Armenta J. M.; Cortes D. F.; Pisciotta J. M.; Shuman J.L.; Blakeslee K.; Rasoloson D.; Ogunbiyi O.; Sullivan D.; Shulaev V. Sensitive and rapid method for amino acid quantitation in malaria biological samples using AccQ-Tag ultra performance liquid chromatography-electrospray ionization-MS/MS with multiple reaction monitoring. *Anal. Chem.* **2010**, 81: 548-558. https://doi.org/10.1021/ac901790q

(146) Bastings J.; van Eijk H. M.; Olde Damink S. W.; Rensen S. S. D-amino acids in health and disease: a focus on cancer. *Nutrients*. **2019**, 11(9):2205. doi:10.3390/nu11092205

(147) Sasamura T.; Matsuda A.; Kokuba Y. Determination of D-amino acid oxidase activity in tumour cells. *Ann. Clin. Biochem.* **2002**, 39(6):595-598. doi:10.1177/000456320203900608

(148) Sakaue H.; Takata T.; Fujii N.; Sasaki H.; Fujii N. Alpha B- and βA3-crystallins containing D-aspartic acids exist in a monomeric state. *Biochim. Biophys. Acta.* **2015**, 1854(1):1-9. doi:10.1016/j.bbapap.2014.10.006

(149) Magami K.; Kim I.; Fujii N.; A single Asp isomer substitution in an αA-crystallin-derived peptide induces a large change in peptide properties. *Exp. Eye Res.* **2020**, 192:107930. doi:10.1016/j.exer.2020.107930

(150) Lyon Y. A.; Collier M. P.; Riggs D. L.; Degiacomi M. T.; Benesch J. L. P.; Julian R. R. Structural and functional consequences of age-related isomerization in α-crystallins. *JBC.* **2019**, 294(19):7546-7555. doi:10.1074/jbc.RA118.007052

(151) Ma T.; Wu Y.; Chen B.; Zhang W.; Jin L.; Shen C; Wang Y.; Liu Y. D-serine contributes to seizure development via ERK signaling. *Front. Neurosci.* **2019**, 13:13. doi:10.3389/fnins.2019.00254

(152) Madeira C.; Freitas M. E.; Vargas-Lopes C.; Wolosker H.; Panizzutti R. Increased brain D-amino acid oxidase (DAAO) activity in schizophrenia. *Schizophr. Res.* **2008**, 101(1):76-83. doi: 10.1016/j.schres.2008.02.002

(153) Verrall L.; Burnet P. W. J.; Betts J. F.; Harrison P. J. The neurobiology of D-amino acid oxidase and its involvement in schizophrenia. *Mol. Psychiatry.* **2010**, 15(2):122-137. doi:10.1038/mp.2009.99

(154) Roher A. E.; Lowenson J. D.; Clarke S.; Wolkow C.; Wang R.; Cotter R. J.; Reardon I. M.; Zurcher-Neely H. A.; Heinrikson R. L.; Ball M. J. Structural alterations in the

peptide backbone of beta-amyloid core protein may account for its deposition and stability in Alzheimer's disease. *JBC*. **1993**, 268(5):3072-3083. doi:10.1016/S0021-9258(18)53661-9

(155) Kaneko I.; Morimoto K.; Kubo T. Drastic neuronal loss in vivo by β-amyloid racemized at Ser26 residue: conversion of non-toxic [D-Ser26] β-amyloid 1–40 to toxic and proteinase-resistant fragments. *Neurosci.* **2001**, 104(4):1003-1011. doi:10.1016/S0306-4522(01)00155-5

(156) Kubo T.; Kumagae Y.; Miller C. A.; Kaneko I. β-Amyloid Racemized at the Ser26 residue in the brains of patients with Alzheimer disease: implications in the pathogenesis of Alzheimer disease. *J. Neuropathol. Exp. Neurol.* **2003**, 62(3): 248-259. doi:10.1093/jnen/62.3.248

(157) Kawamura I.; Mijiddorj B.; Kayano Y.; Matsuo Y.; Ozawa Y.; Ueda K.; Sato H. Separation of D-amino acid-containing peptide phenylseptin using 3,30-phenyl-1,10-binaphthyl-18-crown-6-ether columns. *Biochim Biophys Acta Proteins Proteom BBA-Proteins Proteom.* **2020**, 1868(8):140429. doi:10.1016/j.bbapap.2020.140429

(158) Tai H-C.; Checco J. W.; Sweedler J. V. Non-targeted identification of D-amino acid-containing peptides through enzymatic screening, chiral amino acid analysis, and LC-MS. *Methods Mol. Biol.* **2018**, 1719:107-118. doi:10.1007/978-1-4939-7537-2_7

(159) Abdulbagi M.; Wang L.; Siddig O.; Di B.; Li B. D-amino acids and D-amino acid-containing peptides: potential disease bio-markers and therapeutic targets? *Biomolecules*. **2021**, 11(11):1716. doi:10.3390/biom11111716

(160) Kaiser K.; Benner R. Hydrolysis-induced racemization of amino acids. *Limnol. Oceanogr. - Meth.* **2005**, 3(8):318-325. doi:10.4319/lom.2005.3.318

(161) Broberg A.; Nord C.; Levenfors J. J.; Bjerketorp J.; Guss B.; Öberg B. In-peptide amino acid racemization via inter-residue oxazoline intermediates during acidic hydrolysis. *Amino Acids*. **2021**, 53(3):323-331. doi:10.1007/s00726-021-02951-7

(162) Bellagamba F.; Caprino F.; Mentasti T.; Vasconi M.; Moretti V. M. The impact of processing on amino acid racemization and protein quality in processed animal proteins of poultry origin. *Ital. J. Anim. Sci.* **2015**, 14(2):3770. doi:10.4081/ijas.2015.3770

(163) Morvan M.; Miksík I. Recent advances in chiral analysis of proteins and peptides. *Separations*. **2021**, 8(8):112. https://www.mdpi.com/2297-8739/8/8/112

(164) Armstrong D. W.; Kullman J. P.; Chen X.; Rowe M. Composition and chirality of amino acids in aerosol/dust from laboratory and residential enclosures. *Chirality*. **2001**, 13(3):153-158. doi:10.1002/1520-636X(2001)13:33.0.CO;2-8

(165) Putman J. I.; Lee J. T.; Armstrong D. W. Recent advances in the field of chiral crystallization. *Chirality*. **2022**, 34(10):1338-1354. doi:10.1002/chir.23492

(166) Binda E.; Marinelli F.; Marcone G. L. Old and new glycopeptide antibiotics: action and resistance. *Antibiotics*. **2014**, 3(4):572-594. doi:10.3390/antibiotics3040572

(167) Taurino C.; Frattini L.; Marcone G. L.; Gastaldo L.; Marinelli F. Actinoplanes teichomyceticus ATCC 31121 as a cell factory for producing teicoplanin. *Microb. Cell Fact.* **2011**, 10(1):82. doi:10.1186/1475-2859-10-82

(168) Péter A.; Török G.; Armstrong D. W. High-performance liquid chromatographic separation of enantiomers of unusual amino acids on a teicoplanin chiral stationary phase. *J. Chromatogr. A.* **1998**, 793(2):283-296. doi:10.1016/S0021-9673(97)00938-2

(169) Gasper M. P.; Berthod A.; Nair U. B.; Armstrong D. W. Comparison and modeling study of vancomycin, ristocetin A, and teicoplanin for CE enantioseparations. *Anal. Chem.* **1996**, 68(15):2501-2514. doi:10.1021/ac960154q

(170) Grobuschek N.; Schmid M. G.; Koidl J.; Gübitz G. Enantioseparation of amino acids and drugs by CEC, pressure supported CEC, and micro-HPLC using a teicoplanin aglycone stationary phase. *J. Sep. Sci*. **2002**, 25(15-17):1297-1302. doi:10.1002/1615-9314(20021101)25:15/173.0.CO;2-X

(171) Berthod A.; Liu Y.; Bagwill C.; Armstrong D. W. Facile liquid chromatographic enantioresolution of native amino acids and peptides using a teicoplanin chiral stationary phase. *J. Chromatogr. A.* **1996**, 731(1–2):123-137. doi:10.1016/0021-9673 (95)01198-6

(172) Boger D. L.; Kim S. H.; Miyazaki S.; Strittmatter H.; Weng J-H.; Mori Y.; Rogel O.; Castle S. L.; McAtee J. J. Total synthesis of the teicoplanin aglycon. *J. Am. Chem. Soc.* **2000**, 122(30):7416-7417.doi:10.1021/ja001663j

(173) Xiao T. L.; Tesarova E.; Anderson J. L.; Egger M.; Armstrong D. W. Evaluation and comparison of a methylated teicoplanin aglycone to teicoplanin aglycone and natural teicoplanin chiral stationary phases. *J. Sep. Sci.* **2006**, 29(3):429-445. doi:10.1002/jssc.200500332

(174) Raimbault A.; West C. Effects of high concentrations of mobile phase additives on retention and separation mechanisms on a teicoplanin aglycone stationary phase in supercritical fluid chromatography. *J. Chromatogr. A.* **2019**, 1604:460494. doi:10.1016/j.chroma.2019.460494

(175) Berthod A.; Chen X.; Kullman J. P.; Armstrong D. W.; Gasparrini F.; D'Acquaric I.; Villani C.; Carotti A. Role of the carbohydrate moieties in chiral recognition on

teicoplanin-based LC stationary phases. *Anal. Chem.* **2000**, 72(8):1767-1780. doi:10.1021/ac991004t

(176) Fuqua C.; Greenberg E. Listening in on bacteria: acyl-homoserine lactone signaling, *Nat. Rev. Mol. Cell Biol.* **2002**, 3:685–695, https://doi.org/10.1038/nrm907.

(177) Liu J.; Fu K.; Wu C.; Qin K., Li F.; Zhou L. In-group" communication in marine Vibrio: a Review of N-acyl homoserine lactones-driven quorum sensing, *Front. Cell. Infect. Microbiol*. 2018, 8: 139, https://doi.org/10.3389/fcimb.2018.00139.

(178) Suppiger A.; Schmid N.; Aguilar C.; Pessi G.; Eberl A. Two quorum sensing systems control biofilm formation and virulence in members of the Burkholderia cepacian complex, *Virulence* **2013**, 4 : 400–409, https://doi.org/10.4161/viru.25338.

(179) Smith R. S.; Iglewski B. H. *P. Aeruginosa* quorum-sensing systems and virulence, *Curr. Opin. Microbiol.* **2003**, 6: 56–60, https://doi.org/10.1016/s1369-5274(03)00008-0.

(180) Jimenez P. N.; Koch G.; Thompson J. A.; Xavier K. B.; Cool R.H.; Quax W. J. The multiple signaling systems regulating virulence in Pseudomonas aeruginosa, *Microbiol. Mol. Biol. Rev.* **2012**, 76: 46–65, https://doi.org/10.1128/MMBR.05007-11.

(181) Schuster M. ; Sexton D. J.; Diggle S. P.; Greenberg E. P. Acyl-homoserine lactone quorum sensing: from evolution to application, *Annu. Rev. Microbiol.* **2013**, 67: 43–63, https://doi.org/10.1146/annurev-micro-092412-155635.

(182) Habimana J.D.; Ji J.; Pi F.; Karangwa E.; Sun J.; Guo W.; Cui F.; Shao J.; Ntakirutimana C.; Sun X. A class-specific artificial receptor-based on molecularly imprinted polymer-coated quantum dot centers for the detection of signaling molecules, N-acyl-homoserine lactones present in gram-negative bacteria, *Anal. Chim. Acta*. 2018, 1031:134–144, https://doi.org/10.1016/j.aca.2018.05.018.

(183) Yang X.; Sun J.; Cui F.; Ji J.; Wang L.; Zhang Y.; Sun X. An eco-friendly sensor based on CQD@MIPs for detection of N-acylated homoserine lactones and its 3D printing applications, *Talanta.* 2020, 219: 121343, https://doi.org/10.1016/j.talanta.2020.121343.

(184) Cataldi T. R. I.; Bianco G.; Palazzo L.; Quaranta V. Occurrence of N-acyl-L-homoserine lactones in extracts of some Gram-negative bacteria evaluated by gas chromatography–mass spectrometry, *Anal. Biochem.* **2007**, 361: 226–235, https://doi.org/10.1016/j.ab.2006.11.037.

(185) Reimmann C.; Beyeler M.; Latifi A.; Winteler H.; Foglino M.; Lazdunski A.; Haas D. The global activator GacA of Pseudomonas aeruginosa PAO positively controls the production of the autoinducer N-butyryl-homoserine lactone and the formation of the virulence factors pyocyanin, cyanide, and lipase, *Mol. Microbiol*. **1997**, 24: 309–319, https://doi.org/10.1046/j.1365-2958.1997.3291701.x.

(186) Kuˇsar D.; Srimpf K.; Isakovi´c ˇ P.; Kalˇsek L.; Hosseini J.; Zdovc I.; Kotnik T.; Venguˇst M.; Tavˇcar-Kalcher G. Determination of N-acylhomoserine lactones of Pseudomonas aeruginosa in clinical samples from dogs with otitis externa, *BMC Vet. Res.* **2016**, 12, 233, https://doi.org/10.1186/s12917-016-0843-0.

(187) Kim Y.-W.; Sung C.; Lee S.; Kim K.-J.; Yang Y.-H.; Kim B.-G.; Lee Y.K.; Ryu H.W. Kim Y.- G. MALDI-MS-Based quantitative analysis for ketone containing homoserine lactones in Pseudomonas aeruginosa, *Anal. Chem.* **2015**, 87: 858–863, https://doi.org/10.1021/ac5039362.

(188) Hoang T. P. T.; Barth´elemy M.; Lami R.; Stien D.; Eparvier V.; Touboul D. Annotation and quantification of N-acyl homoserine lactones implied in bacterial quorum sensing by supercritical-fluid chromatography coupled with high resolution mass spectrometry,

Anal. Bioanal. Chem. **2020**, 412: 2261–2276, https://doi.org/10.1007/s00216-019-02265-4.

(189) Cataldi T.R.I.; Bianco G.; Abate S. Profiling of N-acyl-homoserine lactones by liquid chromatography coupled with electrospray ionization and a hybrid quadrupole linear ion-trap and Fourier-transform ion-cyclotron-resonance mass spectrometry (LC-ESI-LTQ-FTICR-MS), *J. Mass Spectrom.* **2007**, 43: 82–96, https://doi.org/10.1002/jms.1275.

(190) Pomini A. M.; Manfio G. P.; Araújo W. L.; Marsaioli A. J. Acyl-homoserine lactones from Erwinia psidii R. IBSBF 435T, a guava phytopathogen (Psydium guajava L.), *J. Agric. Food Chem.* **2005**, 53: 6262–6265, https://doi.org/10.1021/jf050586e.

(191) Malik A.K.; Fekete A.; Gebefuegi I.; Rothballer M.; Schmitt-Kopplin P. Single drop microextraction of homoserine lactones based quorum sensing signal molecules, and the separation of their enantiomers using gas chromatography mass spectrometry in the presence of biological matrices, *Microchim. Acta*. **2009**, 166: 101–107, https://doi.org/10.1007/s00604-009-0183-x.

(192) Gotz C.; Fekete A.; Gebefuegi I.; Forczek S. T.; Fuksov´a K.; Li X.; Englmann M.; Gryndler M.; Hartmann A.; Matucha M.; Schmitt-Kopplin P.; Schroder P. ¨Uptake, degradation and chiral discrimination of N-acyl-D/L-homoserine lactones by barley (Hordeum vulgare) and yam bean (Pachyrhizus erosus) plants, *Anal. Bioanal. Chem*. **2007,** 389: 1447–1457, https://doi.org/10.1007/s00216-007-1579-2.

(193) Ikeda T.; Kajiyama K.; Kita T.; Takiguch N.; Kuroda A.; Kato J.; Ohtake H. The synthesis of optically pure enantiomers of N-Acyl-homoserine lactone autoinducers and their analogues, *Chem. Lett.* **2001**, 30 () 314–315, https://doi.org/10.1246/cl.2001.314.

(194) Readel E.; Portillo A. E.; Talebi M.; Armstrong D. W. Enantiomeric separation of quorum sensing autoinducer homoserine lactones using GC-MS and LC-MS, *Anal. Bioanal. Chem.* **2020**, 412: 2927–2937, https://doi.org/10.1007/s00216-020-02534-7.

(195) Portillo A. E.; Readel E.; Armstrong D. W. Production of both L- and D- N-acyl-homoserine lactones by Burkholderia cepacia and, Vibrio fischeri. *Microbiologyopen* **2021**, 10: e1242, https://doi.org/10.1002/mbo3.1242.

(196) Miyamoto T.; Homma H. D-Amino acid metabolism in bacteria, *J. Biochem.* **2021**, 170: 5–13, https://doi.org/10.1093/jb/mvab043.

(197) Wang J.; Ding L.; Li K.; Schmieder W.; Geng J.; Xu K.; Zhang Y.; Ren H. Development of an extraction method and LC-MS analysis for N-acylated-L-homoserine lactones (AHLs) in wastewater treatment biofilms, *J. Chromatogr. B:Anal. Technol. Biomed. Life Sci.* **2017**, 1041: 37–44, https://doi.org/10.1016/j.jchromb.2016.11.029.

(198) Rodriguez-Mozaz S.; Lopez de Alda M. J.; Barcelo D. Advantages and limitations of on-line solid phase extraction coupled to liquid chromatography-mass spectrometry technologies versus biosensors for monitoring of emerging contaminants in water, *J. Chromatogr. A.* **2007**, 1152: 97–115, https://doi.org/10.1016/j.chroma.2007.01.046.

(199) McClean K. H.; Winson M. K.; Fish L.; Taylor A.; Chhabra S. R.; Camara M.; Daykin M.; Swift S.; Bycroft B. W.; Stewart G. S. A. B.; Williams P. Quorum sensing and Chromobacterium violaceum: exploitation of violacein production and inhibition for the detection of N-acyl homoserine-lactones, *Microbiology*. **1997**, 143 3703–3711, https://doi.org/10.1099/00221287-143-12-3703.

(200) Shaw P. D.; Ping G.; Daly S. L.; Cha C.; Cronan J. E. Jr.; Rinehaert K. L.; Farrand S. K. Detecting and characterizing N-acyl-homoserine lactone signal molecules by thin layer

chromatography, *Proc. Natl. Acad. Sci. USA.* **1997**, 94 () 6036–6041, https://doi.org/10.1073/pnas.94.12.6036.

(201) Pearson J. P.; Gray K. M.; Passador L.; Tucker K. D.; Eberhard A.; Iglewski B. H.; Greenberg E. P. Structure of the autoinducer required for expression of Pseudomonas aeruginosa virulence genes, *Proc. Natl. Acad. Sci. USA.* **1994**, 91: 197–201, https://doi.org/10.1073/pnas.91.1.197.